

# **Evaluation of Acoustic Frequency Methods Coupled to Blade Element Momentum Theory for the Prediction of Propeller Noise**

by

**Mark T. Kotwicz Herniczek**

A thesis submitted to  
the Faculty of Graduate and Postdoctoral Affairs  
in partial fulfilment of  
the requirements for the degree of  
**Master of Applied Science**  
in  
Aerospace Engineering

Ottawa-Carleton Institute for Mechanical and Aerospace Engineering  
Department of Mechanical and Aerospace Engineering  
Carleton University  
Ottawa, Ontario, Canada  
September 2nd, 2017

Copyright ©

2017 - Mark T. Kotwicz Herniczek

# Abstract

The accuracy of several computationally-inexpensive acoustic frequency methods is evaluated across a range of propeller geometries and operational conditions. The acoustic models considered predict far-field harmonic noise. They range in complexity from a direct implementation of the equations derived by Gutin and Deming to Hanson's helicoidal surface theory of propellers. The advantage of these acoustic models is that they do not require chord-wise aerodynamic data and therefore do not need to be coupled to a panel or grid-based aerodynamic solver. Each implemented method is compared to fourteen test cases originating from nine separate published acoustic experiments. The experimental data considered encapsulates a range of propeller geometries, blade numbers, microphone locations, tip speeds, and forward Mach speeds. The implemented acoustic models demonstrate good agreement with the experimental data, particularly for the prediction of the maximum tonal noise for which the model based on Hanson's work has an average error of 7.2 dB. The presented results suggest that the implemented acoustic methods and, in particular, the model based on Hanson's work, remain a valuable resource for propeller noise prediction, especially for design and optimization studies, where a low runtime is important.

# Acknowledgments

First, I would like to thank my supervisor, Daniel Feszty, for his support, guidance and kindness. Secondly, I would like to thank Sid-Ali Meslioui and Jong Park for sharing their expertise in the field of aeroacoustics and for the creative freedom they provided. Thirdly, I would like to acknowledge Fred Nitzsche for his support and for sharing his expertise in aeroelasticity for fixed and rotary winged aircraft. Lastly I would also like to acknowledge Anu Chhetry for the many arduous hours spent proof-reading my work and to my office colleagues for providing a constant source of entertainment.

This work was pursued in collaboration with Pratt & Whitney Canada and was financially supported by the Green Aviation Research and Development Network (GARDN).

# Table of Contents

<b>Abstract</b>	ii
<b>Acknowledgments</b>	iii
<b>Table of Contents</b>	iv
<b>List of Tables</b>	vii
<b>List of Figures</b>	viii
<b>Nomenclature</b>	xiv
<b>1 Introduction</b>	1
1.1 Motivation . . . . .	2
1.2 Literature Review . . . . .	4
1.3 Methodology . . . . .	6
1.4 Programming Framework . . . . .	7
<b>2 Aerodynamic Prediction Methods</b>	9
<b>3 Aerodynamic Results</b>	12
3.1 Selection of Aerodynamic Validation Cases . . . . .	12
3.2 Aerodynamic Results . . . . .	13
3.3 Aerodynamic Impact on Acoustic Solution . . . . .	17
<b>4 Acoustic Prediction Methods</b>	21

4.1	Phase Adjustment . . . . .	22
4.2	Acoustic Theory . . . . .	23
4.2.1	Coordinate System and Reference Frame . . . . .	23
4.2.2	Gutin and Deming . . . . .	24
4.2.3	Barry and Maglione . . . . .	25
4.2.4	Hanson . . . . .	27
<b>5</b>	<b>Acoustic Results</b>	<b>29</b>
5.1	Selection of Acoustic Validation Cases . . . . .	29
5.2	Acoustic Results . . . . .	30
5.2.1	Test Case 1: Soderman and Horne . . . . .	32
5.2.2	Test Case 2: Dittmar ( $M = 0.6$ ) . . . . .	33
5.2.3	Test Case 3: Dittmar ( $M = 0.8$ ) . . . . .	34
5.2.4	Test Cases 4 and 5: Dittmar and Jeracki . . . . .	34
5.2.5	Test Cases 6 and 7: Dittmar and Stang . . . . .	35
5.2.6	Test Cases 8 and 9: Brooks and Metzger . . . . .	36
5.2.7	Test Case 10: Woodward . . . . .	37
5.2.8	Test Case 11: Hubbard . . . . .	38
5.2.9	Test Cases 12 and 13: Brown and Ollerhead . . . . .	38
5.2.10	Test Case 14: Dobrzynski et al. . . . .	39
5.3	Results Summary . . . . .	40
<b>6</b>	<b>Conclusions and Recommendations</b>	<b>45</b>
6.1	Recommendations for Future Work . . . . .	46
<b>References</b>		<b>51</b>
<b>Appendix A Additional Aerodynamic Data</b>		<b>52</b>
A.1	Overall Propeller Performance . . . . .	53

A.2 Thrust and Torque Distributions . . . . .	55
A.3 Adjusted Thrust and Torque Distributions . . . . .	58
A.4 Aerodynamic Impact on Acoustic Solution . . . . .	61
<b>Appendix B Lift and Drag Coefficient Curves</b>	<b>63</b>
<b>Appendix C Propeller Geometry</b>	<b>70</b>
<b>Appendix D Additional Aeroacoustic Data</b>	<b>75</b>
<b>Appendix E Experimental Microphone Locations</b>	<b>81</b>

# List of Tables

1.1	Computational performance of acoustic prediction methods. . . . .	8
3.1	Experimental test cases selected for aerodynamic validation. . . . .	13
3.2	Relative impact of aerodynamic error on acoustic solution. . . . .	20
5.1	Experimental test cases selected for acoustic validation. . . . . . .	31
5.2	Summary of acoustic model performance. . . . . . . . . . . . . . . . .	41
D.1	Summary of acoustic model performance (one mic per data point). . .	80

# List of Figures

1.1	ICAO noise standards (from Ref. 9) . . . . .	3
1.2	Acoustic prediction method genealogy. . . . .	5
1.3	Thesis methodology. . . . .	7
2.1	Flow geometry of blade element (adapted from Ref. 33). . . . .	11
3.1	Propeller aerodynamic performance - test case 1. . . . .	15
3.2	Propeller aerodynamic performance - test case 2. . . . .	15
3.3	Propeller thrust and torque distributions at 27° blade pitch and 1740 RPM - test case 1. . . . .	16
3.4	Adjusted propeller thrust and torque distributions at 27° blade pitch and 1740 RPM - test case 1. . . . .	17
3.5	Impact of thrust and torque variation on acoustic solution - test cases 2, 3, and 14. . . . .	18
3.6	Relative impact of thrust and torque variation on acoustic solution - test cases 2, 3, and 14. . . . .	19
4.1	Sensitivity of results to destructive interference and microphone location. . . . .	22
4.2	Coordinate axis orientation (adapted from Ref. 43). . . . .	24
5.1	Tone directivities - test case 1. . . . .	32
5.2	Tone directivities - test case 2. . . . .	33
5.3	Tone directivities - test case 3. . . . .	34
5.4	Blade passing tone directivities - test cases 4 and 5. . . . .	35
5.5	Blade passing tone directivities - test cases 6 and 7. . . . .	35
5.6	Blade passing tone directivities - test cases 8 and 9. . . . .	36

5.7	Blade passing tone directivities - test case 10. . . . .	37
5.8	Tone directivities - test case 11. . . . .	38
5.9	Blade passing tone directivities - test cases 12 and 13. . . . .	39
5.10	Noise spectra - test case 14. . . . .	39
5.11	Summary of acoustic model performance. . . . .	43
A.1	Propeller aerodynamic performance - test case 3. . . . .	53
A.2	Propeller aerodynamic performance - test case 4. . . . .	54
A.3	Propeller thrust and torque distribution at 12° blade pitch and 2100 RPM - test case 1. . . . .	55
A.4	Propeller thrust and torque distribution at 60° blade pitch and 744 RPM - test case 1. . . . .	56
A.5	Propeller thrust and torque distribution - test case 2. . . . .	57
A.6	Adjusted propeller thrust and torque distribution at 12° blade pitch and 2100 RPM - test case 1. . . . .	58
A.7	Adjusted propeller thrust and torque distribution at 60° blade pitch and 744 RPM - test case 1. . . . .	59
A.8	Adjusted propeller thrust and torque distribution - test case 2. . . . .	60
A.9	Impact of thrust and torque variation on acoustic solution - test cases 9 – 11. . . . .	61
A.10	Relative impact of thrust and torque variation on acoustic solution - test cases 9 – 11. . . . .	62
B.1	Clark-Y lift and drag coefficients. . . . .	63
B.2	NACA-0012 lift and drag coefficients. . . . .	64
B.3	NACA-16-709 lift and drag coefficients. . . . .	64
B.4	NACA-16-712 lift and drag coefficients. . . . .	65
B.5	NACA-16-715 lift and drag coefficients. . . . .	65
B.6	NACA-16002 lift and drag coefficients. . . . .	66

B.7	NACA-16102 lift and drag coefficients.	66
B.8	NACA-16105 lift and drag coefficients.	67
B.9	NACA-16203 lift and drag coefficients.	67
B.10	NACA-65007 lift and drag coefficients.	68
B.11	NACA-65010 lift and drag coefficients.	68
B.12	NACA-65215 lift and drag coefficients.	69
B.13	NACA-65222 lift and drag coefficients.	69
C.1	Geometry of the Model 5 propeller (second from the right) used in aerodynamic test case 1 (from Ref. 37).	70
C.2	Geometry of the Hamilton Standard 6267A-18 propeller and Navy plan form 5868-9 propeller used in aerodynamic test cases 3 and 4 respectively (from Refs. 39 and 40).	71
C.3	Geometry of the SR-2, SR-3 and SR-7 propellers used in aerodynamic test case 3 and acoustic test cases 1–10 (from Refs. 55 and 38).	72
C.4	Geometry of the propeller used by Hubbard in acoustic test case 11 (from Ref. 50).	72
C.5	Geometry of the Sensenich W60K18 propeller used in acoustic test case 12 (from Ref. 28).	73
C.6	Geometry of the W6 STD 8° propeller used in acoustic test case 13 (from Ref. 28).	73
C.7	Geometry of te F8475D-4 propeller (shown left) used in acoustic test case 14 (from Ref. 51).	74
D.1	Tone directivities - test case 1.	76
D.2	Tone directivities - test case 2.	76
D.3	Tone directivities - test case 3.	76
D.4	Blade passing tone directivities - test cases 4 and 5.	77
D.5	Blade passing tone directivities - test cases 6 and 7.	77

D.6	Blade passing tone directivities - test cases 8 and 9. . . . .	77
D.7	Blade passing tone directivities - test case 10. . . . .	78
D.8	Tone directivities - test case 11. . . . .	78
D.9	Blade passing tone directivities - test cases 12 and 13. . . . .	78
D.10	Noise spectra - test case 14. . . . .	79
D.11	Summary of acoustic model performance (one mic per data point). . .	79
E.1	Microphone locations - test case 1 (from Ref. 24). . . . .	82
E.2	Microphone locations - test cases 2, 3, 6 and 7 (from Ref. 46). . . .	83
E.3	Microphone locations - test cases 4 and 5 (from Ref. 6). . . . .	83
E.4	Microphone locations and axial correction factor - test cases 8 and 9 (from Ref. 44). . . . .	84
E.5	Microphone locations - test case 10 (from Ref. 5). . . . .	84
E.6	Microphone locations - test case 14 (from Ref. 51). . . . .	85

# Nomenclature

$A_x$	airfoil cross-sectional area, approximated as $0.6853bh$ , m <sup>2</sup>
$B$	number of blades
$C_P$	power coefficient
$C_Q$	torque coefficient
$C_T$	thrust coefficient
$C_d$	blade section drag coefficient
$C_l$	blade section lift coefficient
$D$	propeller diameter, m
$F$	Prandtl momentum loss factor
$J$	advance ratio
$J_{mB}(x)$	Bessel function of order $mB$ and argument $x$
$M$	freestream Mach number
$MCA$	mid-chord aligment, m
$M_s$	section relative Mach number, $\sqrt{M^2 + r^2 M_t^2}$
$M_t$	tip Mach number, $\Omega r_t/c$
$P$	propeller power, $\Omega Q$ , W
$P_0$	reference sound pressure, $2 \times 10^{-5}$ Pa
$P_{mL}, P_{mT}$	root mean square sound pressure (loading and thickness component), Pa
$Q$	propeller torque, Nm

$R$	radial distance along propeller blade, m
$S$	observer distance from propeller hub, $\sqrt{x^2 + y^2 + z^2}$ , m
$SPL_m$	total sound pressure level at harmonic $m$ , dB
$SPL_{QL}$	tonal loading sound pressure level due to propeller torque, dB
$SPL_{TL}$	tonal loading sound pressure level due to propeller thrust, dB
$S_0$	amplitude radius, $\sqrt{x^2 + (1 - M^2)Y^2}$ , m
$S_r$	distance, $S$ , in retarded reference frame, m
$T$	propeller thrust, N
$V$	freestream velocity, m/s
$W$	total local velocity, m/s
$Y$	observer distance from propeller axis, $\sqrt{y^2 + z^2}$ , m
$a$	axial interference factor
$a'$	rotational interference factor
$b$	blade chord, m
$c$	speed of sound, m/s
$dQ$	discretized propeller torque, Nm
$dT$	discretized propeller thrust, N
$h$	maximum airfoil thickness, m
$k_x$	wave number
$m$	harmonic number
$n$	propeller rotative speed, revolutions per second
$r$	non-dimensional radial distance along propeller blade, $R/r_t$

$r_t$	propeller tip radius, $D/2$ , m
$x, y, z$	observer coordinates relative to propeller hub, m
$\Omega$	propeller angular velocity, $2\pi n$ , rad/s
$\Psi_L, \Psi_V$	normalized loading and thickness source transforms
$\alpha$	pitch angle of propeller shaft axis relative to flight direction, rad
$\alpha_s$	blade section angle of attack, rad
$\beta$	blade section twist angle, rad
$\beta_{75}$	propeller pitch angle at 75% blade radius, deg
$\eta$	propeller efficiency
$\phi$	tangential angle, $\arctan(z/y)$ , rad
$\phi_s$	phase lag due to sweep, rad
$\phi_t$	blade twist angle relative to propeller plane, rad
$\rho$	air density, kg/m <sup>3</sup>
$\sigma$	power loading, $\frac{C_P/J^3}{(C_P/J^3)_{design}}$
$\theta$	observer angle relative to flight direction, $\arccos(x/S)$ , rad
$\theta_r$	angle, $\theta$ , in retarded reference frame, rad
$\theta'_r, \phi'$	angles $\theta_r$ and $\phi$ relative to propeller shaft axis, rad
$\varphi$	flow angle, rad

# Chapter 1

## Introduction

The acoustic signature of commercial propeller aircraft is becoming a key design parameter as airlines shift from turbofan to turboprop engines for short-duration flights [1, 2] and restrictions on the noise pollution surrounding airports become more stringent. Propeller aircraft noise also has a direct impact on passenger comfort and on the health of those living or working near airports [3, 4]. While small propeller aircraft produce negligible noise, there is concern relating to in-flight cabin noise and community noise for larger propeller aircraft, particularly for the high efficiency propfan which operates at supersonic helical tip speeds [5, 6]. Given that propeller aircraft noise originates primarily from the propeller itself, computationally-inexpensive propeller noise prediction methods are necessary such that they can be implemented into the propeller design and optimization process.

The first successful acoustic theory was developed by Gutin in 1936, when he represented the steady aerodynamic forces on the propeller as a ring of acoustic dipole sources acting at a certain effective radius [7]. Since then, there have been many advances in acoustic theory and focus has shifted to the more computationally-expensive Farassat solutions of the Ffowcs Williams-Hawkins (FW-H) equation. Although better suited for design and optimization, earlier acoustic methods lack validation with modern propellers such as the SR-series of propellers developed by NASA. In general,

adequate validation of acoustic methods is missing from the literature due to the high degree of variation in theoretical and experimental results with microphone location, propeller operational parameters, and experimental test-setup.

This thesis investigates the relevance of several early analytical models originating from the work of Gutin and Deming for far-field harmonic noise prediction across a wide range of propeller configurations, including the modern, high speed prop-fan. This thesis also seeks to address the lack of validation present in the literature for the implemented acoustic methods.

## 1.1 Motivation

Studies on the health effects of aircraft noise on local residents have found associations between exposure to aircraft-induced noise and increased stress, sleep problems and cardiovascular diseases [3, 4]. The desirability and land-value of areas surrounding airports are thereby significantly reduced. Similarly, the disruption associated with the higher cabin-noise of propeller aircraft relative to their turbofan counterparts reduces passenger desirability to book flights on such aircraft. In an effort to retain customers, airlines offer reduced ticket prices for flights on propeller aircraft and have lowered the number of seats on those aircraft to increase leg room. Since propeller-aircraft are gaining in popularity due to their lower cost and high efficiency for low-altitude, short-duration flights [1, 2], it is of financial interest for airlines to reduce the acoustic signature of their propeller aircraft such that they do not need to be subsidized.

As a result of the adverse health effects and the annoyance associated with aircraft noise, regulations have been steadily reducing the maximum allowable noise level surrounding airports. The International Civil Aviation Organization (ICAO) has introduced a number of standards, with the latest constituting a further 7 dB increase

in stringency of the Effective Perceived Noise Level (EPNdB). A further reduction in the EPNdB is required for aircraft with a Maximum Takeoff Mass (MTOM) below 10 tonnes, as illustrated in Fig. 1.1. The latest noise standard, defined in Chapter 14, Annex 16 Vol. 1, will apply to propeller aircraft under 55 tonnes in 2020 [8].

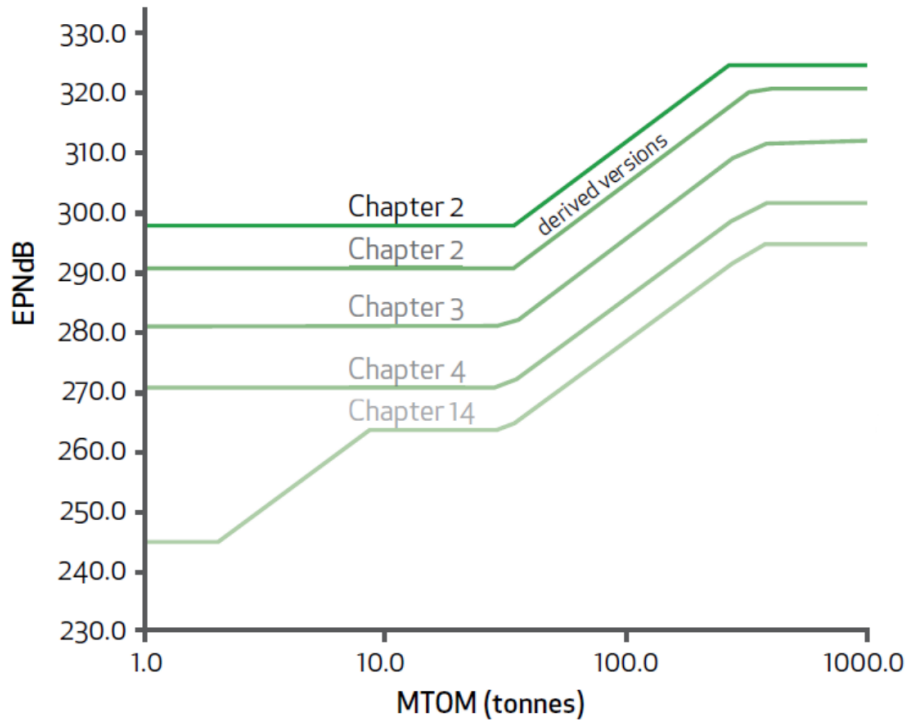


Figure 1.1. ICAO noise standards (from Ref. 9).

As such, propeller-induced noise is becoming a critical design parameter that must be considered during the early stages of the design process. Early acoustic methods have a much lower runtime than formulations which require computational fluid dynamics and are more accurate than the empirical methods typically used by the industry. This makes them well suited for design and optimization. The motivation for this research is two-fold: to evaluate the accuracy of these computationally-inexpensive early acoustic methods for a range of propeller designs and to provide a thorough validation – currently missing in the literature – of the implemented methods.

## 1.2 Literature Review

Propeller noise prediction was first attempted by Lynam and Webb in 1919, for reducing the detectability of military aircraft [10]. The first successful acoustic theory, however, was not formulated until 1936, by Gutin [7]. Gutin's theory was limited to loading noise for propellers with axial flow, simple geometry, low tip speed and no forward speed. Since then, there have been significant advances in acoustic theory due to the work of many researchers who have removed these limitations [11–18]. A thorough review of propeller noise prediction methodology detailing these advances has been published by multiple authors, including Morfey [19], Maglione [20, 21], Farassat [22], and Metzger [23].

Noise predictions methods are typically grouped into two categories: frequency-domain methods and time-domain methods. Time-domain methods, such as the Farassat solution to the FW-H equation, retain the pressure-time history and allow the propeller geometry to be treated with superior precision. However, they require the computation of retarded blade locations and need high quality aerodynamic data to obtain accurate results, particularly if the propeller experiences supersonic flow [21]. Frequency-domain methods eliminate time as a variable by taking the Fourier transform of the wave equation. For this reason, the pressure time history and some information regarding the propeller geometry is lost. Nonetheless, acoustic results are generally not affected up to a fairly high order [21]. Frequency-domain methods are less computationally expensive and have the advantage of being more explicit as to the effects of different parameters on the predicted noise. Modern prediction methods typically require chord-wise pressure or loading data, however, for design or optimization studies, it is often preferable to approximate the chord-wise terms in favor of lower runtimes.

The genealogy of the acoustic methods utilized in this thesis is illustrated in

Fig. 1.2. Acoustic models that originate from Gutin's theory are shown on the left, while those based on Lighthill's acoustic analogy are on the right. The early acoustic methods based on Gutin's method are frequency domain solutions and only consider radial aerodynamic data. The modern models based on Lighthill's acoustic analogy are generally time-domain solutions and all accept surface aerodynamic data. Hanson's acoustic formulations, however, are derived in the frequency domain and include approximations to allow for radial aerodynamic data to be used rather than surface data. With these approximations, Hanson's equations are very similar in form to early acoustic formulations and only minor variable substitutions are needed to obtain the equations by Garrick, Watkins and Arnoldi. The implemented frequency-domain models are highlighted in red, green and blue.

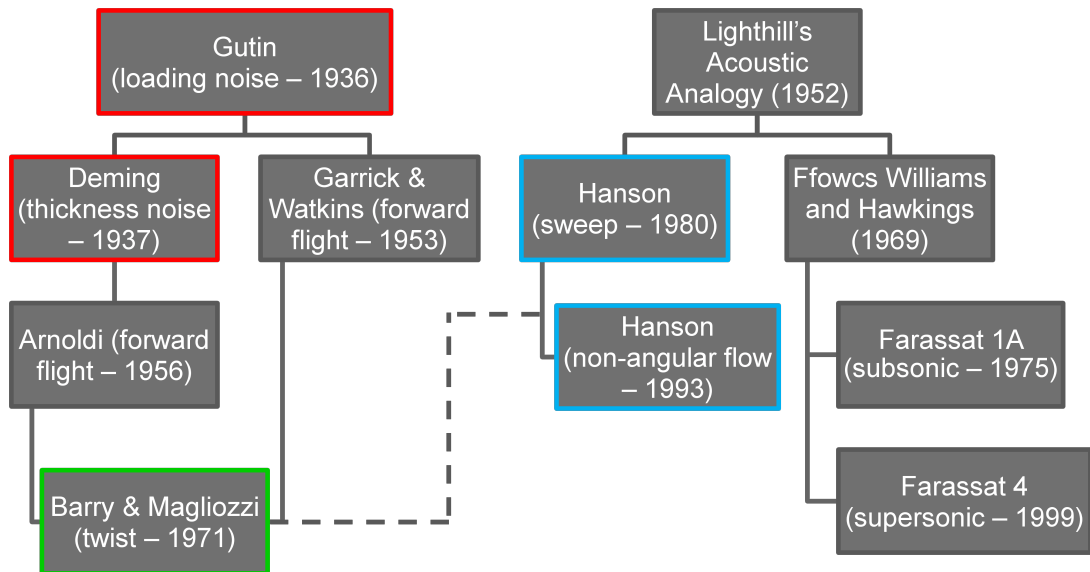


Figure 1.2. Acoustic prediction method genealogy.

In reviewing the literature, a large number of acoustic models were found, yet a significant number lacked sufficient validation with experimental data. This same observation was made by Metzger [23], who also noted that “needs in propeller prediction are not more methods, but a consolidation of the unique features of the many

existing methods”. He called for a comprehensive evaluation of existing methods relative to well documented, high quality data. Due to the significant noise level variation based on microphone location and the measurement fluctuations seen in some acoustics experiments, thorough validation using multiple test cases is essential. One such experiment, performed by Soderman and Horne, saw variations of up to 10 dB for the first harmonic in identical runs [24]. Although the implemented methods have been compared with experimental data [7, 14, 15, 25–31], a comprehensive validation study using multiple experiments with a range of propeller geometries and operational conditions, is lacking. A head-to-head comparison of a number of acoustic models over a range of test cases is also missing from the literature. The objective of this research is to fill the described gap in the literature for frequency-domain, computationally-inexpensive acoustic methods.

### 1.3 Methodology

The methodology followed to accomplish this research objective is summarized in Fig. 1.3. First, the aerodynamic and acoustic models were implemented. An aerodynamic module is necessary to obtain the discretized thrust and torque distributions used by the acoustic equations. Blade Element Momentum Theory (BEMT) was chosen due to its minimal computation time and its popularity with propeller performance prediction in the industry. Three acoustic models were implemented: Gutin & Deming [7, 11], Barry & Maglizzzi [14], and Hanson [15]. The first represents the earliest successful acoustic theory and was included to provide a baseline result. The second represents the most advanced acoustic model derived strictly from early acoustic theory, as shown in Fig. 1.2. The model by Hanson is the most modern frequency-domain method and originates from Lighthill’s acoustic analogy, however, it provides similar computational speed if chord-wise approximations are made.

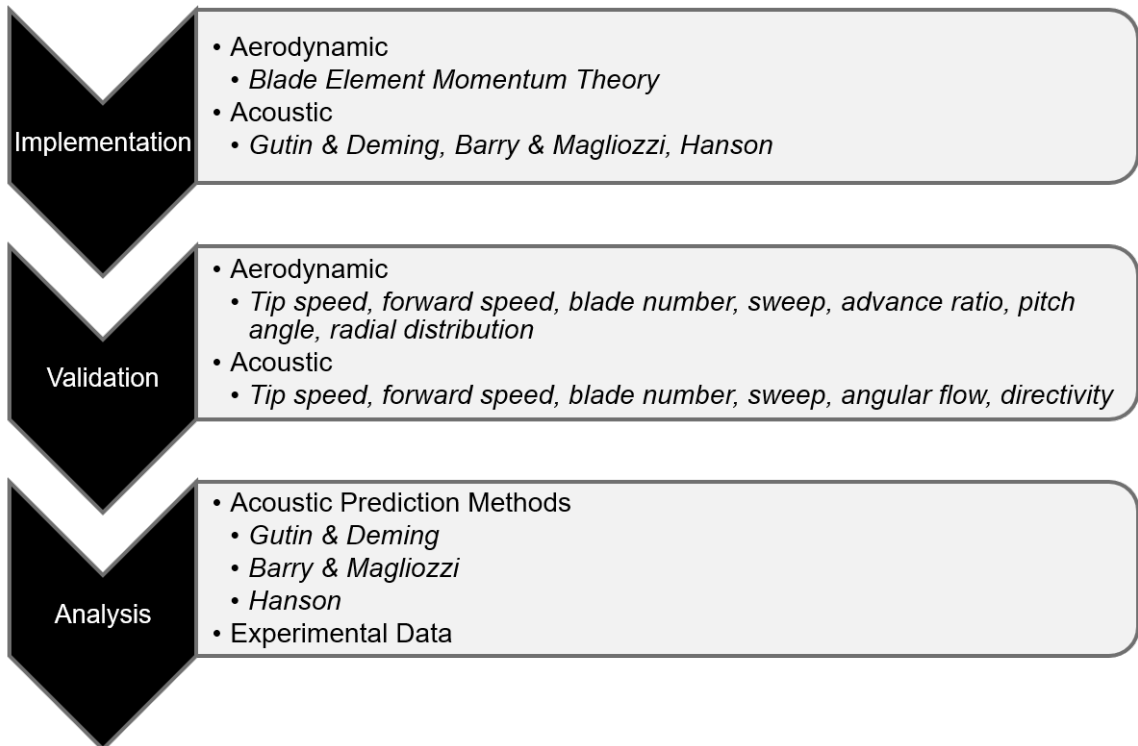


Figure 1.3. Thesis methodology.

Next, both the aerodynamic and acoustic models were validated to ensure proper implementation and evaluate the expected range of error from each model. A variety of parameters were considered during validation to understand their impact on accuracy. Lastly, results from each frequency method were compared to a large number of experiments to evaluate their behavior across a range of propeller geometries and operational conditions.

## 1.4 Programming Framework

Python 3 was chosen as the programming platform due to its flexibility, ease of use and reasonable computational speed for matrix manipulation and mathematical operations. Microsoft Visual Studio Community was used in tandem with Python Tools for Visual Studio as the development environment due to its strong debugging capabilities. The computational performance of the acoustic prediction methods is

detailed in Table 1.1. The speed of the implemented frequency methods is several orders of magnitude faster than acoustic methods coupled to a panel-based or grid-based aerodynamic solver, where typical runtimes span hours to weeks depending on the mesh density and size [32].

Table 1.1. Computational performance of acoustic prediction methods.

<b>Simulation Type</b>	<b>Platform</b>	<b>Processors</b>	<b>Average Performance</b>
Gutin & Deming	Windows		
Barry & Magliozzi	Workstation	6	0.01 seconds / iteration*
Hanson			

\* performance varies slightly with convergence of BEMT module

It should be noted that the computational time stated for the frequency-domain methods is for the prediction of a single harmonic. Time-domain methods, on the other hand, predict all harmonics within a single iteration. The computational performance of the frequency-domain models is fourfold (0.0025 seconds per iteration) if aerodynamic computation is not necessary. This would be the case if multiple harmonics or microphone positions were evaluated with a constant aerodynamic input.

## Chapter 2

# Aerodynamic Prediction Methods

Blade Element Momentum Theory (BEMT) was used to obtain a discretized thrust and torque distribution for each of the implemented frequency-domain acoustic models. Since BEMT is a standard method for propeller design, only a brief description of the theory is provided here.

BEMT is a hybrid method that combines principles from both blade element theory and momentum theory. Blade Element Theory (BET) discretizes the propeller such that each finite element can be considered as a two-dimensional airfoil for which aerodynamic forces and moments can be determined. Momentum theory, on the other hand, applies conservation of mass, momentum and energy to a control volume surrounding the propeller and serves to provide BET with an approximation of the inflow velocity. By dividing the propeller into discrete elements radial variation in twist, chord length and airfoil shape is permitted.

Two variations of BEMT were used; the first is a direct implementation of Ref. 33 and is suited for propellers in its original form. The second, implemented from Refs. 34 and 35, was originally intended for helicopter rotor design and modifications were made to allow for swirl and large induced flow angles. Although both BEMT variations produce similar results, the former was found to be more reliable at high forward flight speeds, while the latter performed better at zero and very low

flight speeds. Both models used lookup tables for lift and drag obtained from the literature or using CFD. The Prandtl-Glauert compressibility correction is utilized, but is capped at Mach 0.7 to avoid divergence. Flow interference factors were limited to 0.7 as suggested by Viterna and Janetzke [36]. Both models had the option of solving for a particular blade pitch angle, or converging to a known thrust or torque value. The latter was utilized to limit the introduction of aerodynamic error into the acoustic solution, however, its implementation generally had a minimal impact.

Both variations of the implemented BEMT models are based on matching the momentum and loading equations for thrust and torque, given in Eqs. (2.1) to (2.4), and iterating until convergence of the flow angle,  $\varphi$ , is achieved. The method of successive substitution with an under-relaxation scheme was used to reach convergence. It should be noted that all symbols are defined in the nomenclature with only a select few explained in the main text.

$$\frac{dT}{dR} = 2\pi R \rho V (1 + a) (2V a F) \quad (2.1)$$

$$\frac{dQ}{dR} = 2\pi R^2 \rho V (1 + a) (2\Omega R a' F) \quad (2.2)$$

$$\frac{dT}{dR} = \frac{1}{2} \rho W^2 B b (C_l \cos \varphi - C_d \sin \varphi) \quad (2.3)$$

$$\frac{dQ}{dR} = \frac{1}{2} \rho W^2 B b (C_l \sin \varphi + C_d \cos \varphi) R \quad (2.4)$$

where  $\varphi$  is the flow angle, defined by the flow geometry illustrated in Fig. 2.1.

$$\varphi = \arctan \left( \frac{V(1 + a)}{\Omega R(1 - a')} \right) \quad (2.5)$$

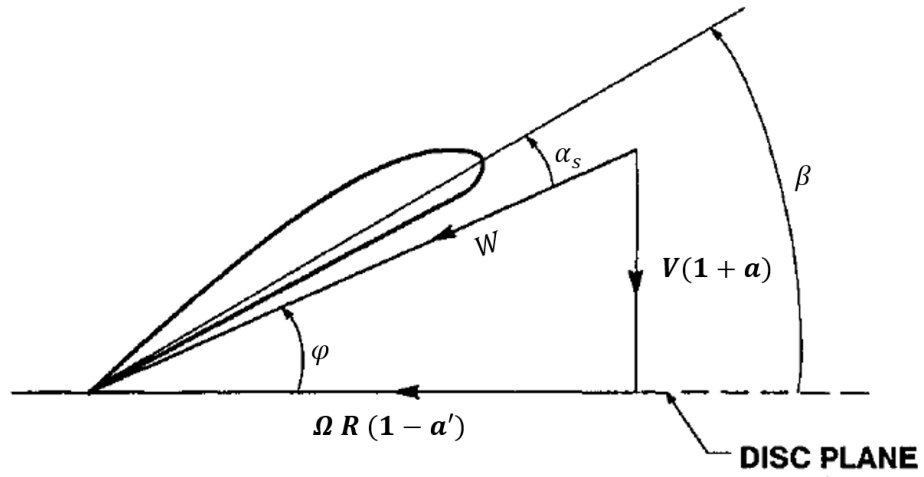


Figure 2.1. Flow geometry of blade element (adapted from Ref. 33).

The equations above were iterated until the difference in the flow angle between successive iterations dropped below 0.1%. One hundred blade elements were used to ensure element independence.

## Chapter 3

# Aerodynamic Results

Correct implementation of each BEMT model was ensured through comparison with test cases supplied with the derivation in Refs. 33 and 34. Focus was therefore placed on determining the error range of the aerodynamic predictions over a variety of input parameters such as tip speed, forward speed, blade number, sweep, advance ratio and pitch angle. Accurate prediction of the radial thrust and torque distributions were of primary interest since these distributions are used directly by the acoustic equations. The capability of the BEMT models in predicting the total thrust and torque values was also tested, however, such predictions are of secondary interest since total thrust or torque values are typically known.

### 3.1 Selection of Aerodynamic Validation Cases

The test cases selected for aerodynamic validation are given in Table 3.1. Test cases were selected on the following basis:

- 1) Blade geometry and operating conditions were clearly defined.
- 2) Both thrust and torque data were provided, with preference given to radially-discretized data.

- 3) Multiple advance ratios and pitch angles were used.

Fulfillment of the first criterion was required to utilize BEMT, the second allowed for the evaluation of BEMT's capability to predict both the overall propeller performance and the discretized thrust and torque distributions, while the third ensured that the full operating range of the propellers were considered.

Table 3.1. Experimental test cases selected for aerodynamic validation.

Test Case	Author	Propeller	No. of Blades	Tip Mach No.	Advance Ratio
1*	Reid [37]	Model 5	3	0.10	0.2 – 3.6
2*	Stefko, Rose and Podboy [38]	SR-7 <sup>†</sup>	8	0.84	2.0 – 4.0
3	Gray [39]	6267A-18	3	0.25	0.2 – 3.2
4	Theodorsen, Stickle and Brevoort [40]	Navy plan form 5868-9	3	0.85	0.1 – 2.5

\* provides discretized thrust and torque data

<sup>†</sup> swept propeller

Propeller geometry is provided for each test case in the reference listed next to the authors in Table 3.1.

## 3.2 Aerodynamic Results

The majority of aerodynamic data available in the literature only considers overall propeller performance and does not provide measurements for discretized thrust and torque along the propeller blade. Overall results are a good indication of BEMT's general prediction accuracy, however, the discretized thrust and torque distributions are of greater interest as they are direct inputs to the acoustic equations used to predict propeller noise. Results for the prediction of overall propeller performance

are provided over a range of advance ratios and pitch angles for test cases 1 and 2 in Figs. 3.1 and 3.2. Results for test cases 3 and 4 are provided in Appendix A.1. Data is presented in standard nondimensional form, where the coefficients of thrust, torque and propeller efficiency are defined as follows:

$$C_T = \frac{T}{\rho n^2 D^4} \quad (3.1)$$

$$C_Q = \frac{Q}{\rho n^2 D^5} \quad (3.2)$$

$$C_P = \frac{P}{\rho n^3 D^5} = 2\pi C_Q \quad (3.3)$$

$$\eta = \frac{C_T}{C_P} J \quad (3.4)$$

and  $J$  is the advance ratio, defined as:

$$J = \frac{V}{nD} \quad (3.5)$$

The agreement with experiment varies depending on the advance ratio as shown in Figs. 3.1 and 3.2. The dashed line in the aforementioned figures represents the rotor BEMT variant, implemented from Ref. 34, while the solid line represents the propeller variant, based on Ref. 33. Both BEMT implementations show good agreement at midrange forward speeds (Mach 0.1 - Mach 0.5). At low speeds, however, the propeller BEMT variant performs poorly, while at high speeds the reverse occurs. At forward speeds greater than Mach 0.8, the rotor-based code fails to converge as is the case in the rightmost graph in Fig. 3.2. Despite some variation in accuracy, the general trend is well captured.

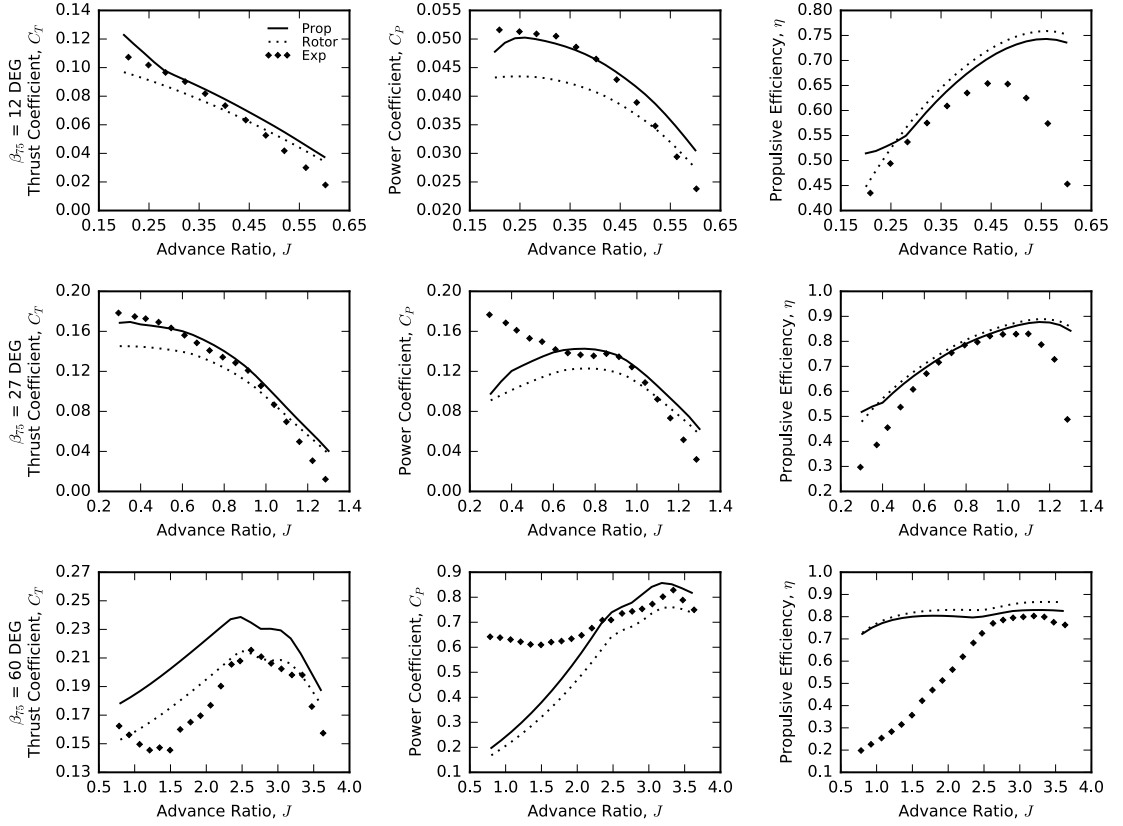


Figure 3.1. Propeller aerodynamic performance - test case 1.

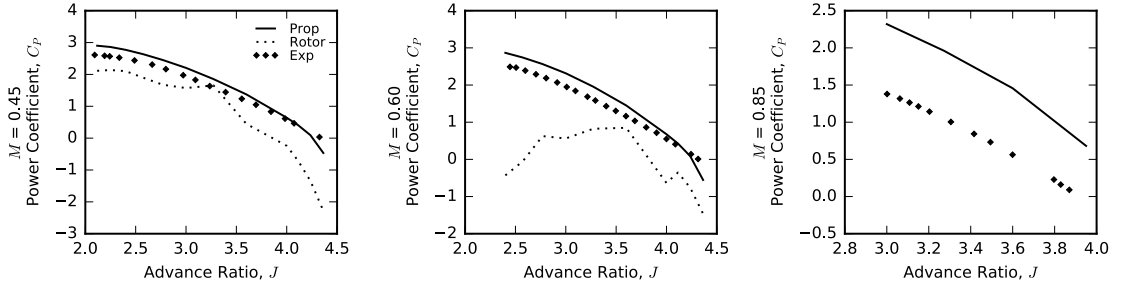


Figure 3.2. Propeller aerodynamic performance - test case 2.

As previously mentioned, since the total thrust or torque is generally known, accurate prediction of these values is not necessary. Prediction of the general shape of the thrust and torque distributions is of higher importance. Results for the thrust and torque distributions for test case 1 are presented in Fig. 3.3. Additional thrust

and torque distributions for test case 1 (at different blade pitch angles and rotational velocities) and for test case 2 are presented in Appendix A.2.

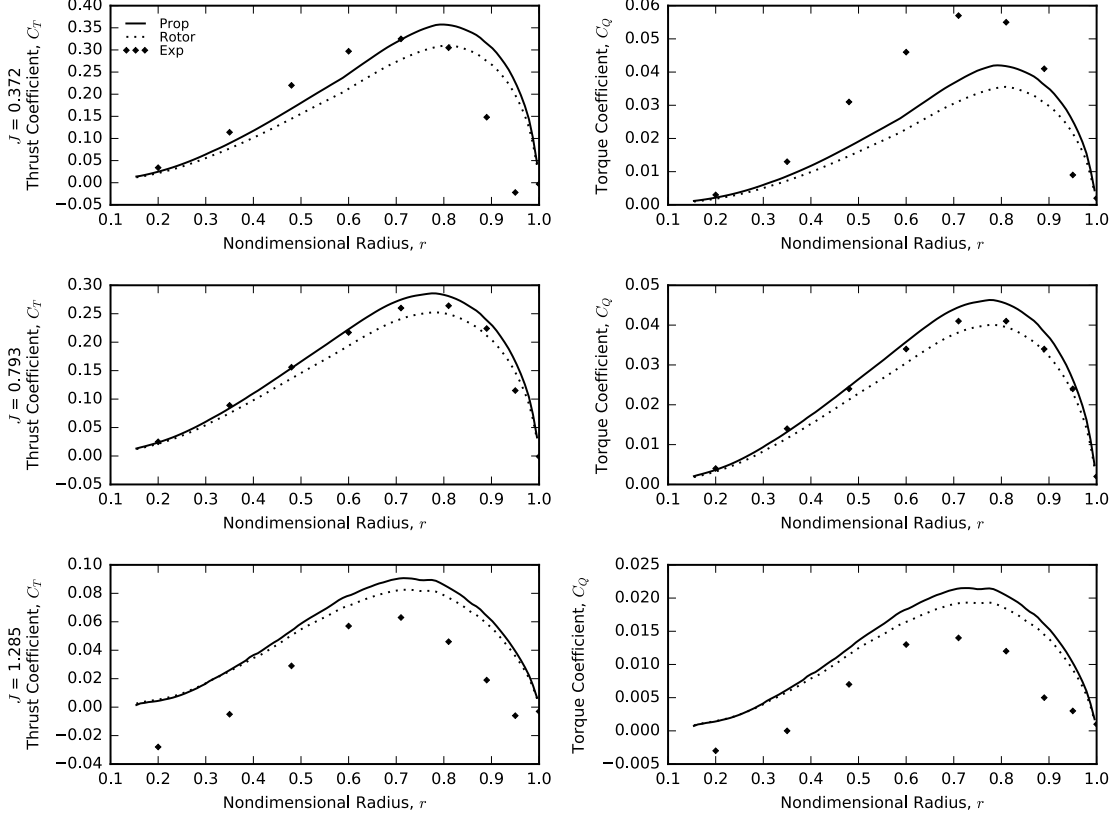


Figure 3.3. Propeller thrust and torque distributions at  $27^\circ$  blade pitch and 1740 RPM - test case 1.

Although the discretized results in Fig. 3.3 and in Appendix A.2 mostly show good agreement, occasionally significant overprediction or underprediction occurs. Nevertheless, because the total thrust or torque values are usually known, the discretized values can be scaled to match the known values and significantly increase agreement with experiment. If solely either the thrust or torque is known, the blade pitch angle is modified to match the known thrust or torque value. If both are known, the pitch angle is modified to match thrust and the torque distribution is subsequently numerically scaled to match the known total torque. The effect of matching thrust and torque, relative to Fig. 3.3, is illustrated in Fig. 3.4. Additional results are presented

in Appendix A.3 and show similar agreement. Minor aerodynamic error (i.e. error in the aerodynamic inputs to the acoustic solution) is still possible if the shapes of the thrust and torque distributions are mischaracterized. An example of this behavior can be observed in Fig. 3.4 for the thrust and torque distributions computed at an advance ratio of 1.285. Such error, however, is infrequent.

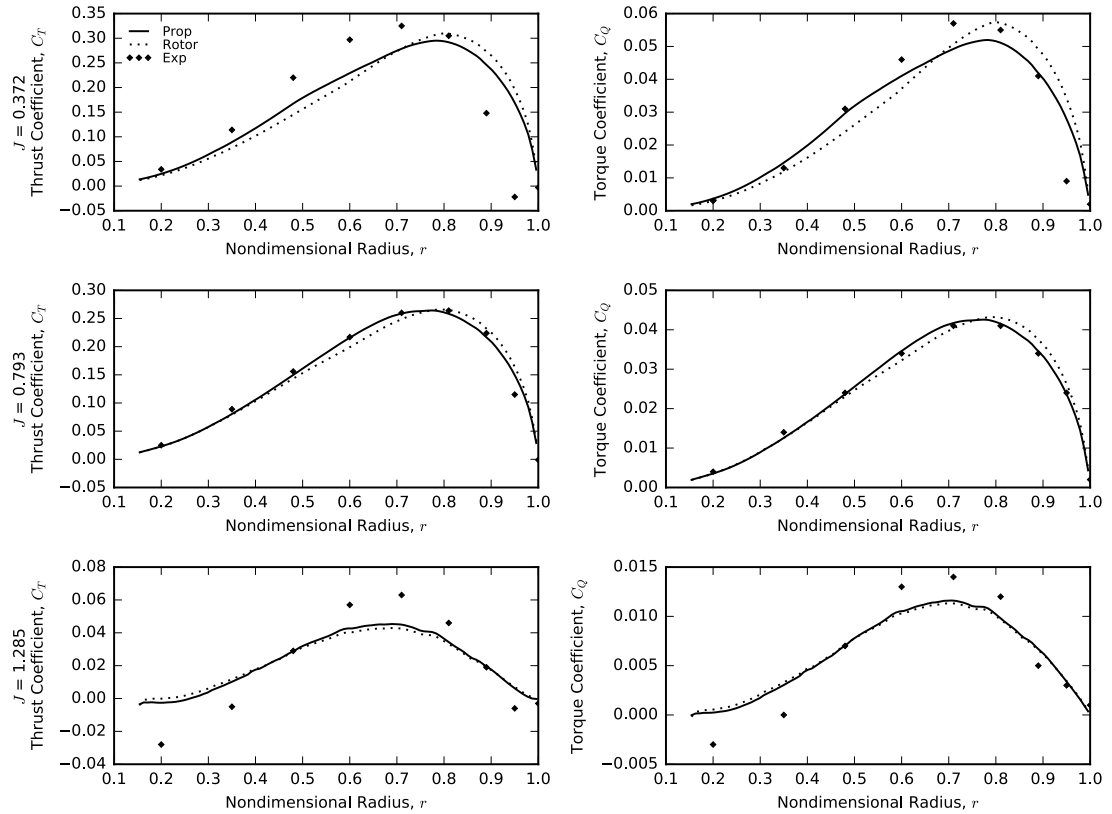


Figure 3.4. Adjusted propeller thrust and torque distributions at  $27^\circ$  blade pitch and 1740 RPM - test case 1.

### 3.3 Aerodynamic Impact on Acoustic Solution

In order to understand the effect of aerodynamic error on the acoustic solution, propeller noise was evaluated at a range of values of thrust and torque while keeping other input parameters constant. To qualify this effect over a variety of propeller

geometries and operational conditions, a number of test cases were selected. The chosen test cases are detailed in Table 3.2. It should be noted that the numbering of the test cases in Table 3.2 refers to the acoustic validation cases presented in Table 5.1, rather than the aerodynamic validation cases detailed in Table 3.1. Results illustrating the relationship between propeller noise (measured in decibels) and the aerodynamic input are shown in Fig. 3.5. The acoustic results in Fig. 3.5 do not represent the complete propeller acoustic signature, but rather the components of noise due to thrust and torque, denoted as  $SPL_{TL}$  and  $SPL_{QL}$ , respectively. Hanson's noise model described in Chapter 4 was used in this analysis but similar results were obtained with the other frequency-domain models. Additional results based on test cases 9, 10 and 11 are included in Appendix A.4.

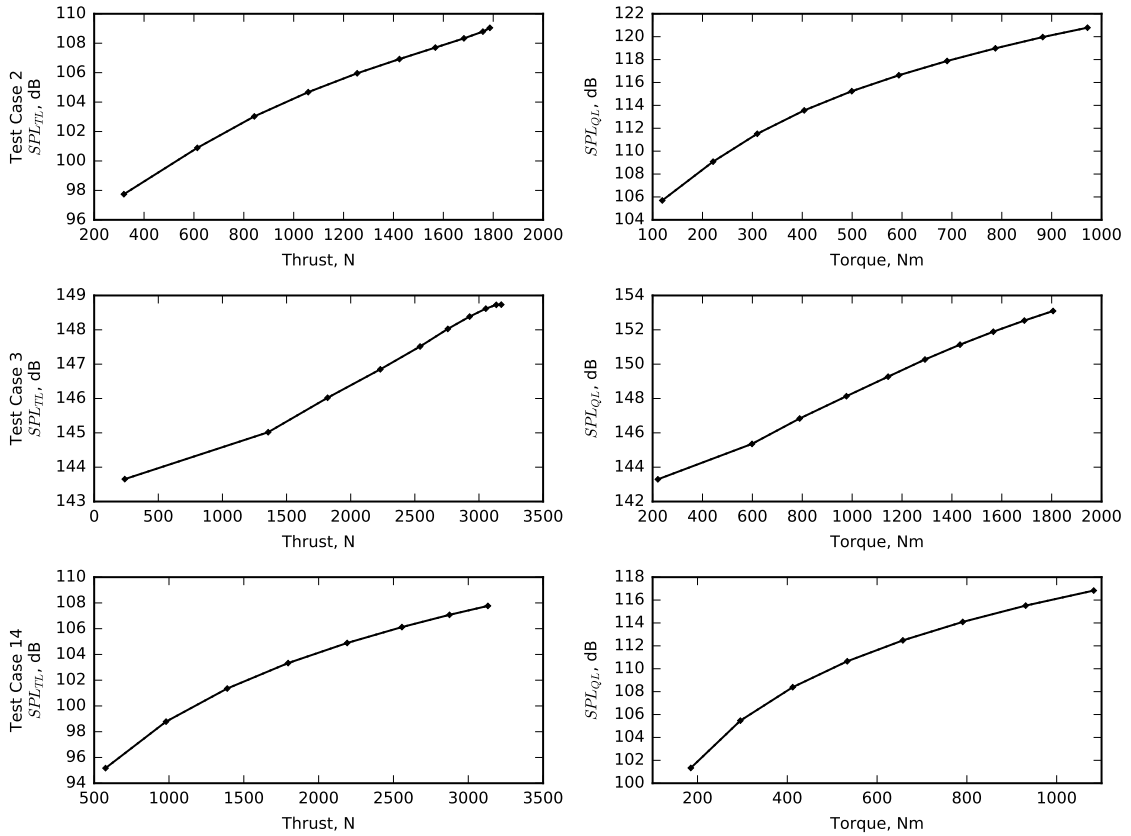


Figure 3.5. Impact of thrust and torque variation on acoustic solution - test cases 2, 3, and 14.

Taking the difference of each axis and non-dimensionalizing the x-axis by thrust or torque, as shown in Fig. 3.6, yields a relatively linear relationship such that the impact of aerodynamic input on propeller noise can be measured by the slope of a fitted trendline (illustrated by the dotted line in Fig. 3.6). The magnitude of the slope for each evaluated test case as well as the coefficient of determination ( $R^2$ ) is presented in Table 3.2.

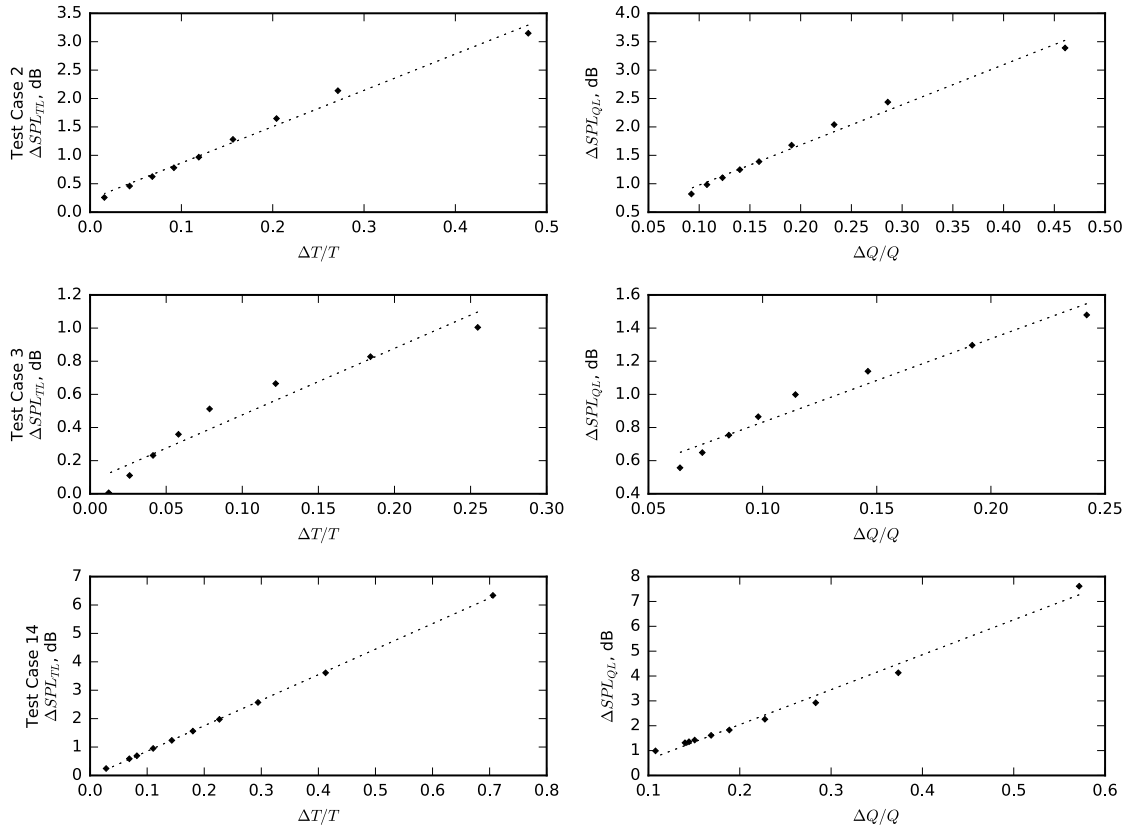


Figure 3.6. Relative impact of thrust and torque variation on acoustic solution - test cases 2, 3, and 14.

The primary observation to be made is the relatively minor impact of aerodynamic input on the acoustic solution, with the full operational range of each propeller (zero to max thrust and torque) only resulting in a 10 dB change. As shown in Fig. 3.6, a significant percentage variation in thrust or torque is required to obtain a 1 dB variation in the acoustic solution. For example, assuming a total thrust of 1000 N

and a slope of 10 dB, a 10% rise in thrust (100 N) is necessary to increase the noise level by 1 dB.

This result is reasonable since other parameters such as propeller rotational frequency and blade number are known to dominate propeller noise. It makes sense, therefore, that the test cases with a lower helical tip speed and lower number of blades (presented in Table 3.2) tend to have slopes with larger magnitudes, indicating a higher aerodynamic dependency. This trend is not followed by test case 10, where the geometry of the propeller significantly lowers the impact of the aerodynamic input.

Table 3.2. Relative impact of aerodynamic error on acoustic solution.

Test Case*	No. of Blades	Helical Tip Mach No.	Thrust Trendline Slope, dB ( $R^2$ )	Torque Trendline Slope, dB ( $R^2$ )
2	8	0.86	6.4, (0.989)	7.1, (0.987)
3	8	1.15	6.0, (0.982)	6.6, (0.980)
9	4	0.91	8.3, (0.990)	8.9, (0.998)
10	8	0.74	2.7, (0.992)	3.9, (0.998)
11	2	0.62	14.9, (0.991)	11.6, (0.993)
14	2	0.86	9.0, (0.999)	14.1, (0.988)

\* test case numbering refers to acoustic test cases detailed in Table 5.1

Given the low impact of aerodynamic error on the acoustic signature of the propeller and the small degree of error expected from the aerodynamic solution, acoustic error introduced in this manner is expected to remain minimal (below 1 dB).

## Chapter 4

# Acoustic Prediction Methods

Acoustic models were selected based on their computational cost, with the desired runtime on a standard desktop computer of less than one second. This criterion severely restricted the complexity of aerodynamic solvers and ruled-out the implementation of models based on the FW-H equation. Frequency-domain methods were selected due to their low computational cost, lower sensitivity to input error, and ease of use. Thus, the acoustic models investigated originate primarily from the work of Gutin, Deming and Hanson due to their minimal need for aerodynamic data. To allow for variable blade geometry without significantly increasing computation time, Blade Element Momentum Theory (BEMT) was implemented to obtain discretized values for thrust and torque along the propeller blade. An additional benefit of the chosen acoustic models is their white-box nature, where the influence of parameters is clear and the user does not need to be concerned with tuning or convergence criteria, therefore eliminating a possible source of error. Three separate frequency methods were implemented and used to produce the results presented in this thesis.

## 4.1 Phase Adjustment

To avoid complete noise cancellation between the thrust, torque, and thickness terms due to their phase difference, the noise was evaluated over a range of  $\pm 5$  degrees relative to the original microphone location rather than at only one microphone location. The microphone position with the least destructive interference was then selected. This generally had a negligible impact on the acoustic signature of the propeller unless the loading or thickness noise terms were close in magnitude. This phenomenon is shown in Fig. 4.1, where a significant difference in the adjusted total noise (shown in black with filled round markers) relative to the total noise evaluated at a single microphone location (shown in black with hollow diamond markers) can be seen when the thrust and thickness noise are very close in magnitude. Near the propeller plane, however, the noise components are dissimilar in magnitude and the difference between the adjusted and non-adjusted total noise terms is negligible. Acoustic results obtained for test cases 1 – 14, using a single microphone location per data point (non-adjusted), show close agreement with the adjusted results and are included in Appendix D.

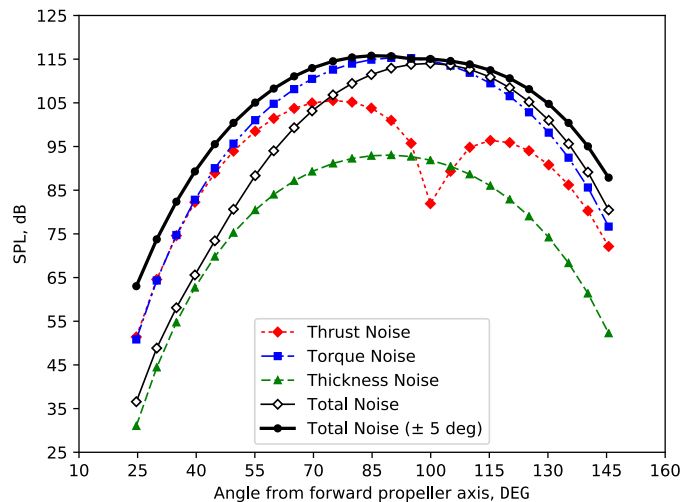


Figure 4.1. Sensitivity of results to destructive interference and microphone location.

## 4.2 Acoustic Theory

The acoustic equations presented in this section give the root-mean-square pressure of the one-sided noise spectrum and are only valid for far-field noise. Near-field versions of these equations exist but were not implemented as they are outside the scope of this thesis. The Sound Pressure Level (SPL) at a given harmonic was obtained using Eq. (4.1).

$$SPL_m = 20 \log \left( \frac{|P_{mL} + P_{mT}|}{P_0} \right) \quad (4.1)$$

Since the implemented noise models are readily available in the literature, only the main loading and thickness noise equations are presented here with comments regarding any modifications made in their implementation. The main equations are, however, described with enough detail for programming to increase the repeatability of the presented results.

Broadband noise models were initially implemented from the literature [14], however, due to their negligible impact on the first few noise harmonic levels and their empirical nature [21, 23, 41], they were later excluded from the results.

### 4.2.1 Coordinate System and Reference Frame

It is important to note that  $x$ ,  $y$ ,  $z$ ,  $\theta$ ,  $\phi$ , and  $S$  represent the physical distances and angles between the microphone or observer location and the propeller hub in a wind-tunnel configuration. In other words, the listed variables are independent of forward Mach speed. This is equivalent to a moving-medium visual reference system. The equations by Gutin & Deming and by Barry & Magliozzi were derived in a visual reference system, allowing direct implementation of the listed variables. Hanson's model, however, was derived in a retarded reference frame, meaning that a

coordinate transformation is necessary before the method can be used. The coordinate transformations from a visual to a retarded reference frame required to implement Hanson's model are included below for clarity and are explained in detail in Refs. 30,42 and 31. The orientation of  $x$ ,  $y$ , and  $z$  is illustrated in Fig. 4.2, where  $x$  is positive in front of the propeller plane. The observer angle  $\theta$  is defined in the  $x - y$  plane, starting from the  $x$ -axis, such that the propeller plane is positioned at  $\theta = 90^\circ$ .

$$\cos \theta_r = \cos \theta \sqrt{1 - M^2 \sin^2 \theta} + M \sin^2 \theta \quad (4.2)$$

$$S_r = \frac{Y}{\sin \theta_r} \quad (4.3)$$

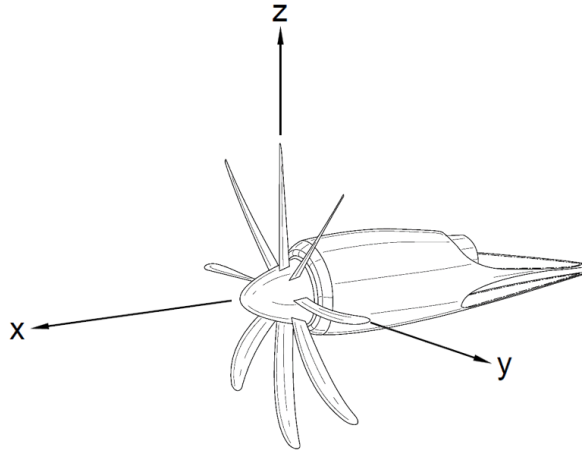


Figure 4.2. Coordinate axis orientation (adapted from Ref. 43).

#### 4.2.2 Gutin and Deming

The first successful analytical acoustic theory was developed by Gutin, who modeled the steady aerodynamic forces acting on a propeller (torque and thrust) as a ring of dipole sources distributed over the propeller disc [7]. Following a similar procedure, Deming was the first to model the noise caused by finite blade thickness using the superposition of a continuous ring of sources and sinks in the propeller plane [11,26].

While not relevant for noise prediction in their original form for the majority of the selected validation cases, they were implemented to provide a baseline for the other acoustic models.

The aforementioned formulations for loading and thickness noise are presented in Eq. (4.4) and Eq. (4.5). Discretized values for thrust and torque were used, rather than the effective-radius approximation used by Gutin and Deming, to maintain a consistent aerodynamic input across all prediction methods.

$$P_{m_L} = \frac{mB\Omega}{2\sqrt{2}\pi cS} \int_{hub}^{tip} \left[ \frac{dT}{dR} \cos \theta - \frac{dQ}{dR} \frac{c}{\Omega R^2} \right] J_{mB} dR \quad (4.4)$$

$$P_{m_T} = \frac{-\rho(mB\Omega)^2 B}{3\sqrt{2}\pi S} \int_{hub}^{tip} bh J_{mB} dR \quad (4.5)$$

$$J_{mB} = J_{mB} \left( \frac{mB\Omega}{c} R \sin \theta \right) \quad (4.6)$$

The directivity of the loading and thickness noise is dictated by the terms  $\cos \theta$  and  $\sin \theta$ , while the pressure amplitude is dictated by the tip speed of the propeller, denoted by  $\Omega R$ . Although the other terms such as the blade number, loading distribution and blade thickness contribute to the noise signature of the propeller, their effect is generally overshadowed by the tip speed of the propeller.

Note that Eqs. (4.4) and (4.5) are limited to far-field predictions for propellers with no forward speed. This was rectified by the work of Garrick and Watkins [12] for loading noise and Arnoldi [13] for thickness noise.

#### 4.2.3 Barry and Magliozzi

The equations of Garrick, Watkins, and Arnoldi for loading and thickness noise were further refined by Barry and Magliozzi to include the effect of blade twist to give Eqs. (4.7) and (4.8) [14]. The alternate Bessel functions ( $J_{mB+1}$  and  $J_{mB-1}$ ) appear because a more exact far field approximation was used by Barry and Magliozzi than

is typically seen in the literature. Some phase terms have also been omitted because they do not alter the relative phase between loading and thickness noise. The absolute phase is not important for this application.

It should be noted that there are two differences between the equations presented below and the equations presented in Ref. 14. The first is a correction to the Bessel function term in Eqs. (4.7) and (4.8), as noted in Ref. 27. The second correction replaces  $(1 - M^2)^4$  with  $(1 - M^2)$  in the loading formulation and makes Eq. (4.7) consistent with other forward flight formulations in the literature. The second correction avoids a large overprediction of noise at higher forward Mach numbers.

$$P_{m_L} = \frac{1}{\sqrt{2}\pi S_0} \int_{hub}^{tip} \frac{R}{b \cos \phi_t} \sin \left( \frac{mBb \cos \phi_t}{2R} \right) \left[ \frac{(M + X/S_0)\Omega}{c(1 - M^2)} \frac{dT}{dR} - \frac{1}{R^2} \frac{dQ}{dR} \right] \\ \left[ J_{mB} + \frac{(1 - M^2)YR}{2S_0^2} (J_{mB-1} - J_{mB+1}) \right] dR \quad (4.7)$$

$$P_{m_T} = -\frac{\rho m^2 \Omega^2 B^3}{2\sqrt{2}\pi(1 - M^2)^2} \frac{(S_0 + MX)^2}{S_0^3} \int_{hub}^{tip} A_x \\ \left[ J_{mB} + \frac{(1 - M^2)YR}{2S_0^2} (J_{mB-1} - J_{mB+1}) \right] dR \quad (4.8)$$

$$J_{mB} = J_{mB} \left( \frac{mB\Omega YR}{cS_0} \right) \quad (4.9)$$

In Eqs. (4.7) to (4.9), the directivity of the noise is dictated by the terms  $X/S_0$  and  $Y/S_0$ , while forward flight is taken into account by the amplitude radius,  $S_0$ , and the Mach number,  $M$ .

The equations derived by Garrick, Watkins, and Arnoldi can be retrieved by setting  $\phi_t$  to zero, removing the alternate Bessel function terms (ie. seting  $J_{mB+1}$  and  $J_{mB-1}$  to zero) and replacing the sinusoid term in the loading equation by its argument.

#### 4.2.4 Hanson

Hanson's formulation for loading and thickness noise extends the work of Garrick, Watkins, and Arnoldi to include the effects of non-compactness, sweep and non-axial flow [15, 16, 21, 31]. The equations for loading and thickness noise are presented below. The reader is reminded that this formulation uses retarded coordinates. Any variables referring to the retarded reference frame are denoted by the subscript  $r$ .

$$P_{m_L} = \frac{imBM_t \sin \theta_r \exp [imB(\frac{\Omega S_r}{c} + (\phi' - \frac{\pi}{2}))]}{2\sqrt{2}\pi Y r_t (1 - M \cos \theta_r)} \int_{hub}^{tip} \left[ \frac{\cos \theta'_r}{1 - M \cos \theta_r} \frac{dT}{dr} - \frac{1}{r^2 M_t r_t} \frac{dQ}{dr} \right] \exp(i\phi_s) J_{mB} \Psi_L dr \quad (4.10)$$

$$P_{m_T} = \frac{-\rho c^2 B \sin \theta_r \exp [imB(\frac{\Omega S_r}{c} + (\phi' - \frac{\pi}{2}))]}{4\sqrt{2}\pi (Y/D)(1 - M \cos \theta_r)} \int_{hub}^{tip} M_s^2(h/b) \exp(i\phi_s) J_{mB} k_x^2 \Psi_V dr \quad (4.11)$$

$$J_{mB} = J_{mB} \left( \frac{mBrM_t \sin \theta'_r}{1 - M \cos \theta_r} \right) \quad (4.12)$$

where  $\theta'_r$  and  $\phi'$  relate to the angular flow angle,  $\alpha$ , and are defined by:

$$\cos \theta'_r = \cos \theta_r \cos \alpha + \sin \theta_r \sin \phi \sin \alpha \quad (4.13)$$

$$\cos \phi' = \frac{\sin \theta_r}{\sin \theta'_r} \cos \phi \quad (4.14)$$

and  $k_x$  is a wave number given by:

$$k_x = \frac{2mBbM_t}{M_s(1 - M \cos \theta_r)} \quad (4.15)$$

and  $\phi_s$  represents phase lag due to sweep:

$$\phi_s = \frac{2mBM_t}{M_s(1 - M \cos \theta_r)} \frac{MCA}{D} \quad (4.16)$$

$\Psi_V$  and  $\Psi_L$  are non-dimensional source transforms that represent the effect of chordwise non-compactness. A parabolic thickness distribution and uniform lift distribution, defined by Eq. (4.17) and Eq. (4.18), were used as per Hanson's suggestion in Ref. 21. However, more exact forms can be employed if necessary.

$$\Psi_V(k_x) = \begin{cases} 2/3 & \text{if } k_x = 0, \\ \frac{8}{k_x^2} \left[ \frac{2}{k_x} \sin\left(\frac{k_x}{2}\right) - \cos\left(\frac{k_x}{2}\right) \right] & \text{if } k_x \neq 0. \end{cases} \quad (4.17)$$

$$\Psi_L(k_x) = \begin{cases} 1 & \text{if } k_x = 0, \\ \frac{2}{k_x} \sin\left(\frac{k_x}{2}\right) & \text{if } k_x \neq 0. \end{cases} \quad (4.18)$$

As noted by Hanson in Ref. 15, the above equations can be related back to earlier formulations by setting  $\alpha$  to zero and with only minor modifications to the  $k_x$  argument of the source functions  $\Psi_V$  and  $\Psi_L$ . Arnoldi's thickness theory can be obtained by setting the  $k_x$  argument of  $\Psi_V$  to zero, while Garrick and Watkin's loading equations can be recovered by setting the argument of  $\Psi_L$  to  $mBb/R$ .

## **Chapter 5**

# **Acoustic Results**

Due to the minimal impact of aerodynamic error on the acoustic solution and all other input parameters, such as propeller radius and rotational velocity having no error associated to them, any error in the acoustic prediction can safely be assumed to be a result of either experimental error or a shortcoming of the prediction method. A large number of experiments were replicated in order to mitigate the inconsistencies seen in some acoustic experiments [24], limit the effect of experimental error, caused, for example, by wind-tunnel effects [44], and properly characterize the flexibility and general prediction ability of the acoustic models.

### **5.1 Selection of Acoustic Validation Cases**

Acoustic validation cases were selected such that they represented a wide range of propeller geometries and operating conditions. The following criteria were used in their selection:

- 1) Blade geometry and operating conditions were clearly defined.
- 2) Aerodynamic data, such as total thrust, was provided.
- 3) Multiple far-field microphone locations were used.

Fulfillment of the first criterion was required to implement the prediction models, the second ensured accuracy of the aerodynamic solvers and limited the introduction of aerodynamic error, while the third allowed for the evaluation of the capability of the acoustic models to predict directivity.

A total of fourteen validation cases, summarized in Table 5.1, were selected for this thesis, with nine from separate experiments. The propeller operational conditions and microphone locations of each test case are available in the references listed next to the authors in the table below. The propeller geometries are available from the same references with the exception of the SR-2, SR-3 and SR-7 propellers which were obtained from Refs. 24, 45 and 38, respectively. Images of each of the propellers, illustrating their general shape, are included in Appendix C. If additional aerodynamic data was used, separate from the reference listed next to the author, it is listed next to the propeller name.

## 5.2 Acoustic Results

Results for each of the validation cases are presented in Figs. 5.1 to 5.10. Tone levels (SPL) are presented as a function of the angular position,  $\theta$ , of the observer. Predictions are provided for the first and second harmonic for test cases 1, 2, 3, and 11, while results are provided for solely the first harmonic for test cases 4–10, 12, and 13. A full spectrum of twenty harmonics is provided for test case 14 due to the fact that experimental data for only two microphones was available. No adjustments were made to any of the predicted results, with the exception of test cases 8 and 9 where corrected microphone locations were used as directed by the authors of the experiment.

It should also be noted that the results below have not been normalized to a

Table 5.1. Experimental test cases selected for acoustic validation.

Test Case	Author	Propeller	No. of Blades	Free Stream Mach No.	Helical Tip Mach No.
1	Soderman and Horne [24]	SR-2	4	0.2	0.77
2	Dittmar [46]	SR-2	8	0.6	0.86
3	Dittmar [46]	SR-2	8	0.8	1.15
4	Dittmar and Jeracki [6]	SR-3	8	0.5	0.72
5	Dittmar and Jeracki [6]	SR-3	8	0.8	1.14
6	Dittmar and Stang [47]	SR-7 [48]	8	0.6	0.86
7	Dittmar and Stang [47]	SR-7 [48]	8	0.8	1.15
8	Brooks and Metzger [44]	SR-3	2	0.2	0.78
9	Brooks and Metzger [44]	SR-3	4	0.32	0.91
10 <sup>†</sup>	Woodward [5]	SR-7 [49]	8	0.2	0.74
11	Hubbard [50]	*	2	0.0	0.62
12	Brown and Ollerhead [28]	Sensenich W60LK18	2	0.0	0.40
13	Brown and Ollerhead [28]	W6 STD 8°	6	0.0	0.40
14	Dobrzynski et al. [51]	F8475D-4	2	0.2	0.86

\* propeller geometry included in Ref. 50

<sup>†</sup> provides acoustic data for non-axial flow

constant sideline distance and represent a direct implementation of the experimental data from the literature. As such, Figs. 5.1 to 5.10 are not consistent in their representation of the distance between the observer and the microphone. The chosen format does, however, provide a compact means of comparing unaltered experimental data to predictions from each acoustic model. The exact placement of transducers relative to the propeller is included in Appendix E for every validation case.

Experimental data is not presented at some microphone locations due to experimental data not being available at those stations. This is occasionally due to transducer malfunction, but is more generally a result of the wind-tunnel background noise exceeding the propeller harmonic at that location.

### 5.2.1 Test Case 1: Soderman and Horne

Acoustic results for test case 1, performed with a four-bladed NASA SR-2 propeller at a freestream Mach number of 0.2 and helical tip Mach number of 0.76, are shown in Fig. 5.1.

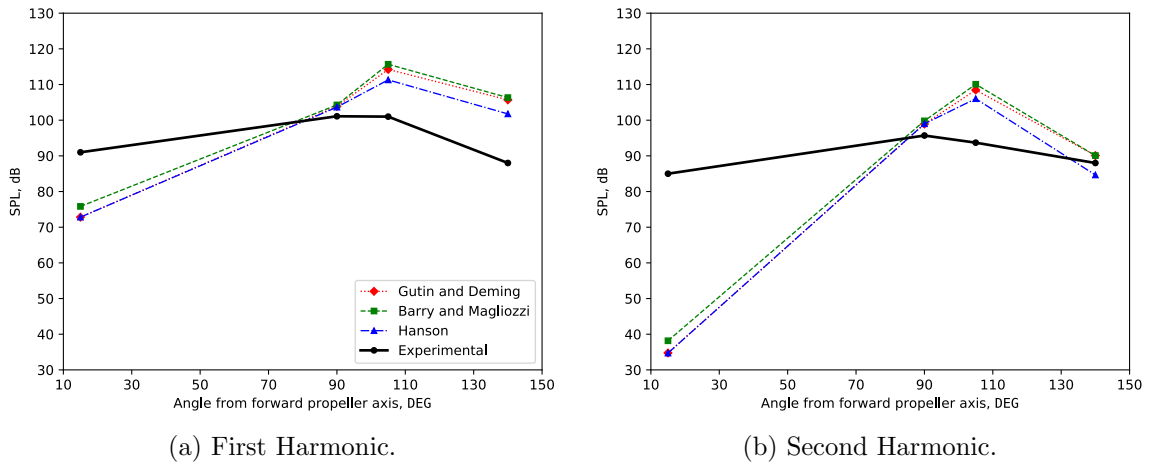


Figure 5.1. Tone directivities - test case 1.

It is important to note that the microphones, whose locations are detailed in Appendix E, are not at the same distance from the propeller hub. Transducer 7 and

8 are 1.4 meters from the hub, while transducers 9 and 12 are 2.4 and 4.3 meters from the hub, respectively. It is therefore unexpected that the experimentally measured noise at transducers 7 and 12 (positioned 105° and 90° downstream of the propeller axis) are almost identical. Reasons for this behavior are discussed by Soderman and Horne in Ref. 24.

Poor prediction accuracy near the propeller axis is expected from the frequency methods since they do not consider broadband noise and theoretically predict zero noise at the axis. This is caused by the sinusoidal or  $Y$  term in the Bessel functions (Eqs. (4.6), (4.9) and (4.12)) which reduce the noise to zero at propeller axis.

### 5.2.2 Test Case 2: Dittmar ( $M = 0.6$ )

Acoustic results for test case 2 are presented in Fig. 5.2. The second validation case uses similar propeller geometry as test case 1, but has eight blades and was performed at a forward Mach speed of 0.6 which is representative of cruise conditions. Poor agreement is obtained with Gutin and Deming's model, however, this is expected since the model does not take forward flight into account.

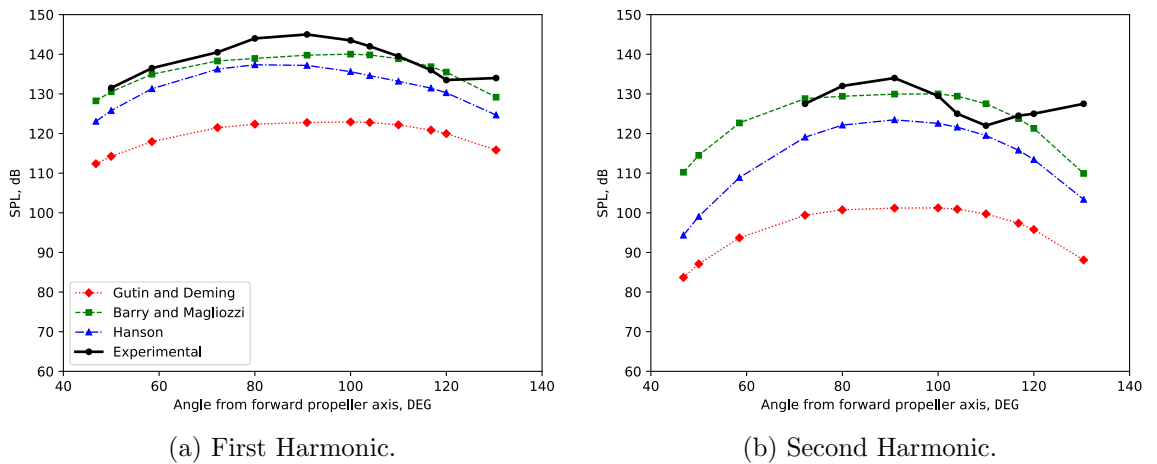


Figure 5.2. Tone directivities - test case 2.

### 5.2.3 Test Case 3: Dittmar ( $M = 0.8$ )

Acoustic results for test case 3 are shown in Fig. 5.3. The propeller geometry is identical to test case 2 and differs only in the freestream Mach number and rotational speed. Poor agreement is found with Barry and Magliozi's method at high forward Mach speeds due to the improper characterization of the chord-wise compactness term as noted by Hanson in Ref. 15.

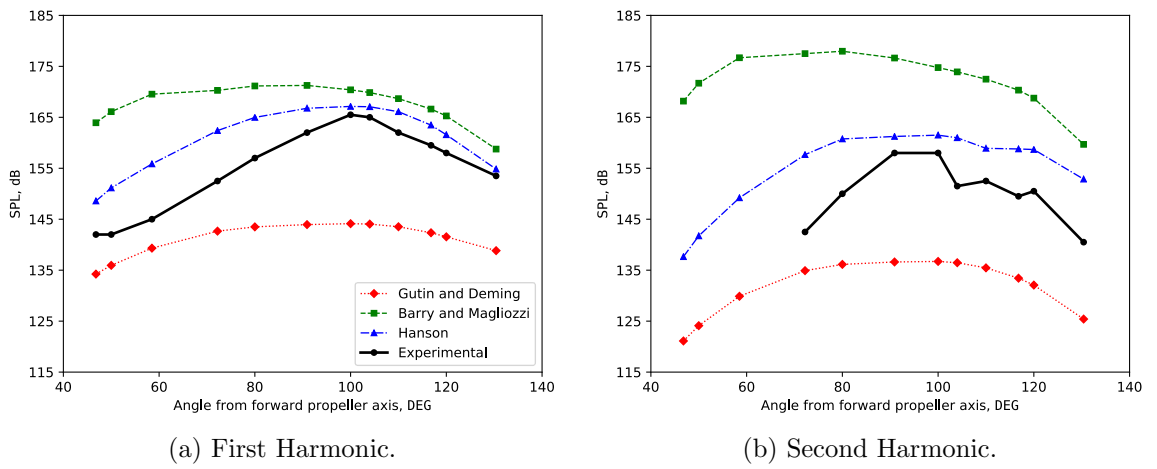


Figure 5.3. Tone directivities - test case 3.

### 5.2.4 Test Cases 4 and 5: Dittmar and Jeracki

Blade passing tone levels for test cases 4 and 5 are presented in Figs. 5.4a and 5.4b, respectively. Both utilize an eight-bladed SR-3 propeller and differ only in the freestream Mach number and rotational speed. The better accuracy of Gutin and Deming's model at forward Mach speeds of 0.8 relative to forward Mach speeds of 0.6 is due to a cancellation of two errors: lack of consideration of forward speed reduces the noise prediction while incorrect characterization of the chord-wise compactness term increases the noise prediction. Since Barry and Magliozi's model considers forward flight, significant overprediction is obtained at high forward speeds.

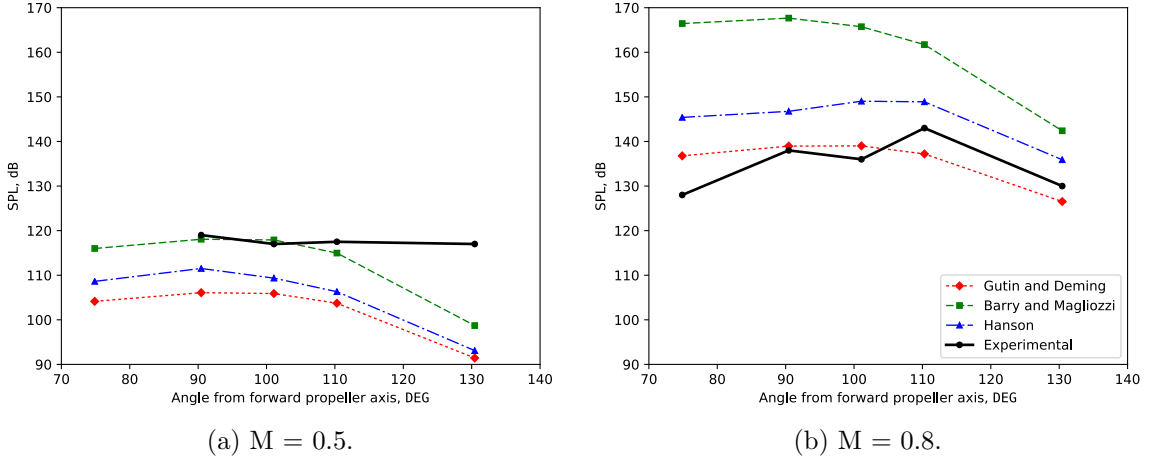


Figure 5.4. Blade passing tone directivities - test cases 4 and 5.

### 5.2.5 Test Cases 6 and 7: Dittmar and Stang

Blade passing tone levels for test cases 6 and 7 are presented in Figs. 5.5a and 5.5b, respectively. Both utilize an eight-bladed SR-7 propeller and, again, differ only in the freestream Mach number and rotational speed.

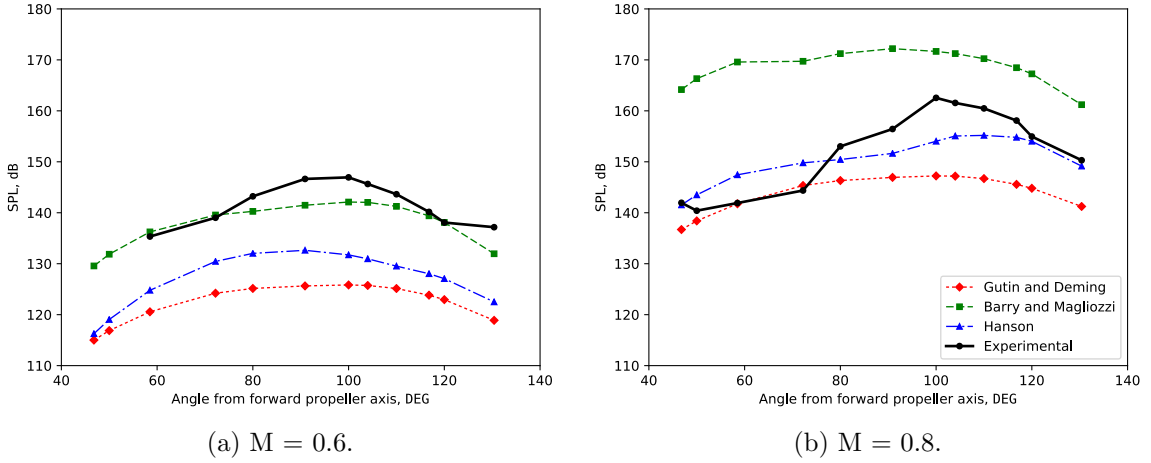


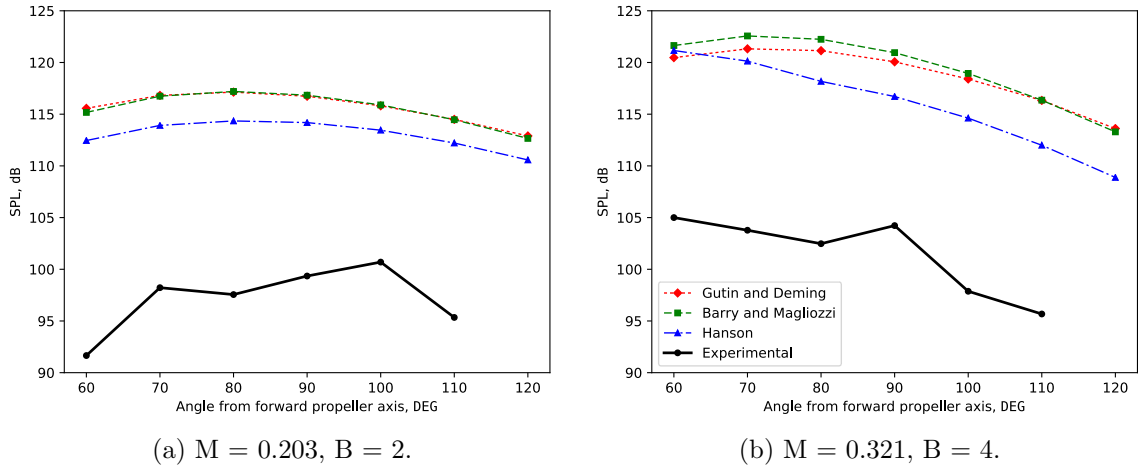
Figure 5.5. Blade passing tone directivities - test cases 6 and 7.

The mischaracterization of the chord-wise compactness term by Barry & Magliozzi's model leads to a more accurate prediction at a forward speed of Mach 0.6 but results in a large overprediction at Mach 0.8. Gutin and Demin's model suffers

from the same error, however, since it does not consider forward flight its prediction is significantly lower. The model by Hanson is the only one that correctly formulates the noise for high speed propellers, but underpredicts the noise at the slower freestream velocity of Mach 0.6. The underprediction of Hanson's model relative to Barry and Magliozzi's model is accentuated by propeller sweep, which reduces the noise signature of the propeller and is only considered by Hanson's model.

### 5.2.6 Test Cases 8 and 9: Brooks and Metzger

Blade passing tone levels for test cases 8 and 9 are presented in Figs. 5.6a and 5.6b, respectively. An eight-blade configuration was not used for the SR-3 due to limitations in the power output of the propeller drive rig. Test case 8 is meant to simulate takeoff and approach conditions, while test case 9 was performed to simulate cruise. Since the flight velocity of the wind-tunnel facility employed by Brooks and Metzger was limited to Mach 0.32, the model was oversped to achieve a helical tip mach number representative of cruise conditions [44].



(a) M = 0.203, B = 2.

(b) M = 0.321, B = 4.

Figure 5.6. Blade passing tone directivities - test cases 8 and 9.

It should be noted that although results are plotted using the azimuth locations in Fig. E.4a, they were produced using the corrected axial microphone locations, as described in Appendix E. A discrepancy between the prediction models can be seen,

even though the forward Mach speed is small, in part due to propeller sweep which is only taken into account by Hanson's model. The overprediction of the experimental values by all three frequency methods is unexpected and suggests an error in the experimental data or misinterpretation of the propeller geometry and operational conditions by the prediction models.

### 5.2.7 Test Case 10: Woodward

Blade passing tone levels for test case 10 are shown in Fig. 5.7. The experimental data obtained by Woodward, described in Ref. 5, specifically simulates takeoff and approach conditions and includes the effects of non-axial flow. Figure 5.7a corresponds to axial flow and serves as a baseline result, while Fig. 5.7b presents data for a propeller with a positive 10 degree angle of attack. Results for a negative angle of attack are not presented here, but produced a similar yet opposite effect on the propeller acoustic signature. The introduction of non-axial flow had minimal impact on the acoustic prediction of Hanson's model, particularly near the propeller plane, where noise output is generally the highest. Experimental results, on the other hand, showed a notable upwards shift with the introduction of non-axial flow. The significant difference between prediction methods is, again, in part due to sweep.

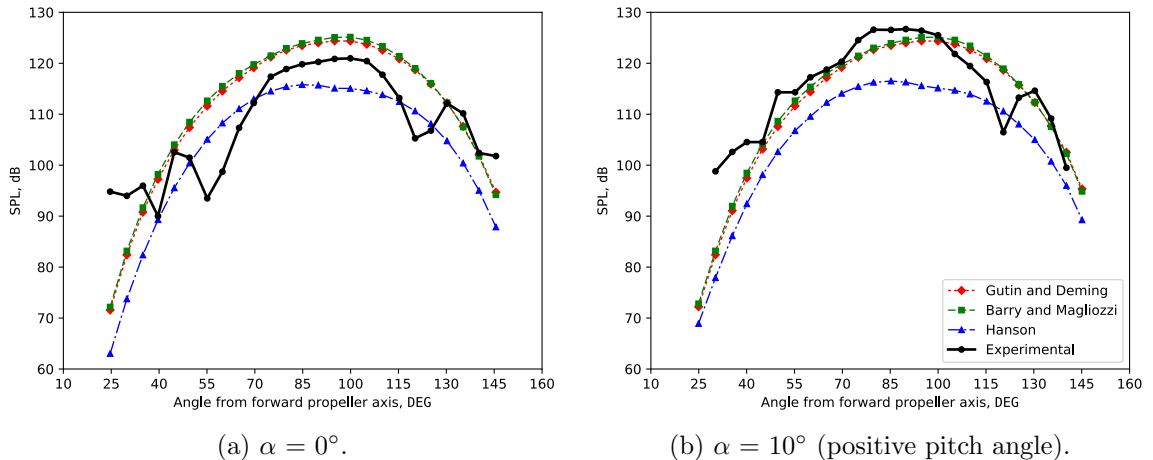


Figure 5.7. Blade passing tone directivities - test case 10.

### 5.2.8 Test Case 11: Hubbard

Acoustic results for the blade passing frequency and second harmonic of test case 11 are given in Fig. 5.8. Experimental data for test case 11 was obtained using an outdoor static test stand and a two-bladed propeller. The geometry of the propeller is given in Ref. 50. Close agreement between all three methods is observed in test case 11 because a non-swept propeller operating at a low forward speed is used. The predicted noise is nonzero at the propeller axis since multiple microphone locations are used for each data point, as described in Section 4.1. If only one microphone is used, the predicted noise at the propeller axis is zero as shown in Fig. D.8.

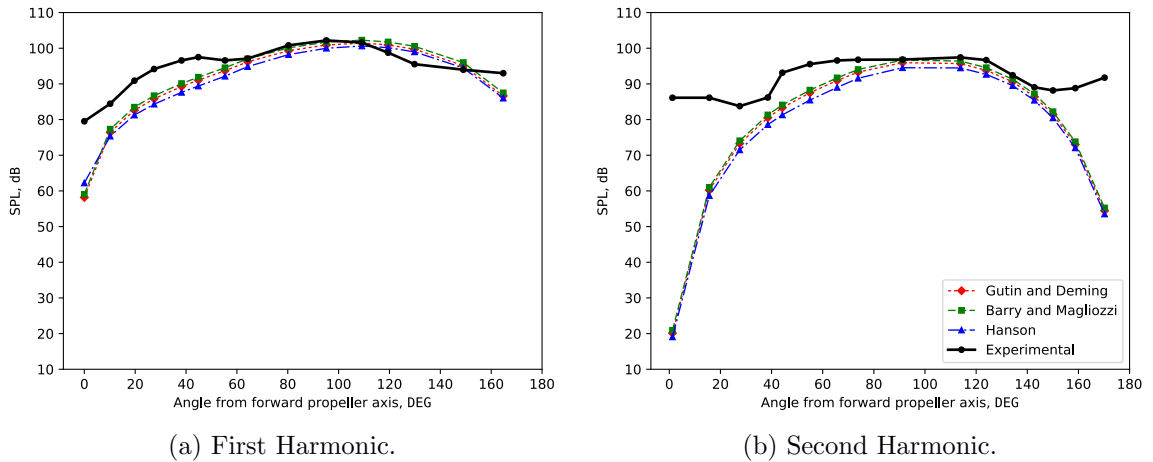


Figure 5.8. Tone directivities - test case 11.

### 5.2.9 Test Cases 12 and 13: Brown and Ollerhead

Blade passing tone levels for test cases 12 and 13 are presented in Figs. 5.9a and 5.9b, respectively. Both test cases were performed under static conditions, but differ in blade geometry and number. The geometry of each propeller is provided in Ref. 44. It is interesting to note that the experimental data remains relatively constant regardless of the observer angle for both test cases 12 and 13, but decreases significantly near the axis for test case 11. This may be due to the lower blade loading in test cases 12 and 13, where unaccounted noise sources, such as broadband noise, may be dominant.

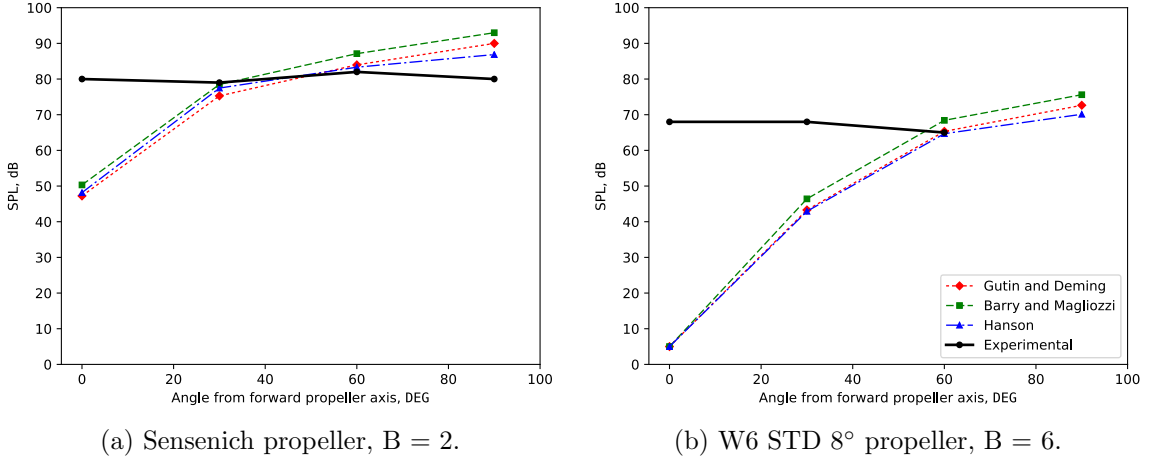


Figure 5.9. Blade passing tone directivities - test cases 12 and 13.

### 5.2.10 Test Case 14: Dobrzynski et al.

The harmonic noise spectra of test case 14, performed with a full-scale two-bladed propeller at a freestream Mach number of 0.2 and helical tip Mach number of 0.86, is shown in Fig. 5.10. Only two microphone locations (microphones 4 and 5) were considered due to the fact that data for other transducer locations was not readable from the source document. Since data for only two transducer positions was available, the harmonic spectrum of the first twenty harmonics was plotted instead.

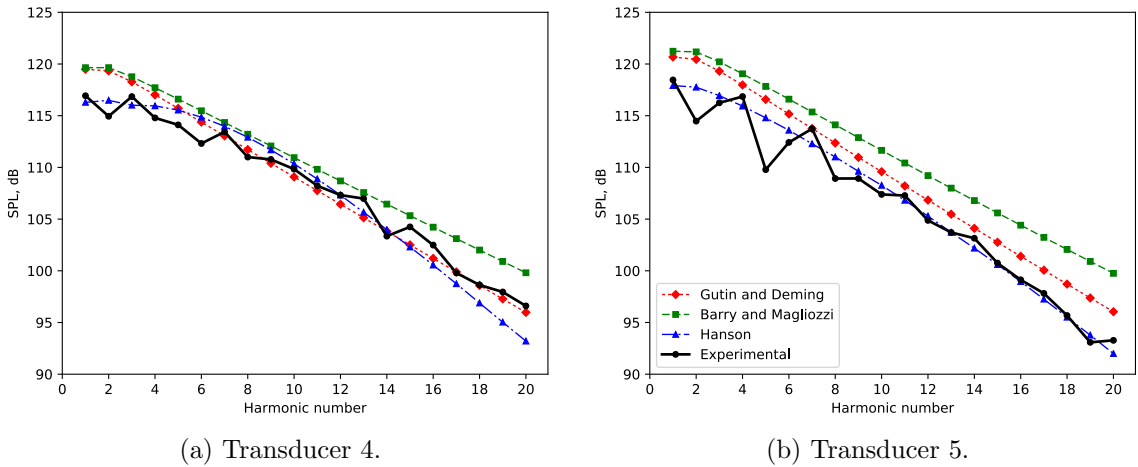


Figure 5.10. Noise spectra - test case 14.

The close agreement with the experiment up to the twentieth harmonic is unexpected as Gutin and Deming's noise formulations are known to only be accurate at low order harmonics [22, 28].

### 5.3 Results Summary

Acoustic prediction accuracy of each noise model for every test case is presented in Table 5.2. The non-bracketed term qualifies the capability of the models in predicting the maximum noise level and usually corresponds to the prediction error of transducers near the propeller plane. The term in brackets, on the other hand, is a measure of the consistency of the models at different transducer locations and typically matches the prediction error at the transducer closest to the propeller axis. It can be seen from Table 5.2 that Hanson's model outperforms the other prediction methods with an average 7.2 dB overprediction or underprediction of the maximum sound pressure level. The large errors in maximum error (bracketed term) are expected due to the nature of the prediction methods, which theoretically predict zero noise at the propeller axis.

Table 5.2. Summary of acoustic model performance.

Test	Error at location of maximum noise*, dB (Maximum error†, dB)		
Case	Gutin and Deming	Barry and Magliozzi	Hanson
1‡	13.1 (-18.2)	14.6 (18.3)	10.2 (-18.2)
	12.8 (-50.3)	14.4 (-46.8)	10.3 (-50.3)
2‡	-22.1 (-22.2)	-4.97 (-5.23)	-7.65 (-9.34)
	-32.8 (-39.4)	-4.00 (-17.6)	-10.5 (-24.1)
3‡	-21.4 (-21.4)	5.76 (24.5)	1.64 (10.9)
	-21.3 (-21.4)	20.0 (35.0)	3.50 (15.2)
4	-12.9 (-25.6)	-0.93 (-18.3)	-7.48 (-23.9)
5	-4.00 (8.78)	24.7 (38.4)	6.02 (17.4)
6	-21.1 (-21.1)	-4.84 (-5.21)	-14.3 (-15.2)
7	-15.3 (-15.3)	9.65 (27.7)	-7.37 (-8.52)
8	16.4 (23.9)	16.5 (23.5)	13.7 (20.8)
9	16.3 (20.7)	17.6 (21.1)	16.2 (16.7)
10§	3.41 (-23.2)	4.16 (-22.6)	-5.18 (-31.8)
	-2.32 (-16.4)	-1.58 (-15.6)	-10.2 (-20.9)
11‡	-0.74 (-21.3)	0.07 (-20.5)	-1.56 (-17.3)
	-1.48 (-66.0)	-0.77 (-65.2)	-2.89 (-67.0)
12	7.99 (-32.8)	11.0 (-29.7)	4.86 (-31.8)
13	4.65 (-63.0)	7.61 (-63.0)	2.12 (-63.0)
14	1.67 (1.67)	2.23 (2.23)	-1.09 (-1.71)
Avg.¶	12.2 (27.0)	8.70 (26.3)	7.20 (24.4)

\* difference between maximum experimental and maximum predicted noise; locations of maximum noise are not necessarily identical between experimental and predicted results

† maximum error between experimental and predicted data across all transducer locations

‡ the fundamental harmonic is presented first, followed by the second harmonic

§ error for axial flow is presented first, followed by non-axial flow

¶ the modulus of the error values is taken before averaging

Independent of individual validation cases, some general trends were observed:

- 1) Good acoustic results were obtained with an aerodynamic-acoustic solution with a total runtime of 0.01 seconds, many orders of magnitude faster than acoustic methods coupled to panel or grid-based aerodynamic solvers.
- 2) The formulations by Gutin and Deming showed good agreement with experiment up to freestream velocities of Mach 0.3.
- 3) The formulations by Barry and Magliozzi showed good agreement with experiment up to freestream velocities of Mach 0.6.
- 4) The formulations by Hanson showed the best consistency and accuracy of the three frequency methods but tended to underpredicted the noise at lower freestream speeds, particularly for swept propellers.
- 5) Better acoustic predictions were obtained near the propeller plane, with poor accuracy near the axis.
- 6) The implementation of non-axial flow into Hanson's model using Refs. 16 and 31 had limited success as angle of attack was found to have only a minor impact on the predicted noise signature of the propeller. This can likely be attributed to the fact that only steady loading was considered.
- 7) Experimental and predicted results varied significantly across test cases and microphone locations, emphasizing the need for thorough validation of acoustic models with multiple test cases and a range of microphone positions being considered.
- 8) The impact of aerodynamic error on the acoustic solution was minimal and could be described by a linear relationship.

The error at the location of maximum noise (non-bracketed term) is shown graphically in Fig. 5.11. Figure 5.11a on the left shows the variation of error by test case and depicts the outlying behavior of test cases 8 and 9, where all acoustic methods significantly overpredict the noise. Figure 5.11b on the right shows the variation of error with freestream Mach number and illustrates the trends outlined above. The dotted lines in Fig. 5.11b represent the general behavior of each model and were formed by taking the average error of test cases for each Mach number. From this trendline, the significant underprediction by Gutin and Deming's model at Mach numbers above 0.3 is visible. This behavior, however, is expected since Gutin and Deming's model does not consider forward flight. The better accuracy of Gutin and Deming's model at forward Mach speeds of 0.8 relative to forward Mach speeds of 0.6 is due to a cancellation of two errors: lack of consideration of forward speed reduces the noise prediction while incorrect characterization of the chord-wise compactness term increases the noise prediction. At very high forward speeds, such as Mach 0.8, the latter starts to dominate.

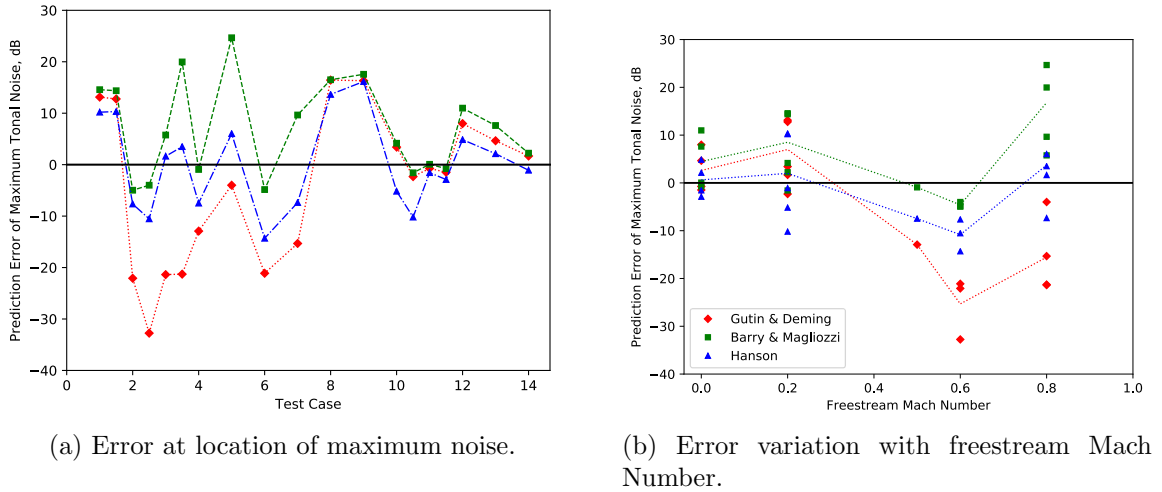


Figure 5.11. Summary of acoustic model performance.

For the same reason, Barry and Magliozzi's model, which considers forward flight, predicts higher noise relative to Hanson's model for test cases with a freestream Mach

number above 0.2. For the selected test cases, this tends to increase the accuracy of the results at freestream Mach numbers of 0.5 and 0.6 but leads to significant overprediction at forward speeds above Mach 0.6. The higher acoustic prediction of Barry and Magliozzi's model at low forward Mach speeds is in part due to the modified Bessel function it employs while the lower prediction of Hanson's model at low forward speeds is primarily due to the consideration of sweep. Hanson's model, as stated earlier, shows the best overall accuracy and consistency, particularly at forward flight speeds of Mach 0.8, where it is the only model capable of producing reasonable results. It should be noted that test cases 8 and 9 were omitted from Fig. 5.11b due to their outlying behavior.

Acoustic results for test cases 1, 2 and 3 were obtained with time-domain methods by Boots [52] and Hambrey [53] using a panel method and a grid-based computational fluid dynamics solver coupled to the Ffowcs Williams-Hawkins equation. The time-domain models implemented by Boots and Hambrey demonstrated lower accuracy relative to the significantly faster implemented frequency methods, however, it is not clear if the results presented in Refs. 52 and 53 are representative of the accuracy of panel and grid-based time-domain solutions. As such, they are not included in this thesis.

Results for the validation cases presented demonstrate the capability of early acoustic methods for the prediction of far-field, propeller-alone harmonic noise across a range of propeller configurations, including the modern, high speed prop-fan.

## **Chapter 6**

# **Conclusions and Recommendations**

Three different acoustic prediction methods based on early acoustic theory were implemented from the literature and validated against fourteen test cases. The implemented methods only required easily obtainable geometric and operational data and used blade element momentum theory to approximate the radial thrust and torque distributions. The predicted thrust and torque distributions were found to be in good agreement with experiment for a range of aerodynamic test cases and any aerodynamic error introduced by BEMT was found to have minimal impact on the acoustic solution. The selected aerodynamic and acoustic test cases ranged in propeller configuration and operational conditions to characterize the limits of BEMT and the acoustic prediction methods. A substantial number of acoustic validation cases were used in an effort to identify the general behavior of each prediction method and limit the influence of inconsistencies within the predicted and experimental results.

The acoustic predictions showed significant variation in accuracy across test cases and at different microphone locations, highlighting the need for multiple test cases to be considered in the validation of acoustic models. Nevertheless, noise comparisons of the implemented acoustic models showed good agreement with experiment. Hanson's model was the most consistent and accurate of the evaluated methods, with an

average error of 7.2 dB in the maximum tonal noise relative to experiment. The presented results indicate the potential of early acoustic methods, particularly for design and optimization studies, and demonstrate their relevance for the noise prediction of modern, high speed, prop-fan configurations.

## 6.1 Recommendations for Future Work

Although the completed work clearly demonstrates the ability of early acoustic theory and frequency methods in the prediction of propeller noise, additional results in a number of areas would enhance the presented work. These are, in order of importance:

- 1) Compare results obtained with the implemented frequency methods to time-domain methods such as ANOPP-PAS or STAR-CCM+ to determine the relative accuracy of the implemented frequency methods.
- 2) Incorporate the near-field equations for the implemented acoustic models.
- 3) Implement and assess the accuracy of the FW-H equation coupled to BEMT, with approximations made for the chord-wise pressure distribution.
- 4) Investigate the possibility of merging acoustic equations such that different acoustic model variants are used based on input parameters such as the freestream velocity. It should be noted that a very large data set would be required for this endeavor to correctly formulate such a model.

# References

- [1] R. Peterson. Regional turboprop resurgence continues; jet demand shifts upward. *Aircraft Engineering and Aerospace Technology*, 80(2), 2004.
- [2] M. S. Ryerson and M. Hansen. The potential of turboprops for reducing aviation fuel consumption. *Transportation Research Part D: Transport and Environment*, 15(6):305–314, 2010.
- [3] E. Franssen, C. van Wichen, N. Nagelkerke, and E. Lebret. Aircraft noise around a large international airport and its impact on general health and medication use. *Occupational and Environmental Medicine*, 61(5):405–413, 2004.
- [4] H. Swift. A review of the literature related to potential health effects of aircraft noise. PARTNER-COE-2010-003, Partnership for Air Transportation Noise and Emissions Reduction, Cambridge, MA, July 2010.
- [5] R. P. Woodward. Measured noise of a scale model high speed propeller at simulated takeoff/approach conditions. NASA-TM-88920, Lewis Research Center, Cleveland, OH, January 1987.
- [6] J. H. Dittmar and R. J. Jeracki. Additional noise data on the SR-3 propeller. NASA-TM-81736, Lewis Research Center, Cleveland, OH, May 1981.
- [7] L. Gutin. On the sound field of a rotating propeller. NACA-TM-1195, National Advisory Committee for Aeronautics, Washington, DC, October 1948.
- [8] C. Holsclaw. Stage 5 airplane noise standards. 81 FR 1923, Federal Aviation Administration, Washington, DC, January 2016.
- [9] N. Dickson. ICAO noise standards. In *ICAO Symposium on Aviation and Climate Change*, Montreal, Canada, 2013.
- [10] F. J. H. Lynam and H. A. Webb. The emission of sound by airscrews. *Technical Report of the Advisory Committee for Aeronautics for the Year 1918-1919*, 2:792–801, 1919.

- [11] A. F. Deming. Noise from propellers with symmetrical sections at zero blade angle II. NACA-TN-679, National Advisory Committee for Aeronautics, Washington, DC, December 1938.
- [12] I. E. Garrick and C. E. Watkins. A theoretical study of the effect of forward speed on the free-space sound-pressure field around propellers. NACA-TN-3018, National Advisory Committee for Aeronautics, Washington, DC, October 1953.
- [13] R. A. Arnoldi. Propeller noise caused by blade thickness. R-0896-1, United Aircraft Corporation Research Department, East Hartford, CT, January 1956.
- [14] F. W. Barry and B. Maglizzi. Noise detectability prediction method for low tip speed propellers. AFAPL-TR-71-37, Hamilton Standard, Wright-Patterson Air Force Base, OH, June 1971.
- [15] D. B. Hanson. Helicoidal surface theory for harmonic noise of propellers in the far field. *AIAA Journal*, 18(10):1213–1220, 1980.
- [16] D. B. Hanson. Sound from a propeller at angle of attack: A new theoretical viewpoint. *Proceedings: Mathematical and Physical Sciences*, 449(1936):315–328, 1995.
- [17] J. E. Ffowcs Williams and D. L. Hawkings. Sound generation by turbulence and surfaces in arbitrary motion. *Philosophical Transactions of the Royal Society of London. Series A, Mathematical and Physical Sciences*, 264(1151):321–342, 1969.
- [18] F. Farassat. Derivation of formulations 1 and 1A of Farassat. NASA-TM-2007-214853, Langley Research Center, Hampton, VA, March 2007.
- [19] C. L. Morfey. Rotating blades and aerodynamic sound. *Journal of Sound and Vibration*, 28(3):587–617, 1973.
- [20] B. Maglizzi, F. B. Metzger, W. Baush, and R. J. King. A comprehensive review of helicopter noise literature. FAA-RD-75-79, Federal Aviation Administration, Washington, DC, June 1975.
- [21] B. Maglizzi, D. B. Hanson, and R. K. Amiet. Propeller and propfan noise. In H. H. Hubbard, editor, *Aeroacoustics of Flight Vehicles: Theory and Practice*, volume 1, pages 1–61. NASA, Hampton, VA, 1991.

- [22] F. Farassat and G. P. Succi. A review of propeller discrete frequency noise prediction methodology with emphasis on two current methods for time domain calculations. *Journal of Sound and Vibration*, 71(3):399–419, 1980.
- [23] B. Metzger. A review of propeller noise prediction methodology: 1919-1994. NASA-CR-198156, Langley Research Center, Hampton, VA, June 1995.
- [24] P. T. Soderman and W. C. Horne. Acoustic and aerodynamic study of a pusher-propeller aircraft model. NASA-TP-3040, Ames Research Center, Moffet Field, CA, September 1990.
- [25] H. H. Hubbard and L. W. Lassiter. Sound from a two blade propeller at supersonic tip speeds. NACA-Report-1079, Lewis Research Center, Cleveland, OH, September 1952.
- [26] A. F. Deming. Propeller rotation noise due to torque and thrust. *Journal of the Acoustical Society of America*, 12(1):173–182, 1940.
- [27] E. D. Griffith and J. D. Revell. Low noise propeller technology demonstration. AFA1L-TR-73-115, Lockheed-California Company, Burbank, CA, January 1974.
- [28] D. Brown and J. B. Ollerhead. Propeller noise at low tip speeds. AFAPL-TR-71-55, Wyle Laboratories, Hampton, VA, September 1971.
- [29] C. E. Whitfield, P. R. Gliebe, R. Mani, and P. Mungur. High speed turboprop aeroacoustic study (single rotation). NASA-CR-182257, GE Aircraft Engines, Cincinnati, OH, May 1989.
- [30] D. B. Hanson. Influence of propeller design parameters on far-field harmonic noise in forward flight. *AIAA Journal*, 18(11):1313–1319, 1980.
- [31] D. B. Hanson and D. J. Parzych. Theory for noise of propellers in angular inflow with parameteric studies and experimental verification. NASA-CR-4499, Hamilton Standard, Windsor Locks, CT, March 1993.
- [32] J. R. Hambrey, M. T. Kotwicz Herniczek, D. Feszty, S. Meslioui, and J. Park. Comparison of three popular methods for the prediction of high speed propeller noise. In *Proceedings of the 23rd AIAA/CEAS Aeroacoustics Conference*, Denver, CO, 2017. AIAA.
- [33] C. N. Atkins and R. H. Leibek. Design of optimum propellers. *Journal of Propulsion and Power*, 10(5):676–682, 1994.

- [34] G. Leishman. *Principles of Helicopters Aerodynamics*. Cambridge University, New York, 2006.
- [35] D. H. Hodges. An extension of blade element momentum theory to incorporate nonlinear lift and drag coefficients. *Journal of the American Helicopter Society*, 25(4):48–50, 1981.
- [36] L. A. Viterna and D. C. Janetzke. Theoretical and experimental power from large horizontal-axis wind turbines. NASA-TM-82944, Lewis Research Center, Cleveland, OH, September 1982.
- [37] E. G. Reid. The influence of blade-width distribution on propeller characteristics. NACA-TN-1834, Stanford University, Stanford, CA, March 1949.
- [38] G. L. Stefko, G. E. Rose, and G. G. Podboy. Wind tunnel performance results of an aeroelastically scaled 2/9 model of the PTA flight test prop-fan. NASA-TM-89917, Lewis Research Center, Cleveland, OH, July 1987.
- [39] W. H. Gray. Wind-tunnel tests of two hamilton standard propellers embodying Clark Y and NACA 16-series blade section. NACA-WR-L-530, Langley Aeronautical Laboratory, Langley Field, VA, August 1941.
- [40] T. Theodorsen, G. W. Stickle, and M. J. Brevroort. Characteristics of six propellers including the high-speed range. NACA-TR-594, Langley Aeronautical Laboratory, Langley Field, VA, January 1937.
- [41] J. E. Marte and D. W. Kurtz. A review of aerodynamic noise from propellers, rotors and lift fans. NASA-TR 32-1462, California Institute of Technology, Pasadena, CA, January 1970.
- [42] J. Jacques. Wind-tunnel simulation of the effects of flight on radiated sound. C.P. No. 1351, Aeronautical Research Council, London, England, 1976.
- [43] B. Saint-Jalmes, J. Zaneboni, and B. Rumeau. Engine nacelle with propeller. U.S. Patent D633429 S1, 2009.
- [44] B. M. Brooks and F. B. Metzger. Acoustic test and analysis of three advanced turboprop models. NASA-CR-159667, Hamilton Standard, Windsor Locks, CT, January 1980.
- [45] L. C. Billman, R. M. Ladden, J. E. Turnberg, C. J. Gruska, and D. K. Leishman. Large scale prop-fan structural design study: Volume II - preliminary design of SR-7. NASA-CR-174993, Hamilton Standard, Washington, DC, August 1989.

- [46] J. H. Dittmar. Cruise noise of the SR-2 propeller model in a wind tunnel. NASA-TM-101480, Lewis Research Center, Cleveland, OH, April 1989.
- [47] J. H. Dittmar and D. B. Stang. Cruise noise of the 2/9 scale model SR-7A propeller. *Journal of Aircraft*, 25(8):740–746, 1988.
- [48] D. Parzych, S. Cohen, and A. Shenkman. Large-scale advanced propfan (lap) performance, acoustic and weight estimation. NASA-CR-174782, Hamilton Standard, Washington, DC, February 1985.
- [49] M. Nallasamy, R. P. Woodward, and J. F. Groeneweg. High-speed propeller performance and noise predictions at takeoff/landing conditions. *Journal of Aircraft*, 26(6):563–569, 1989.
- [50] H. H. Hubbard. Sound measurements for five shrouded propellers at statics conditions. NACA-TN-2024, Langley Aeronautical Laboratory, Cleveland, OH, April 1950.
- [51] W. M. Dobrzynski, H. H. Heller, J. O. Powers, and J. E. Densmore. Propeller noise tests in the german-dutch wind tunnel DNW. Report No. AEE 86-3, Federal Aviation Administration, Washington, DC, December 1986.
- [52] D. Boots. Numerical predictions of propeller-wing interaction induced noise in cruise and off-design conditions. Master’s thesis, Carleton University, Ottawa, ON, August 2016.
- [53] J. Hambrey. Computational aeroacoustic prediction of propeller noise using grid-based and grid-free cfd methods. Master’s thesis, Carleton University, Ottawa, ON, August 2016.
- [54] W. F. Lindsey, D. B. Stevenson, and B. N. Daley. Aerodynamic characteristics of 24 NACA 16-series airfoils at Mach numbers between 0.3 and 0.8. NASA-TN-1546, Langley Aeronautical Laboratory, Washington, DC, September 1948.
- [55] J. H. Dittmar, B. J. Blaha, and R. J. Jeracki. Tone noise of three supersonic helical tip speed propellers in a wind tunnel at 0.8 Mach number. NASA-TM-79046, Lewis Research Center, Cleveland, OH, December 1978.

## **Appendix A**

### **Additional Aerodynamic Data**

Additional data on validation of the blade element momentum theory implementation is presented in Figs. A.1 to A.8. Supplementary data on the impact of aerodynamic error on the acoustic solution is given in Figs. A.9 and A.10. The reader is reminded that the test case numbering in Figs. A.1 to A.8 refers to the aerodynamic validation cases described in Table 3.1, while the numbering in Figs. A.9 and A.10 refers to the acoustic validation cases detailed in Table 5.1.

## A.1 Overall Propeller Performance

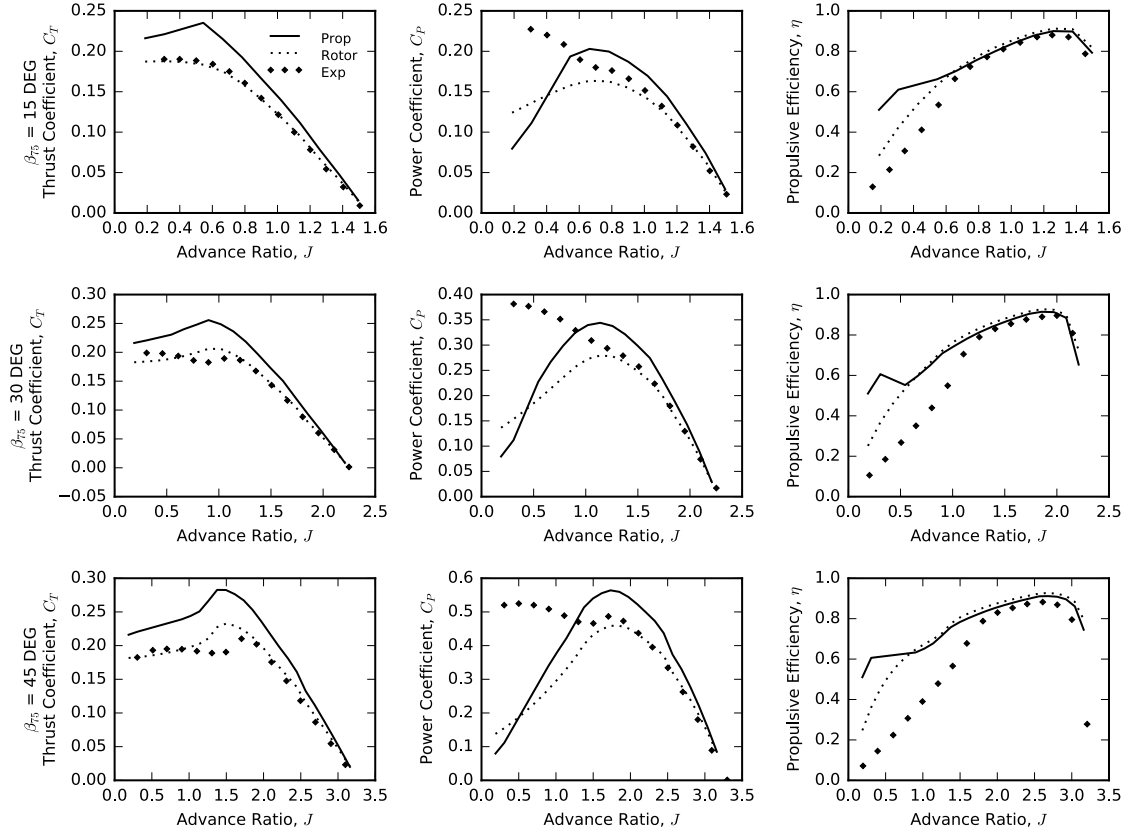


Figure A.1. Propeller aerodynamic performance - test case 3.

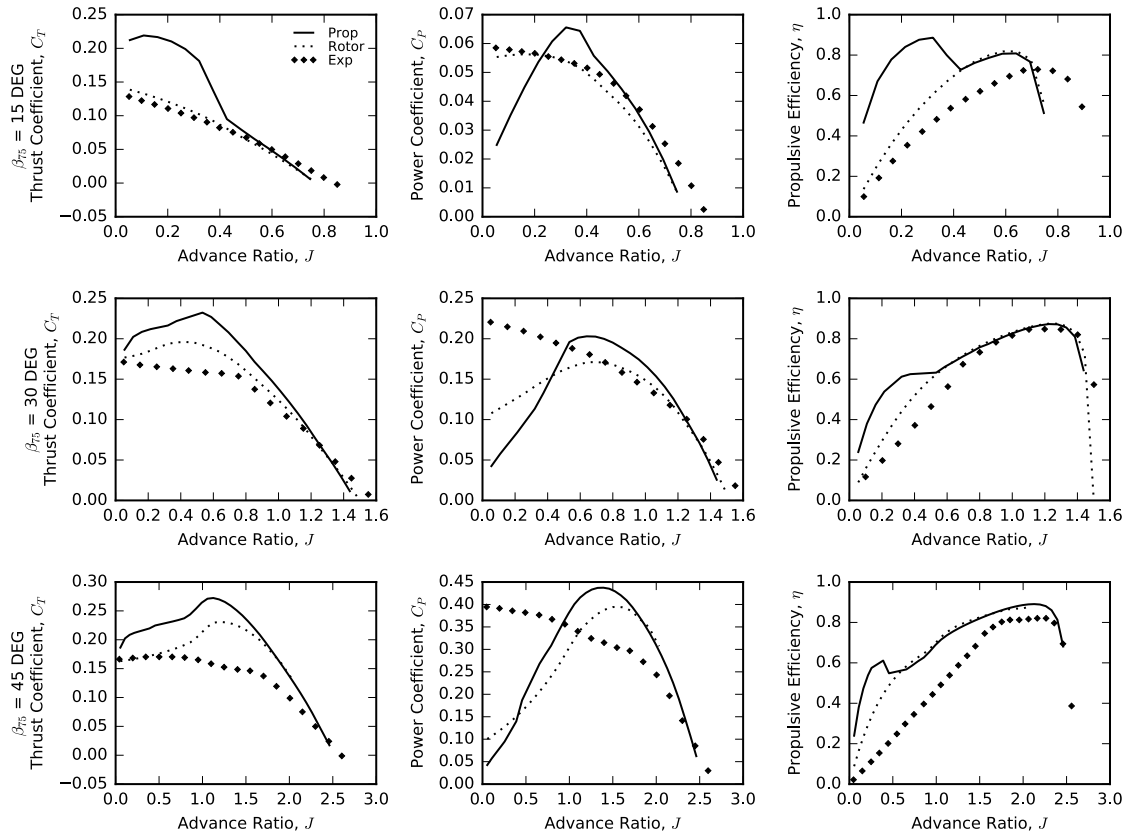


Figure A.2. Propeller aerodynamic performance - test case 4.

## A.2 Thrust and Torque Distributions

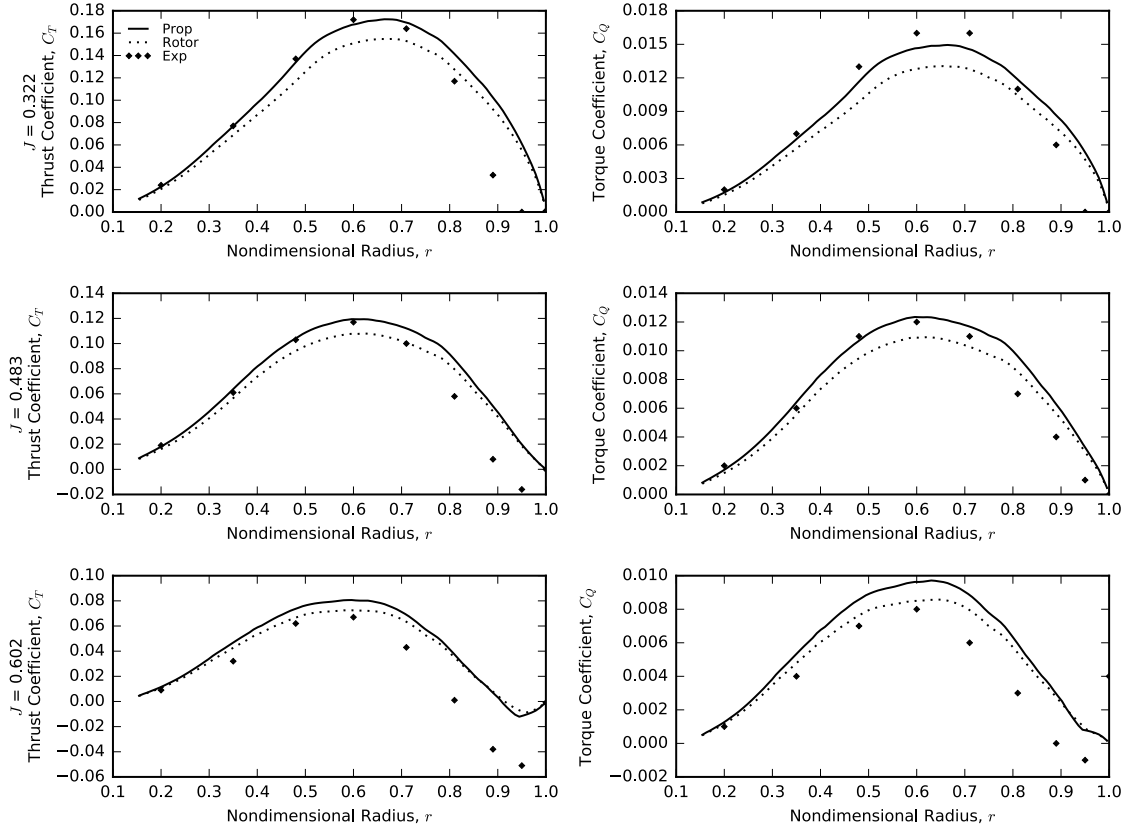


Figure A.3. Propeller thrust and torque distribution at  $12^\circ$  blade pitch and 2100 RPM - test case 1.

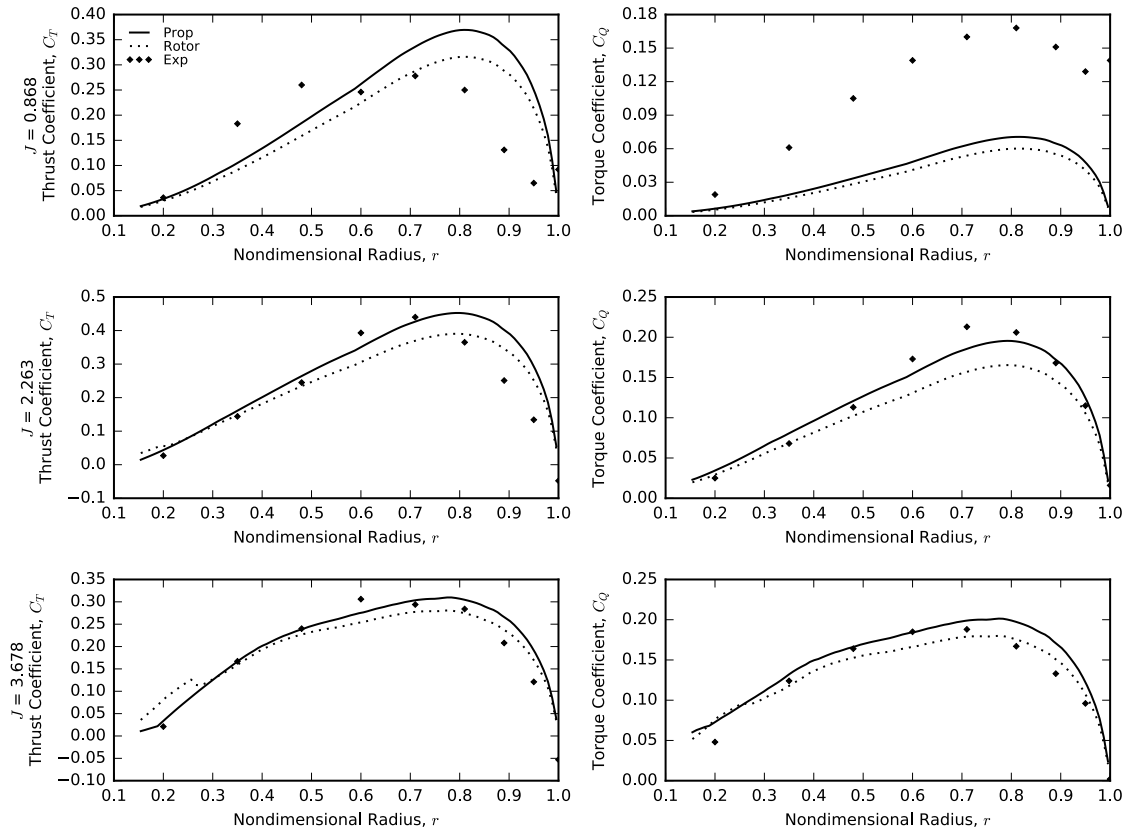


Figure A.4. Propeller thrust and torque distribution at  $60^\circ$  blade pitch and 744 RPM - test case 1.

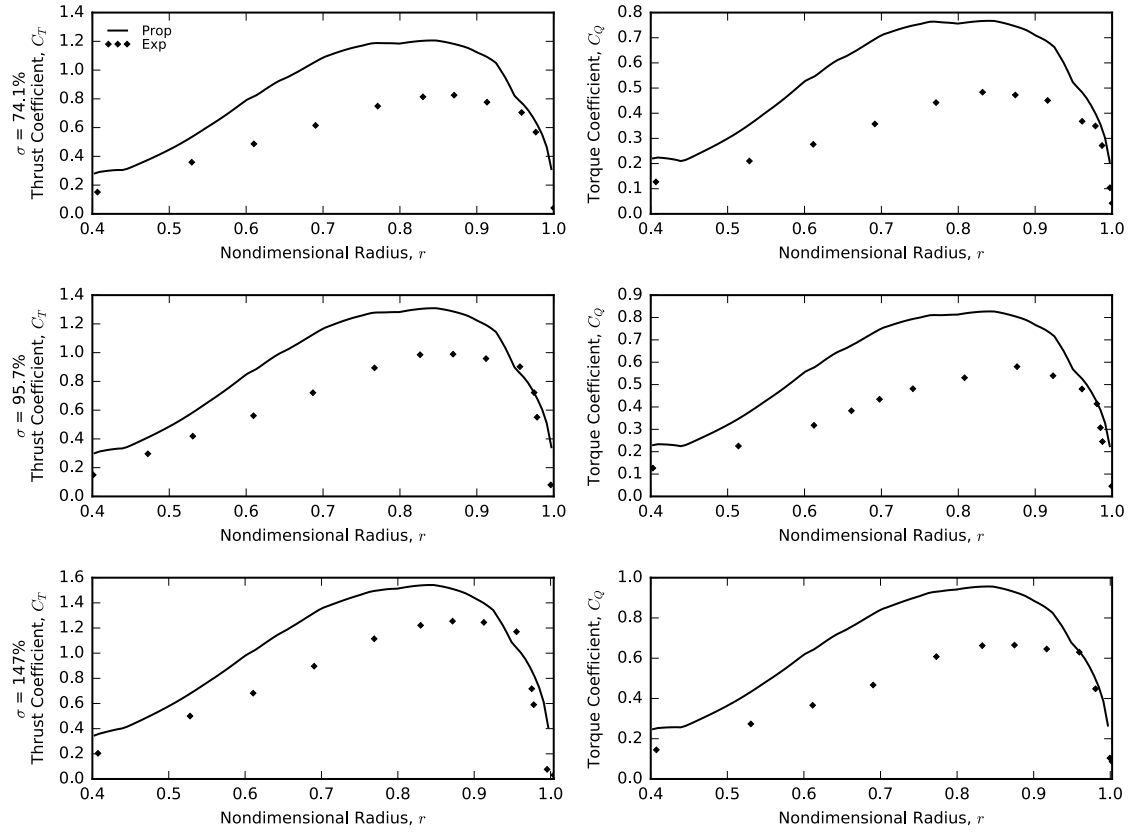


Figure A.5. Propeller thrust and torque distribution - test case 2.

### A.3 Adjusted Thrust and Torque Distributions

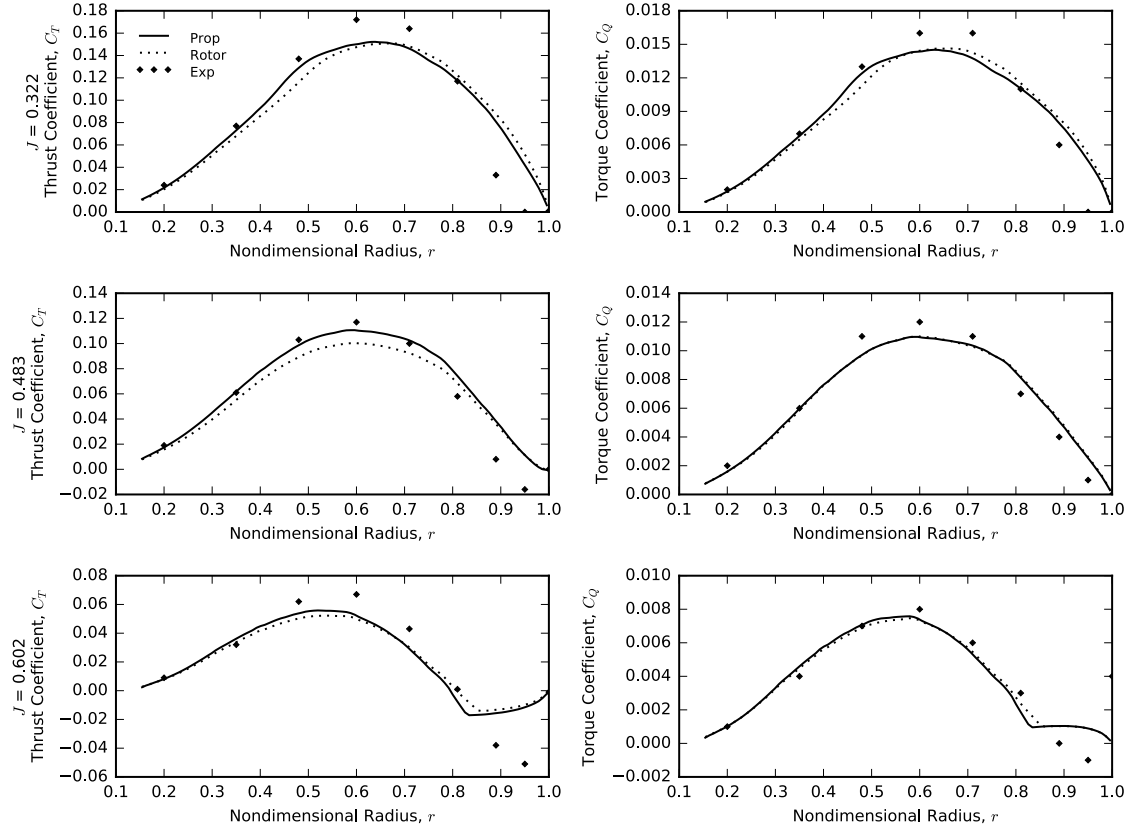


Figure A.6. Adjusted propeller thrust and torque distribution at  $12^\circ$  blade pitch and 2100 RPM - test case 1.

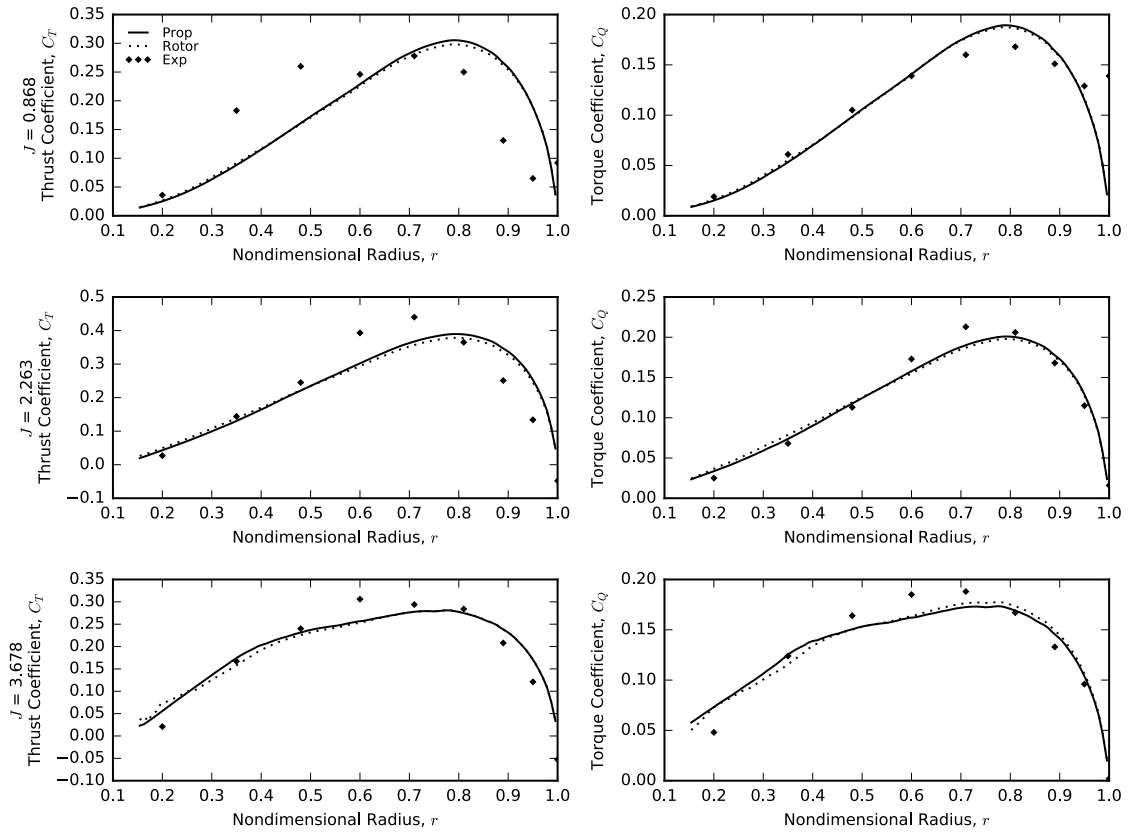


Figure A.7. Adjusted propeller thrust and torque distribution at  $60^\circ$  blade pitch and 744 RPM - test case 1.

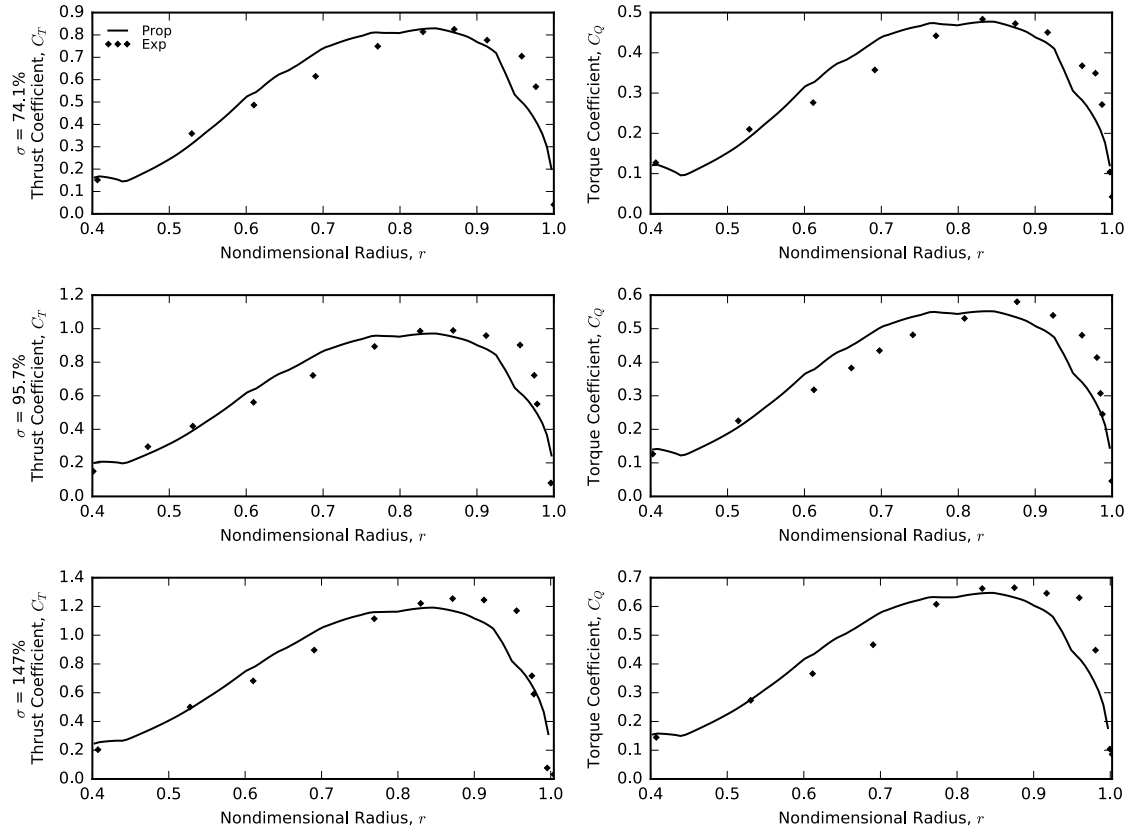


Figure A.8. Adjusted propeller thrust and torque distribution - test case 2.

## A.4 Aerodynamic Impact on Acoustic Solution

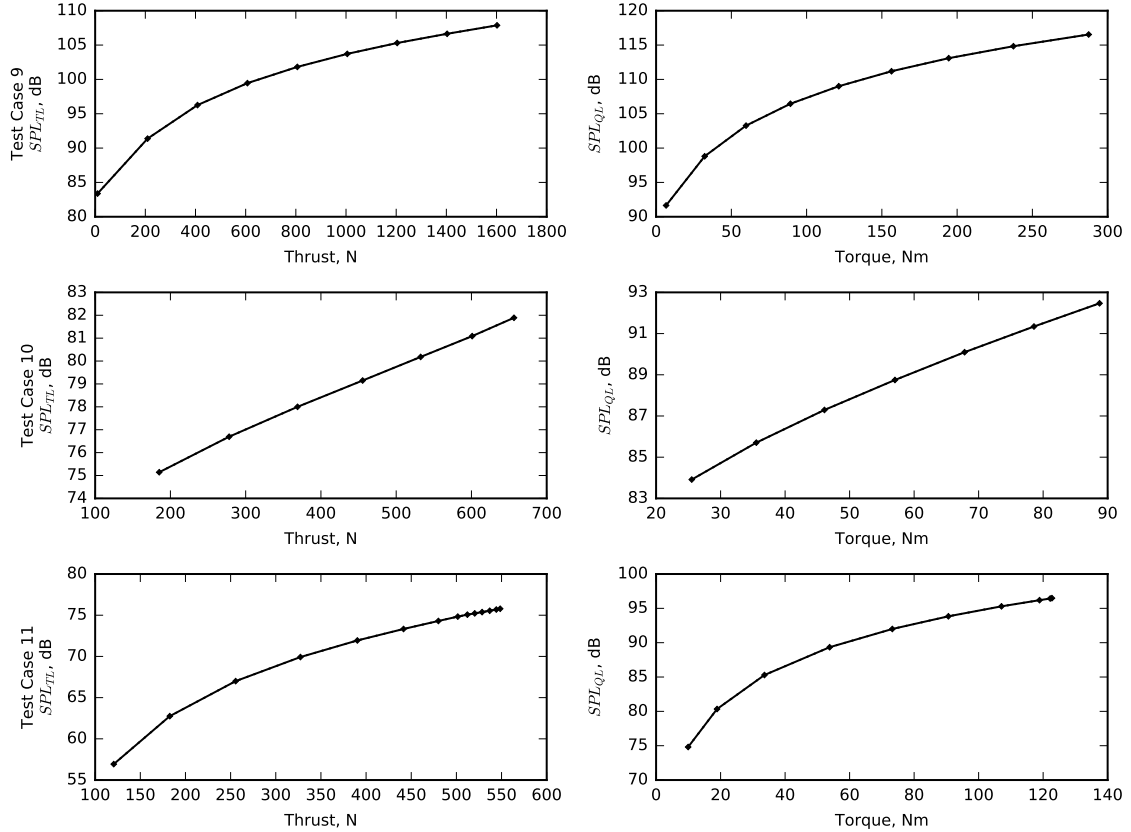


Figure A.9. Impact of thrust and torque variation on acoustic solution - test cases 9 – 11.

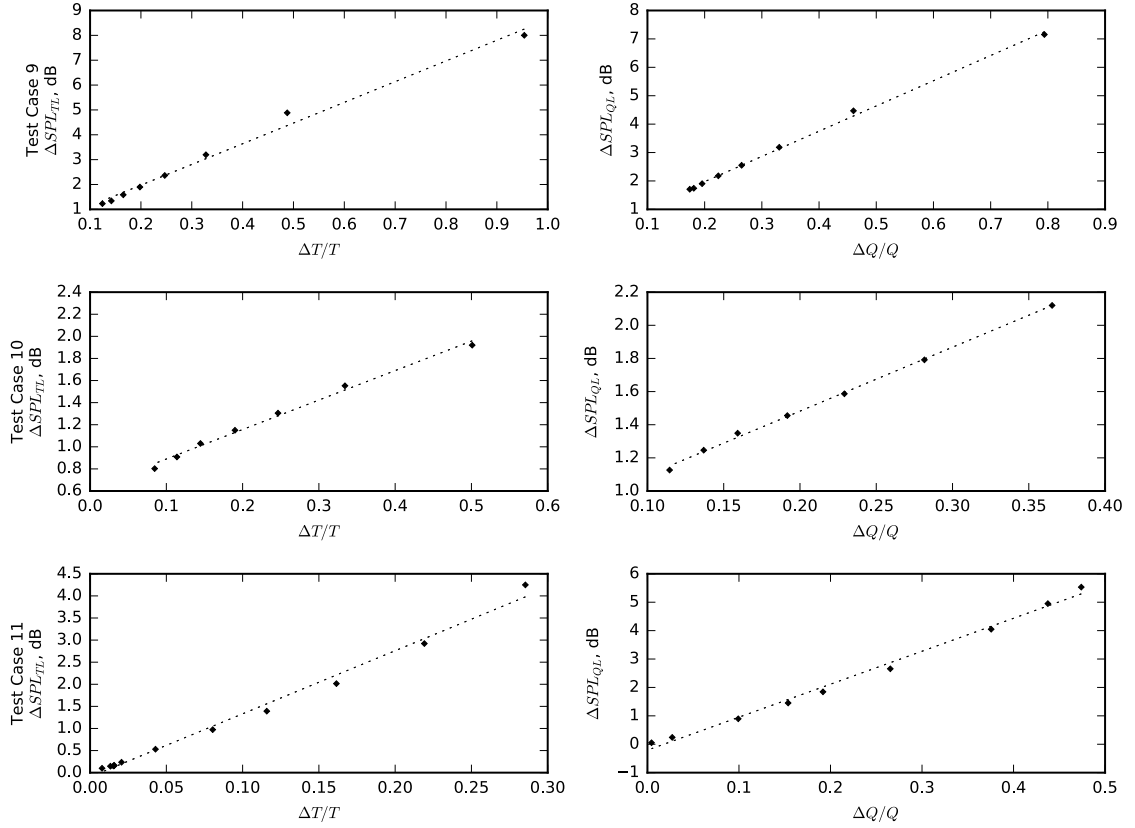


Figure A.10. Relative impact of thrust and torque variation on acoustic solution - test cases 9 – 11.

## Appendix B

### Lift and Drag Coefficient Curves

The lift and drag coefficient curves used by Blade Element Momentum Theory to produce aerodynamic and acoustic results are included below for completeness. The lift and drag curves presented in Figs. B.1 to B.13 were obtained by different means. Clark-Y airfoil data was obtained using XFOIL, NACA-16 series airfoil data is experimental data from Ref. 54 while NACA 4-digit and 5-digit series airfoil data was obtained using STAR-CCM+.

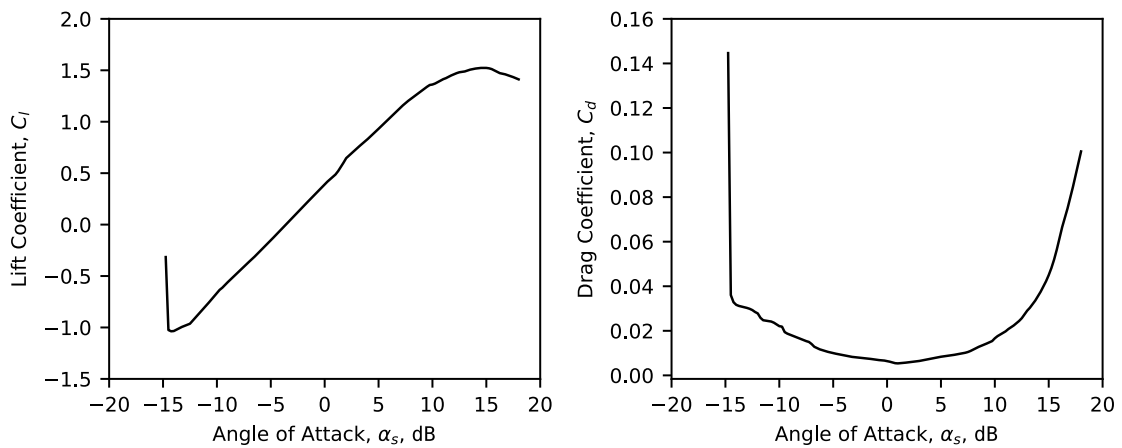


Figure B.1. Clark-Y lift and drag coefficients.

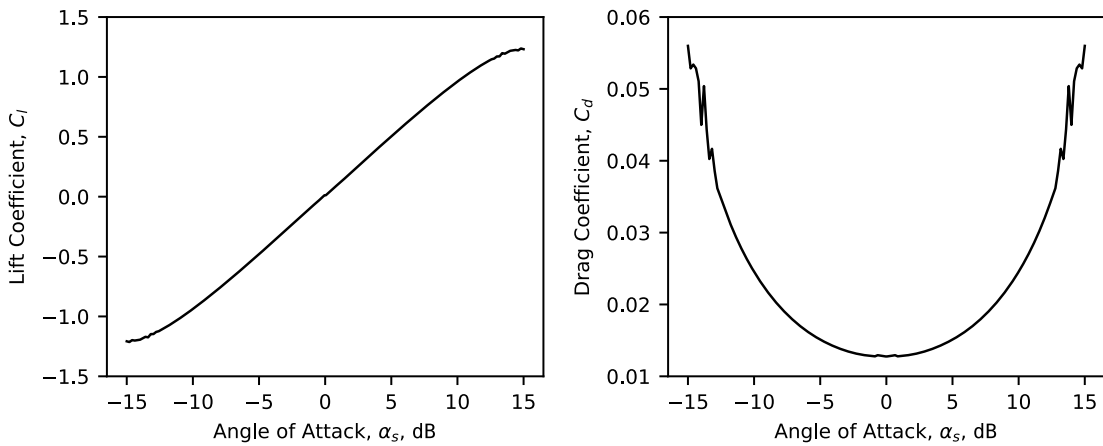


Figure B.2. NACA-0012 lift and drag coefficients.

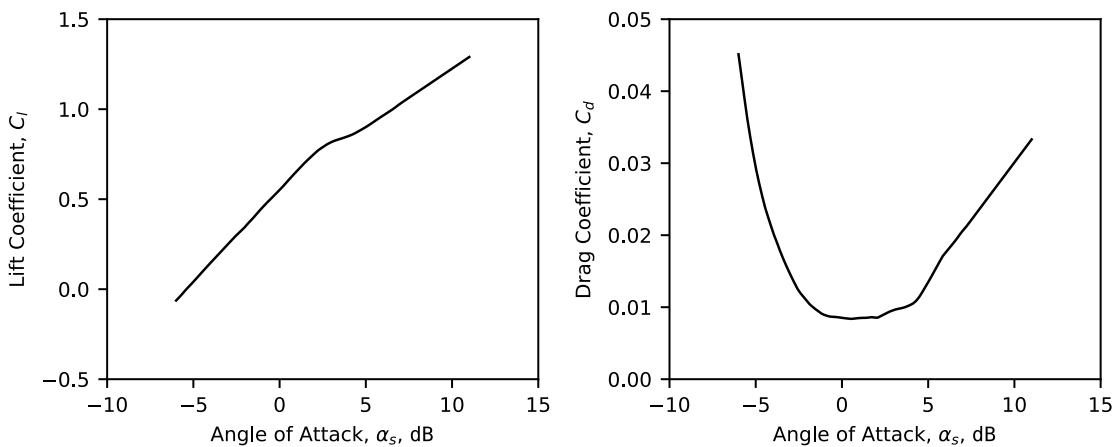


Figure B.3. NACA-16-709 lift and drag coefficients.

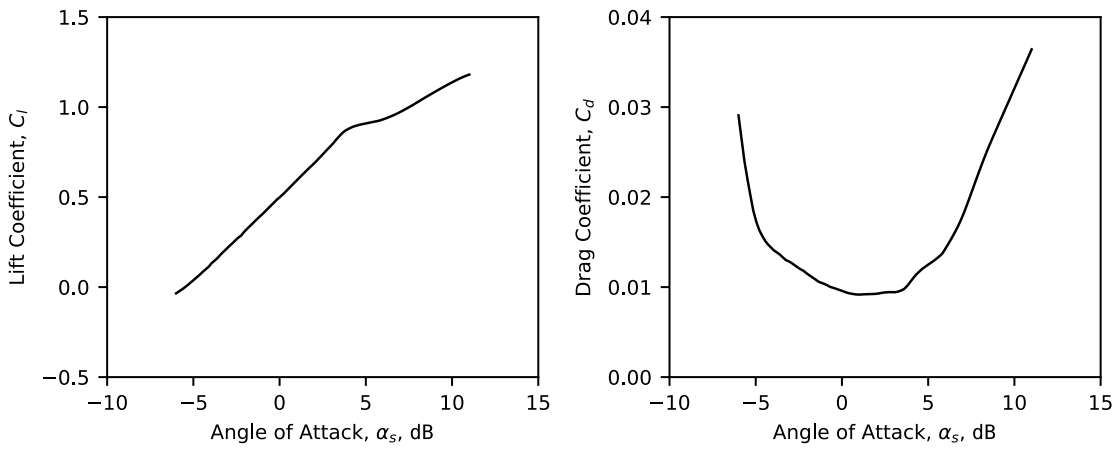


Figure B.4. NACA-16-712 lift and drag coefficients.

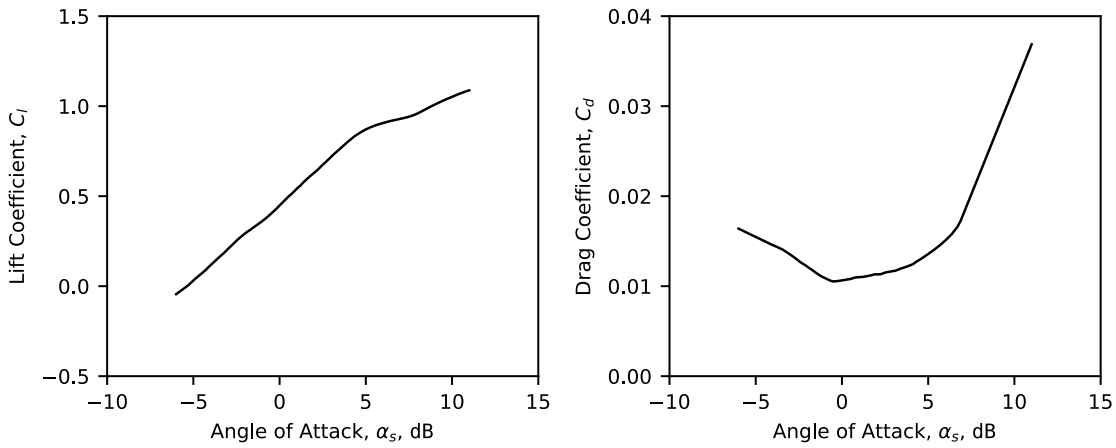


Figure B.5. NACA-16-715 lift and drag coefficients.

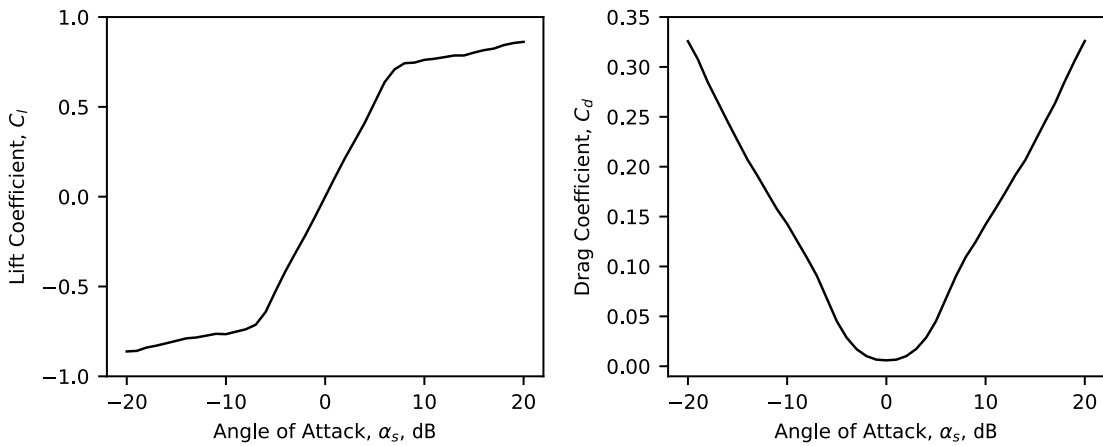


Figure B.6. NACA-16002 lift and drag coefficients.

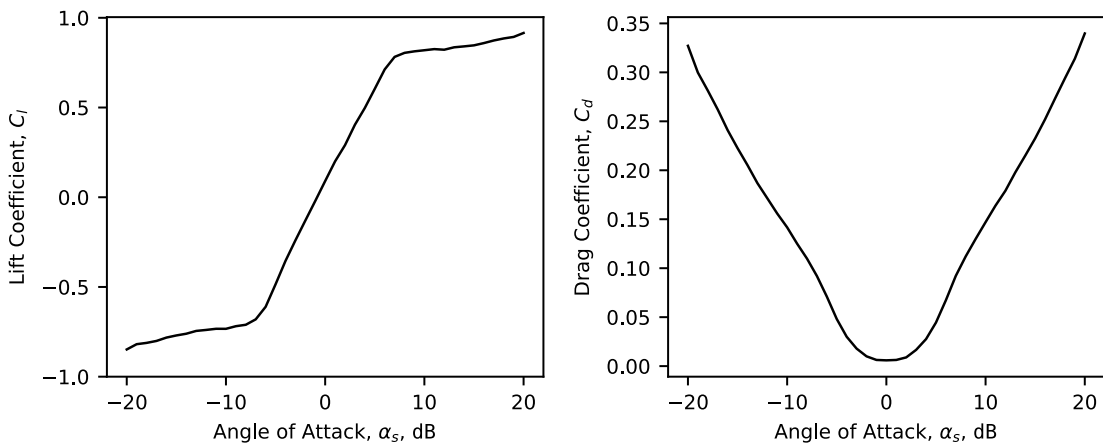


Figure B.7. NACA-16102 lift and drag coefficients.

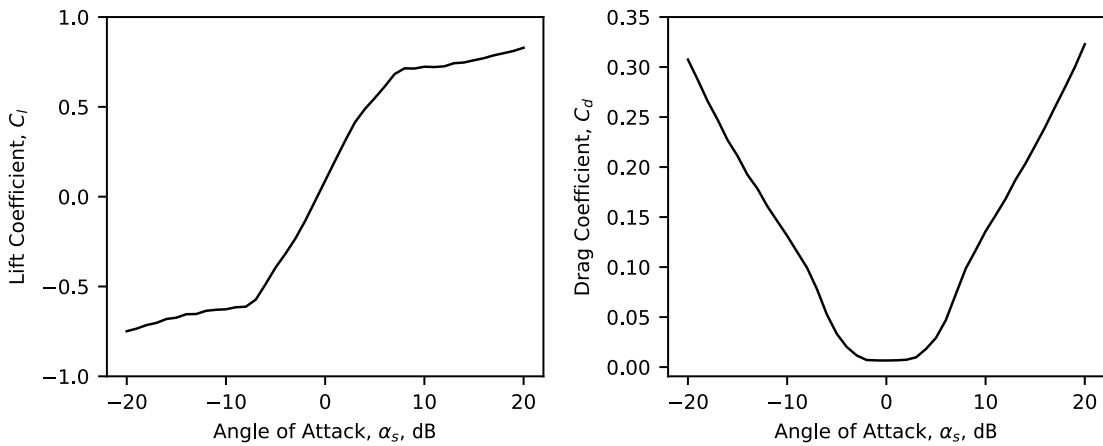


Figure B.8. NACA-16105 lift and drag coefficients.

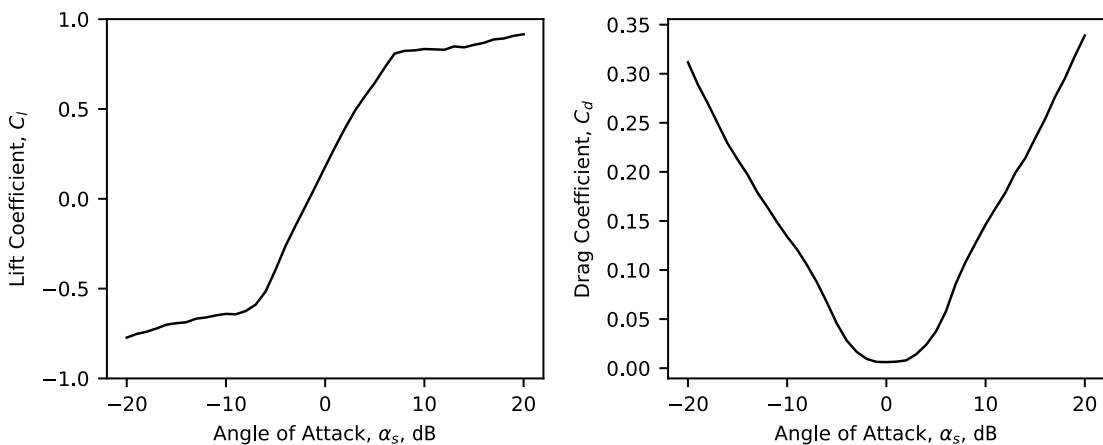


Figure B.9. NACA-16203 lift and drag coefficients.

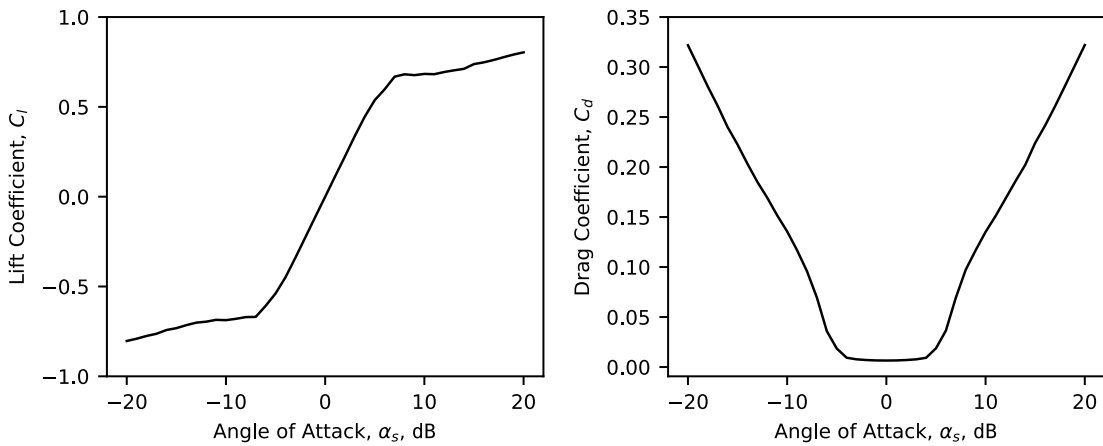


Figure B.10. NACA-65007 lift and drag coefficients.

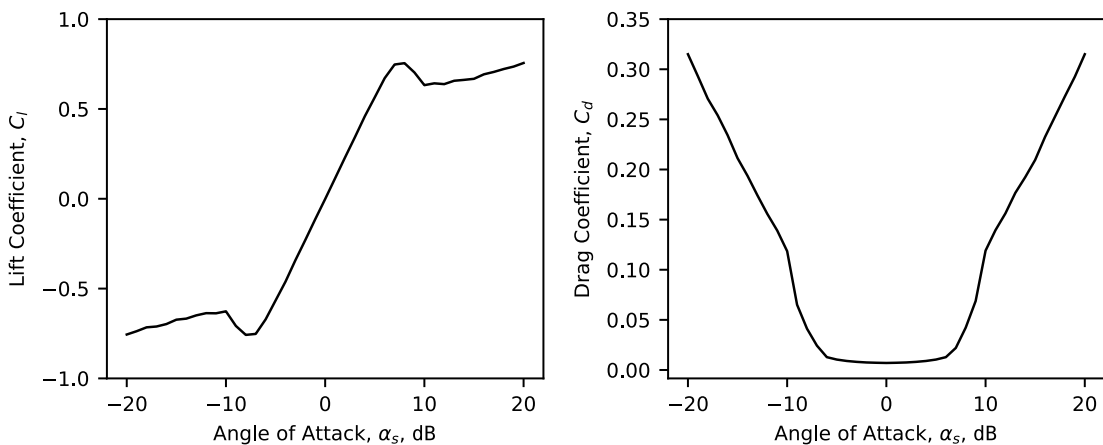


Figure B.11. NACA-65010 lift and drag coefficients.

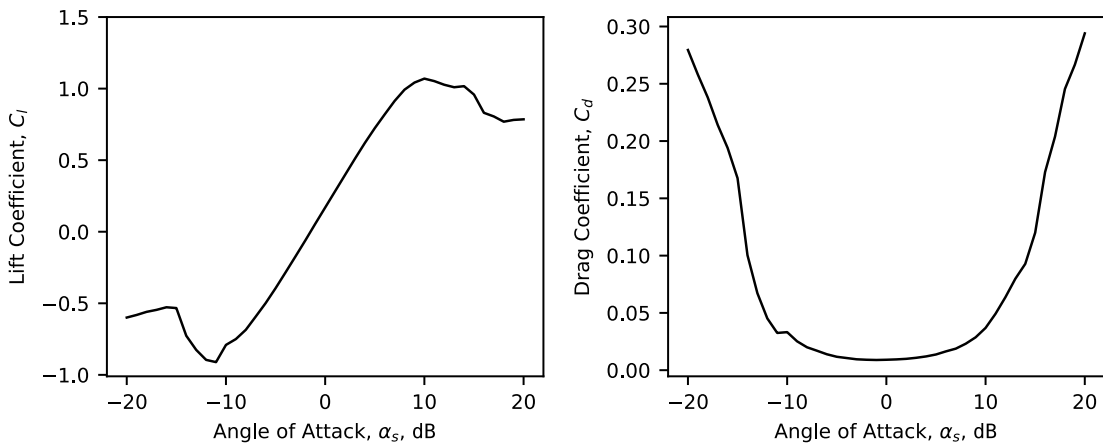


Figure B.12. NACA-65215 lift and drag coefficients.

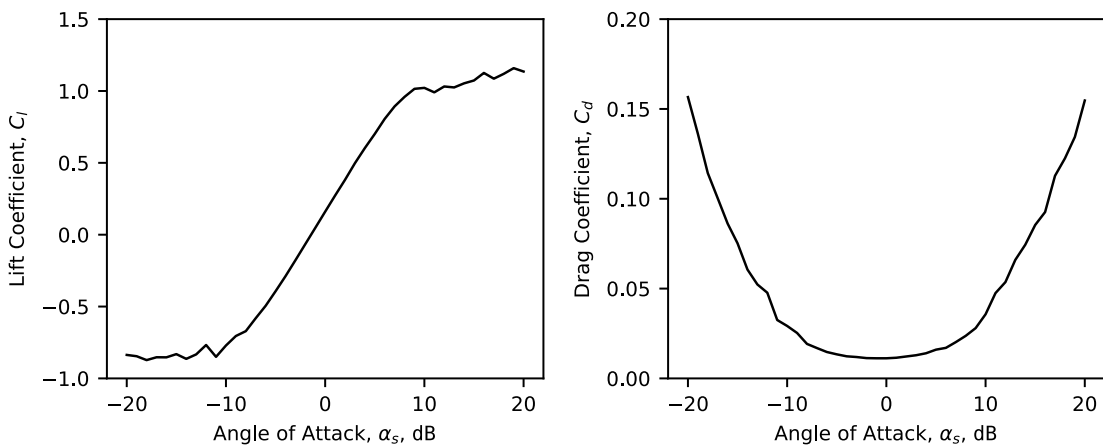


Figure B.13. NACA-65222 lift and drag coefficients.

## Appendix C

### Propeller Geometry

The general shapes of each of the propellers used in this thesis are illustrated below. The exact geometries of the majority of these propellers, described in enough detail to produce 3D solid models, are available from the references listed next to the authors in Table 3.1 and Table 5.1. The geometries of the remaining propellers, the SR-2, SR-3 and SR-7, are available from Refs. 24, 45 and 38, respectively.

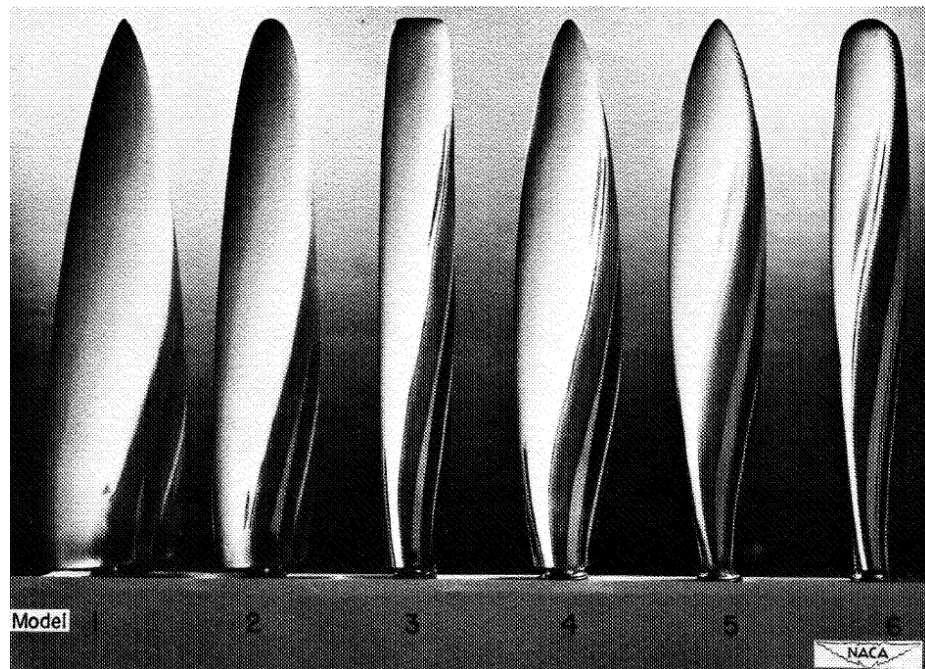
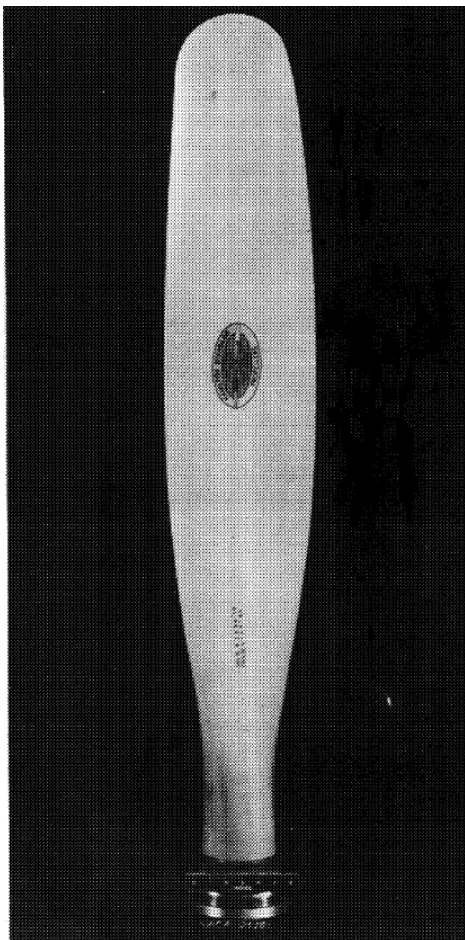
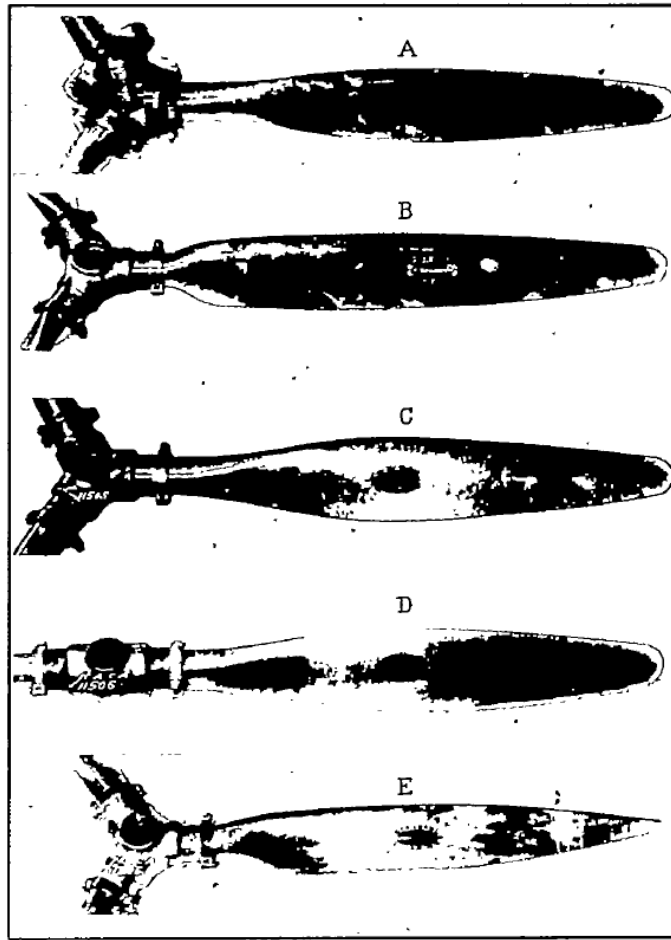


Figure C.1. Geometry of the Model 5 propeller (second from the right) used in aerodynamic test case 1 (from Ref. 37).



(a) Hamilton Standard 6267A-18 propeller.



(b) Navy plan form 5868-9 propeller (Model C).

Figure C.2. Geometry of the Hamilton Standard 6267A-18 propeller and Navy plan form 5868-9 propeller used in aerodynamic test cases 3 and 4 respectively (from Refs. 39 and 40).

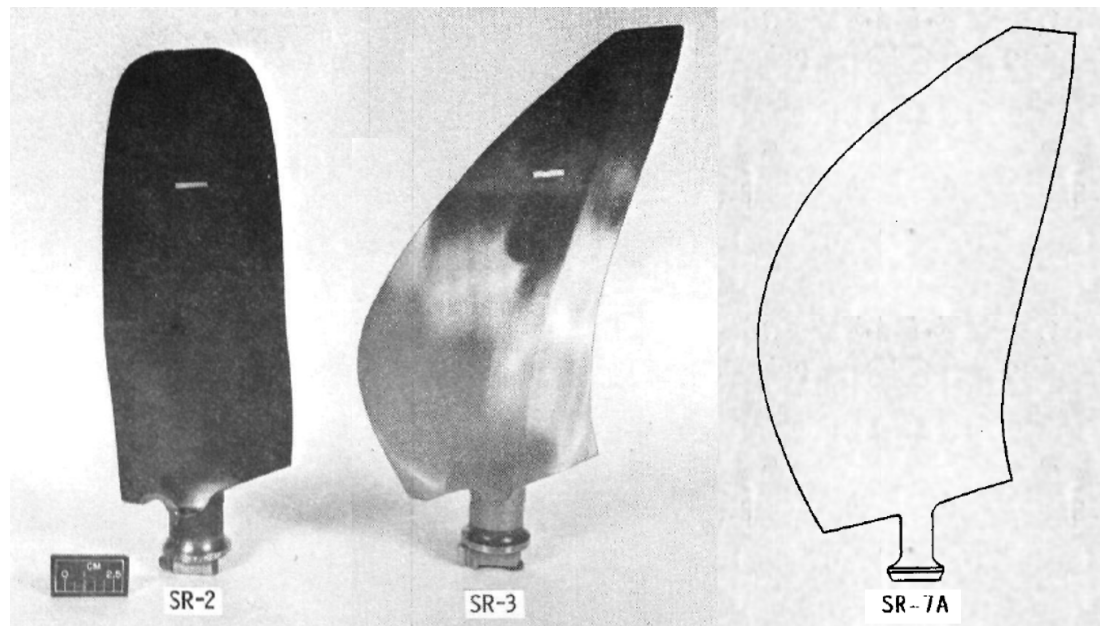


Figure C.3. Geometry of the SR-2, SR-3 and SR-7 propellers used in aerodynamic test case 3 and acoustic test cases 1–10 (from Refs. 55 and 38).

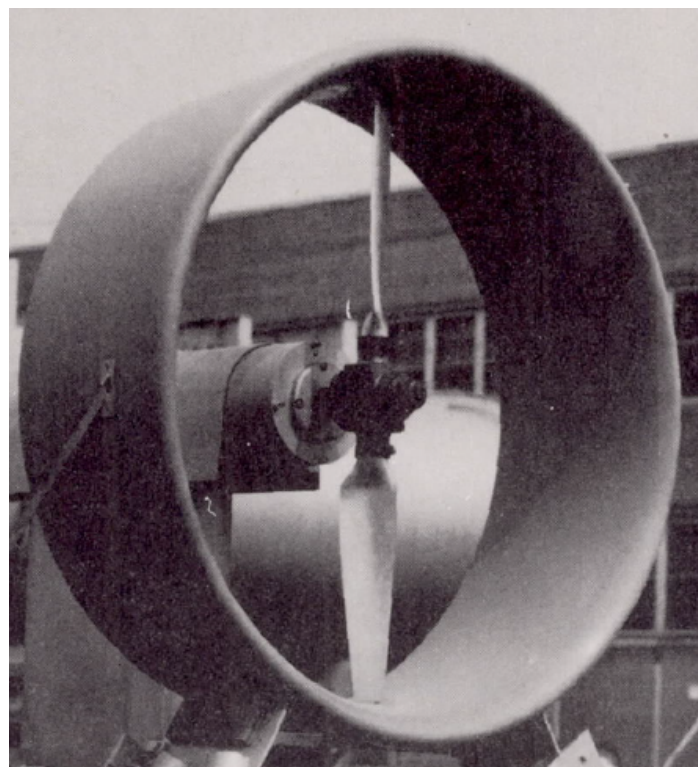


Figure C.4. Geometry of the propeller used by Hubbard in acoustic test case 11 (from Ref. 50).

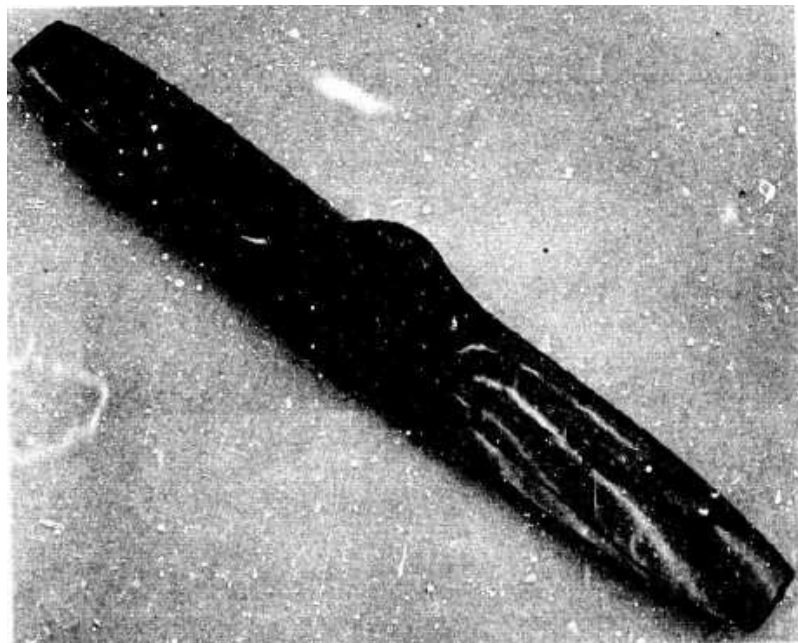


Figure C.5. Geometry of the Sensenich W60K18 propeller used in acoustic test case 12 (from Ref. 28).

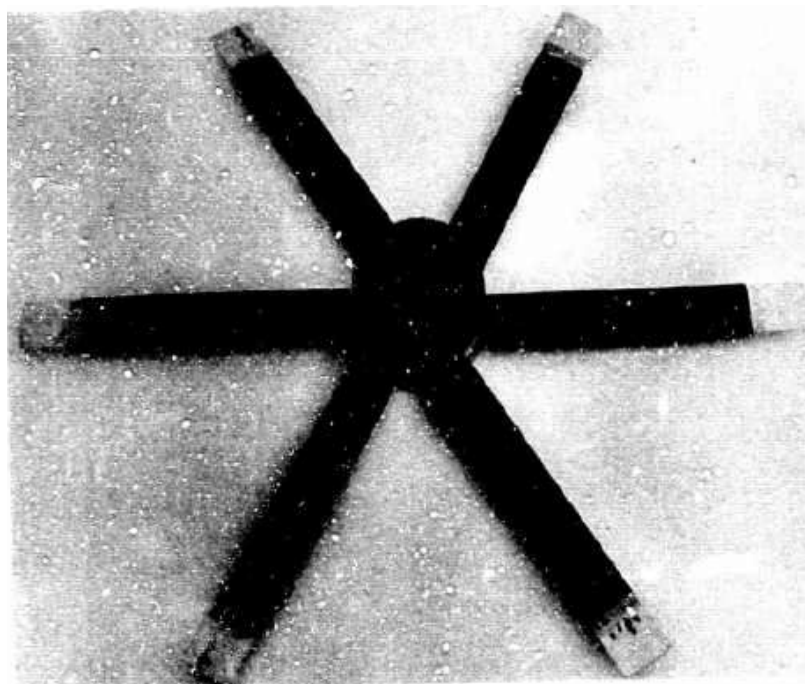


Figure C.6. Geometry of the W6 STD 8° propeller used in acoustic test case 13 (from Ref. 28).

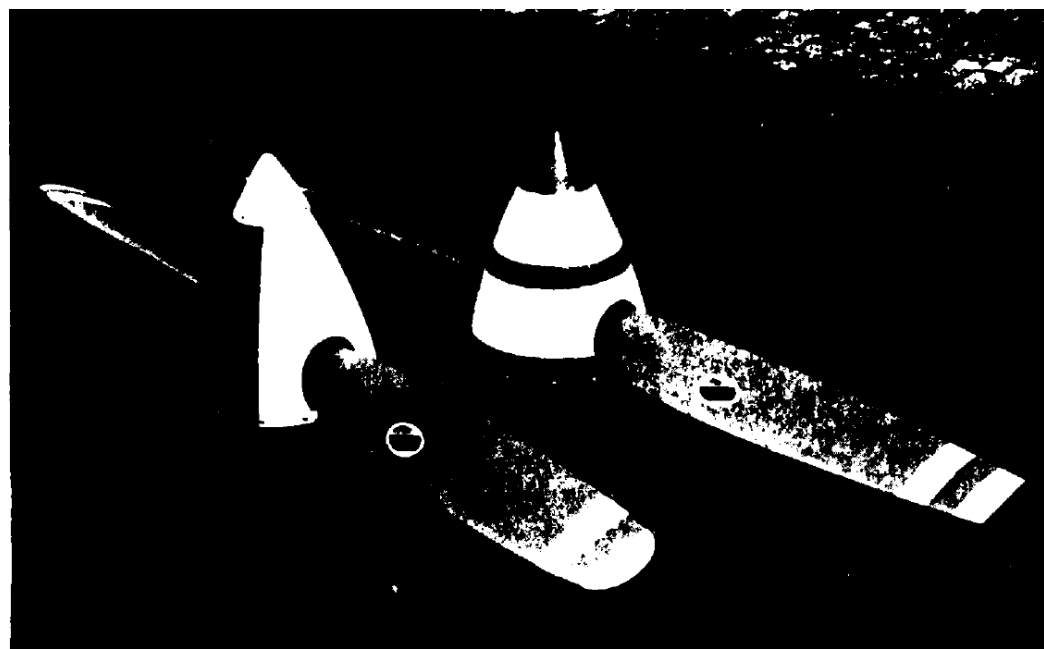


Figure C.7. Geometry of te F8475D-4 propeller (shown left) used in acoustic test case 14 (from Ref. 51).

## Appendix D

# Additional Aeroacoustic Data

Aeroacoustic data obtained using only a single microphone position per data point, as described in Section 4.1, is included below. Figs. D.1 to D.10 feature the same setup and test cases as the results presented in the main text. Acoustic prediction accuracy of each noise model is summarized in Table D.1. As in the main text, the non-bracketed term qualifies the capability of the models in predicting the maximum noise level and usually corresponds to the prediction error of transducers near the propeller plane. Likewise, the term in brackets is a measure of the consistency of the models at different transducer locations and typically matches the prediction error at the transducer closest to the propeller axis. The significant difference in the maximum error is expected since the acoustic theory predicts zero noise at the propeller axis if a single microphone location is used. The error at the location of maximum noise is shown graphically in Fig. D.11. Figure D.11a on the left shows the variation of error by test case, while Fig. D.11b on the right shows the variation of error with freestream Mach number (test cases 8 and 9 omitted). The dotted lines in Fig. D.11b represent the general trend of each model and were formed by taking the average error of test cases for each Mach number. Comparison of Table D.1 and Table 5.2 shows only a minor difference in the predicted maximum tonal noise between the two sets of results.

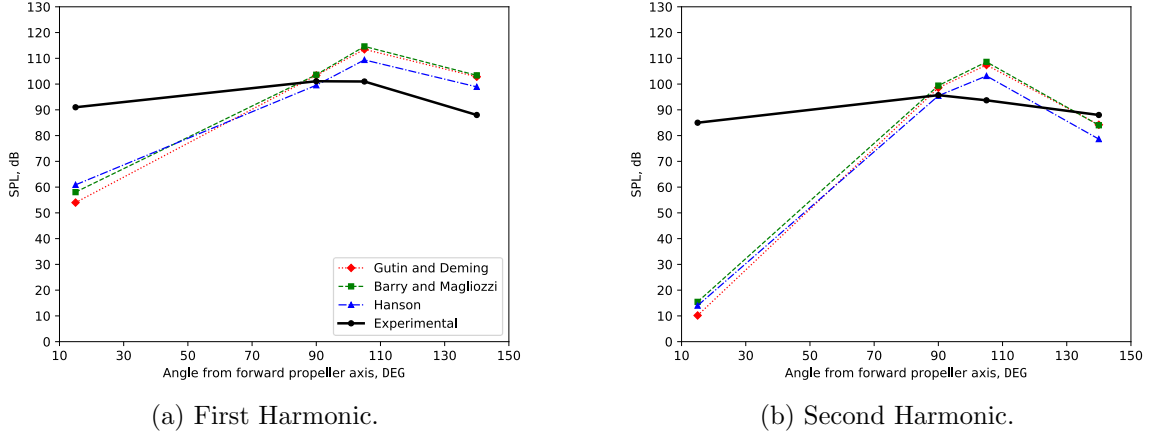


Figure D.1. Tone directivities - test case 1.

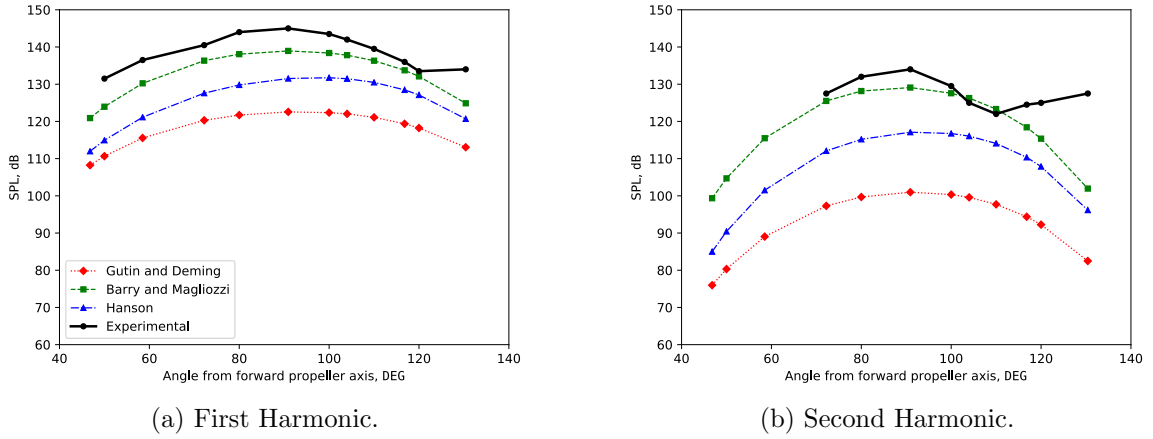


Figure D.2. Tone directivities - test case 2.

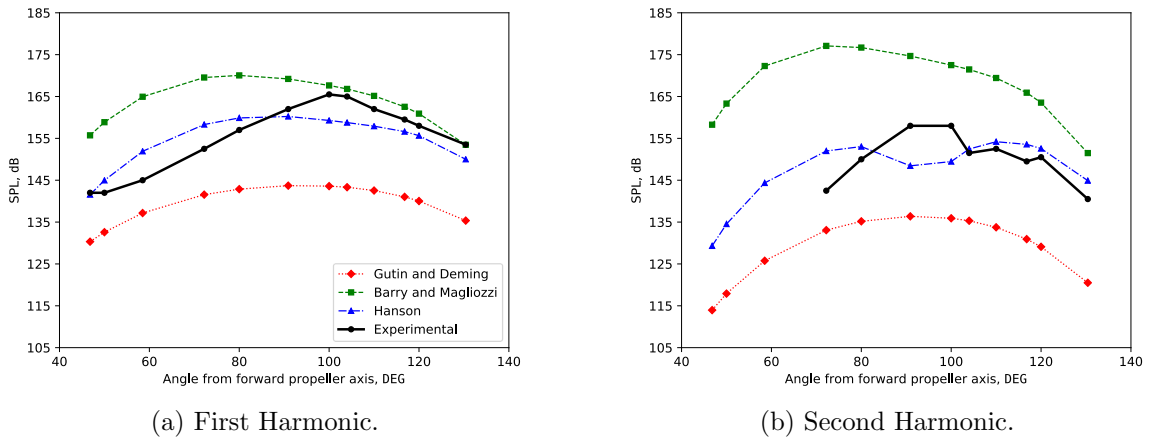


Figure D.3. Tone directivities - test case 3.

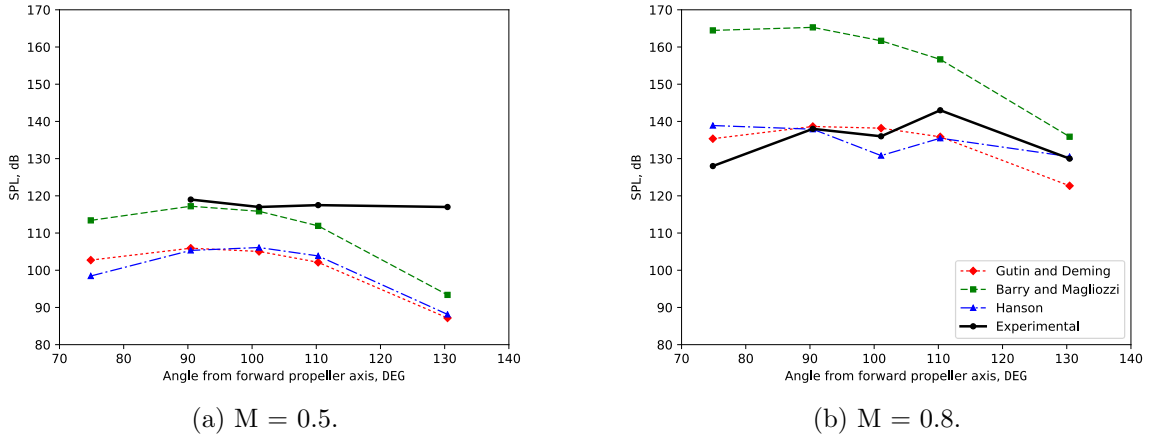


Figure D.4. Blade passing tone directivities - test cases 4 and 5.

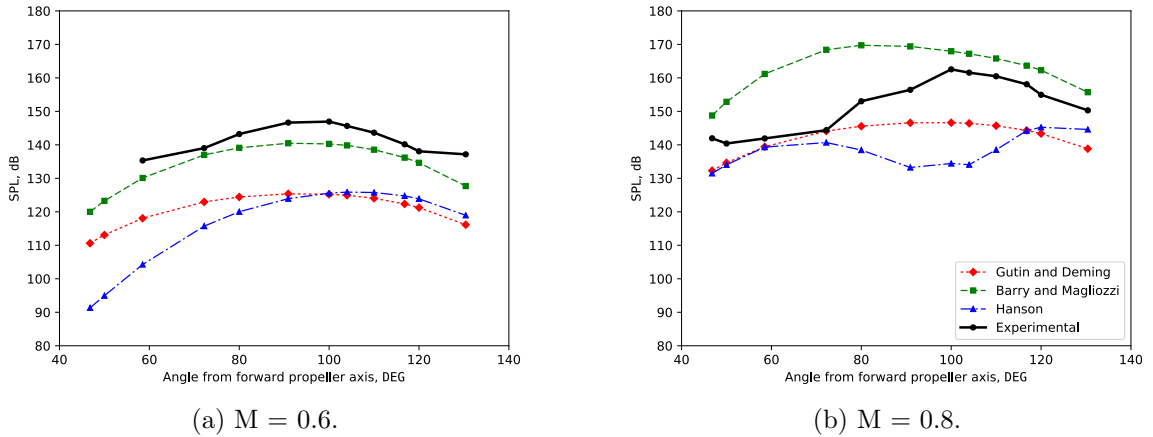


Figure D.5. Blade passing tone directivities - test cases 6 and 7.

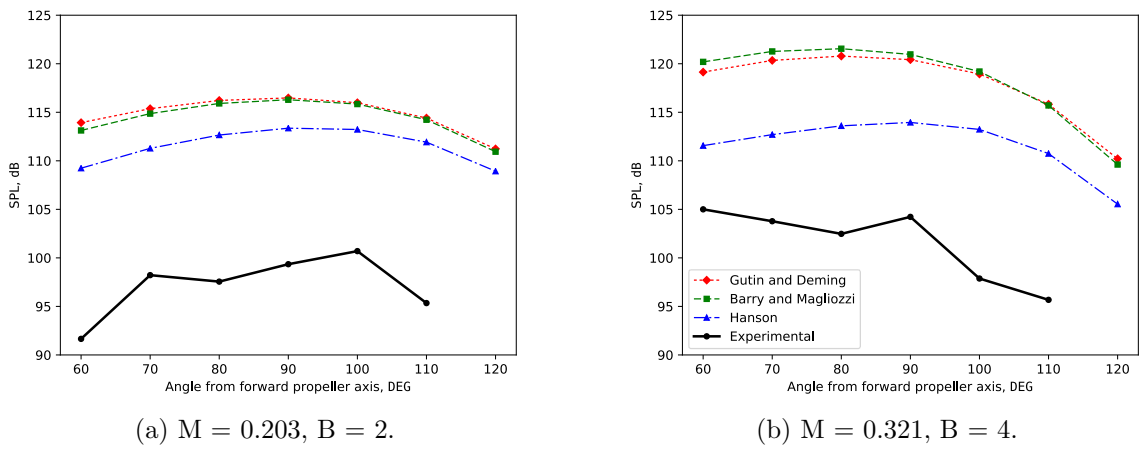


Figure D.6. Blade passing tone directivities - test cases 8 and 9.

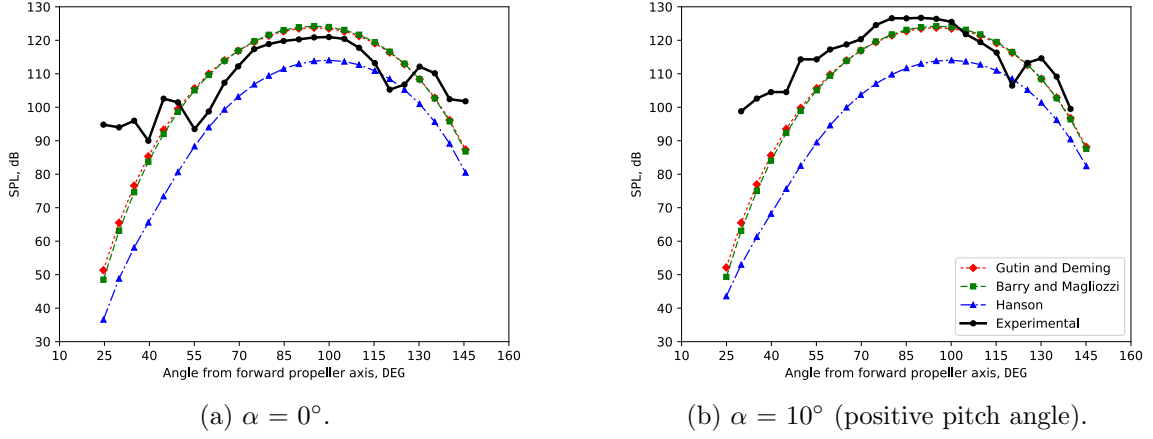


Figure D.7. Blade passing tone directivities - test case 10.

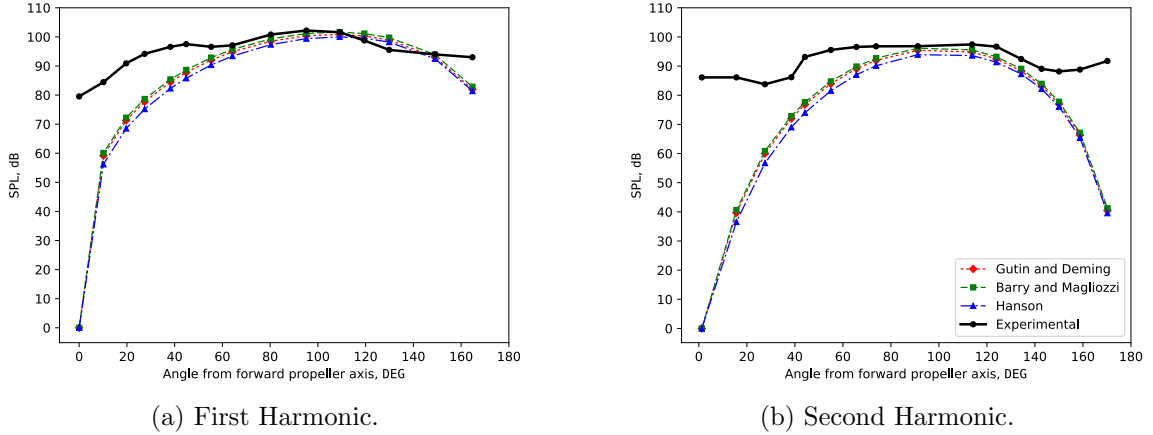


Figure D.8. Tone directivities - test case 11.

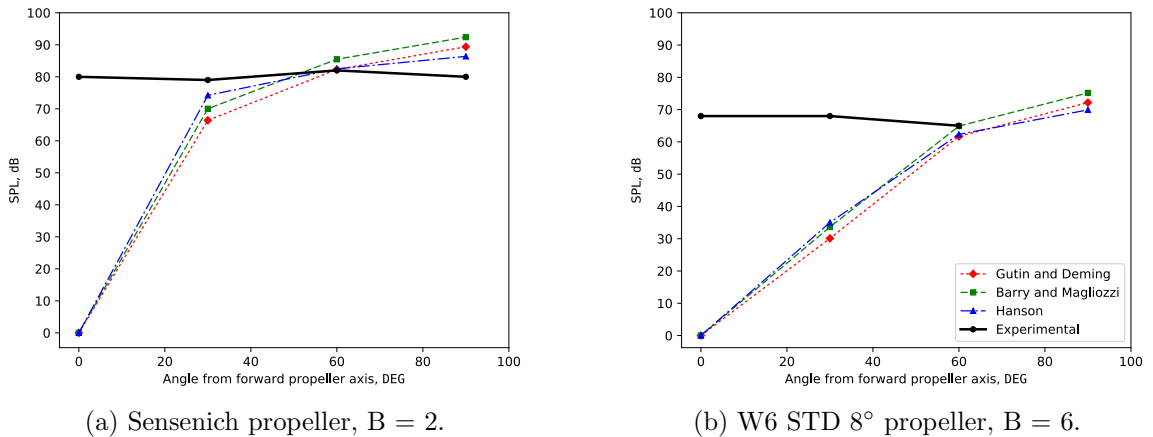


Figure D.9. Blade passing tone directivities - test cases 12 and 13.

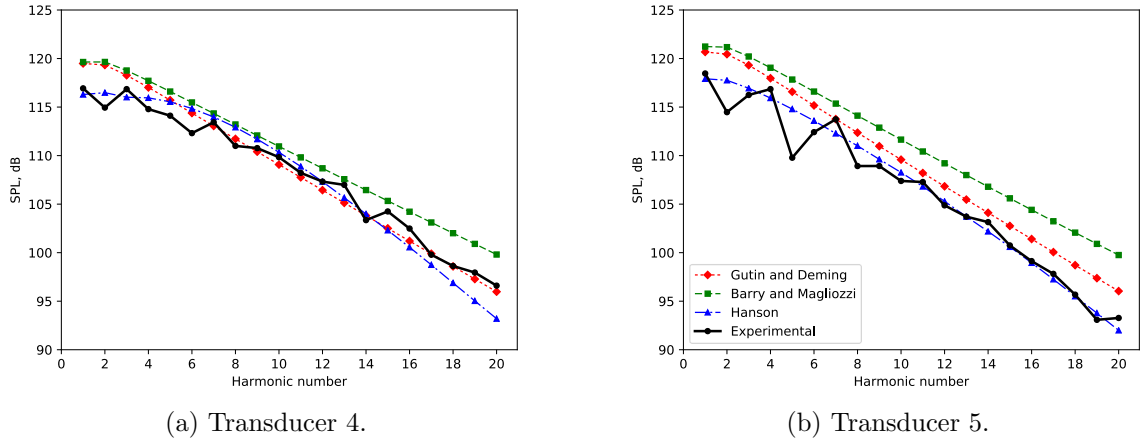


Figure D.10. Noise spectra - test case 14.

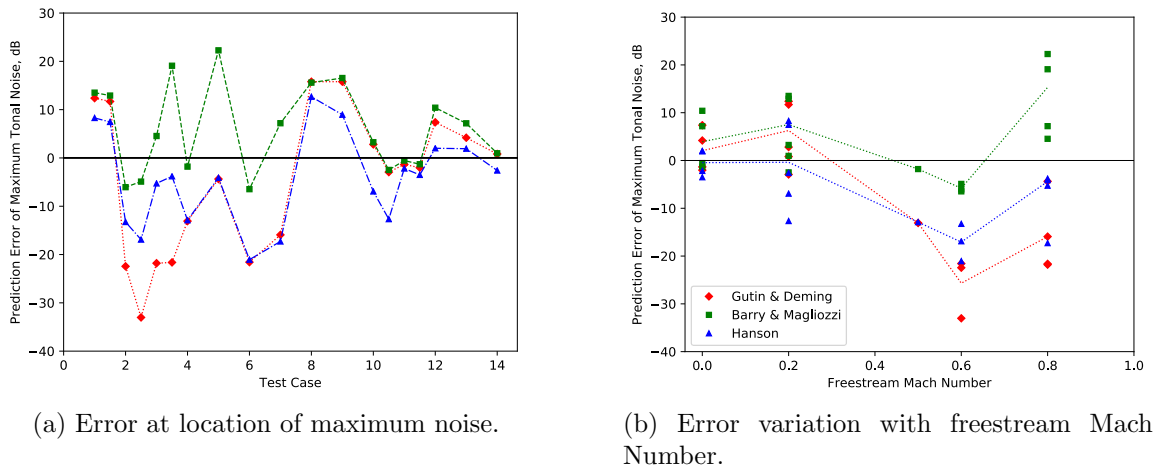


Figure D.11. Summary of acoustic model performance (one mic per data point).

Table D.1. Summary of acoustic model performance (one mic per data point).

Test	Error at location of maximum noise*, dB (Maximum error†, dB)		
Case	Gutin and Deming	Barry and Magliozzi	Hanson
1‡	12.4 (-37.0)	13.5 (-32.9)	8.28 (-30.1)
	11.7 (-74.8)	12.9 (-69.6)	7.45 (-71.0)
2‡	-22.4 (-22.4)	-6.05 (-9.13)	-13.3 (-16.6)
	-33.0 (-45.0)	-4.90 (-25.5)	-16.9 (-31.3)
3‡	-21.8 (-21.9)	4.54 (19.9)	-5.27 (6.91)
	-21.6 (-22.1)	19.1 (34.6)	-3.80 (-9.56)
4	-13.1 (-29.8)	-1.80 (-23.6)	-12.9 (-28.9)
5	-4.36 (7.35)	22.3 (36.5)	-4.11 (10.9)
6	-21.6 (-21.7)	-6.47 (-9.47)	-21.1 (-31.1)
7	-15.9 (-15.9)	7.19 (24.0)	-17.3 (-28.1)
8	15.8 (22.3)	15.6 (21.5)	12.7 (17.6)
9	15.8 (21.1)	16.5 (21.3)	8.95 (15.4)
10§	2.81 (-43.5)	3.25 (-46.3)	-6.94 (-58.2)
	-2.92 (-33.3)	-2.49 (-35.7)	-12.7 (-45.8)
11‡	-1.35 (-79.5)	-0.54 (-79.5)	-2.19 (-79.5)
	-2.02 (-86.1)	-1.30 (-86.1)	-3.51 (-86.1)
12	7.39 (-80.0)	10.4 (-80.0)	4.38 (-80.0)
13	4.19 (-68.0)	7.17 (-68.0)	1.91 (-68.0)
14	0.82 (0.82)	0.96 (0.96)	-2.60 (-3.84)
Avg.¶	12.2 (38.6)	8.26 (38.1)	8.74 (37.8)

\* difference between maximum experimental and maximum predicted noise; locations of maximum noise are not necessarily identical between experimental and predicted results

† maximum error between experimental and predicted data across all transducer locations

‡ the fundamental harmonic is presented first, followed by the second harmonic

§ error for axial flow is presented first, followed by non-axial flow

¶ the modulus of the error values is taken before averaging

## Appendix E

### Experimental Microphone Locations

The positions of the microphones in the experiments selected for validation are described below. The circled microphones in Figs. E.1 and E.6 represent microphones for which valid experimental data was available. Those circled in Fig. E.1 represent locations for which propeller-alone or propeller-fuselage data was available. Acoustic data for the other microphone locations was only available with the aircraft tail present in the wind-tunnel, which alters the harmonic SPL and is therefore not used for comparison. The fuselage itself was shown by Soderman and Horne to have negligible impact on the harmonic sound level [24]. Only microphones 4 and 5 were used in test case 14 (circled in red in Fig. E.6), as data for the other microphones was illegible from the source document.

The microphone positions of test cases 8 and 9 were adjusted using Fig. 3.5 from Ref. 44 to correct for tunnel shear layer effects as directed by Brooks and Metzger. This correction factor translates to a shift in the axial microphone position that is described by Fig. E.4b. A third order polynomial fit of the curve defined in Fig. E.4b was used such that  $x_c = 0.0229x^3 - 0.149x^2 + 0.927x - 0.834$ , where  $x_c$  is the corrected axial location used to produce results for test cases 8 and 9.

The translating microphone probe used in test case 10 (depicted in Fig. E.5) is in plane with the propeller axis and maintains a sideline distance of 1.68 meters.

The microphone positions for test case 11 were distributed along an arc 9.14 meters from the propeller hub (30 feet). The microphones in test cases 12 and 13 were positioned along an arc 3.66 meters (12 feet) from the hub at azimuth locations of  $0^\circ$ ,  $30^\circ$ ,  $60^\circ$  and  $90^\circ$ . In both experiments, the observer angle is taken relative to the forward propeller axis and the microphones are assumed to be in plane with the propeller axis ( $z = 0$ ).

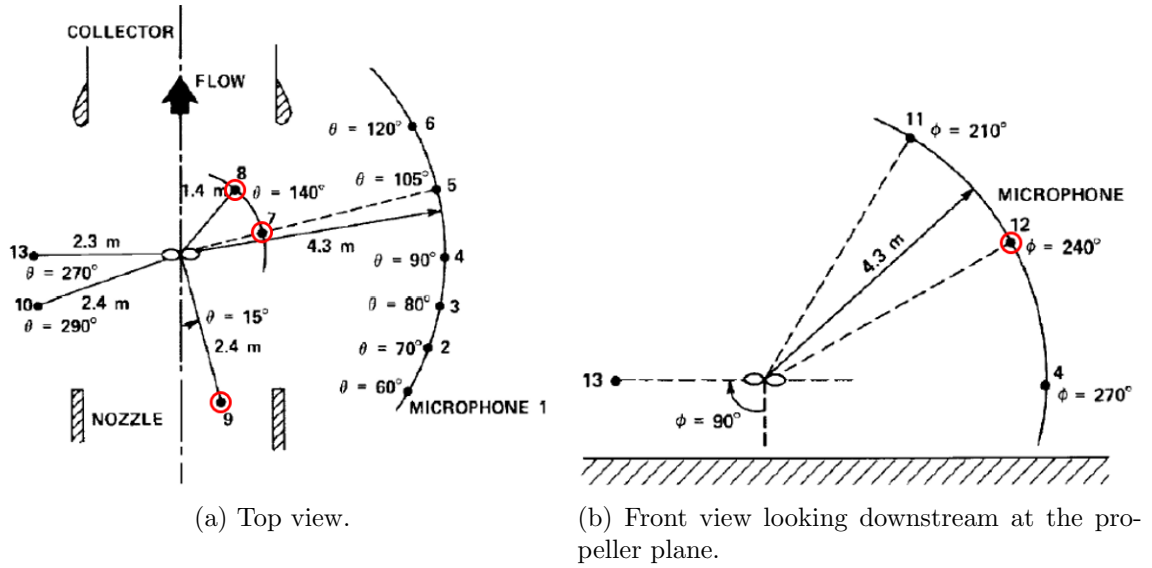
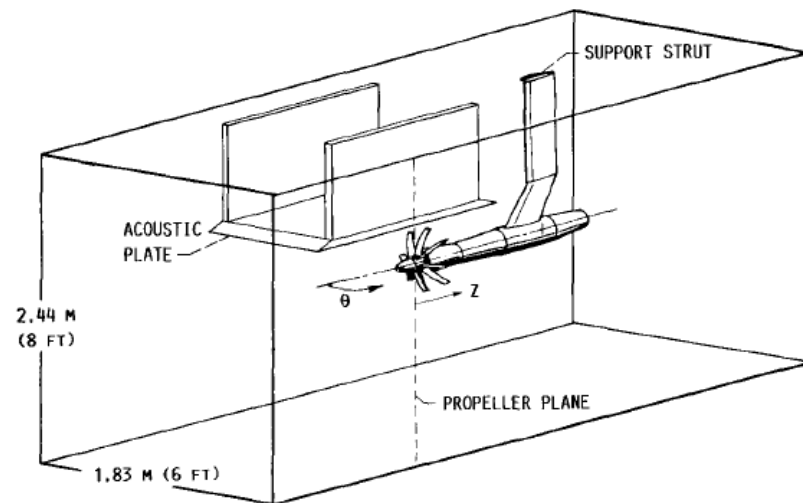


Figure E.1. Microphone locations - test case 1 (from Ref. 24).



TRANSDUCER (PLATE 0.3 DIAMETER FROM TIP)											
1	2	3	4	5	6	7	8	9	10	11	12
TRANSDUCER DISTANCE FROM PROPELLER PLANE, Z, CM (IN.)											
-46.7 (-18.4)	-41.7 (-16.4)	-30.5 (-12.0)	-16.0 (-6.3)	-8.9 (-3.5)	0.8 (0.3)	8.9 (3.5)	12.4 (4.9)	18.0 (7.1)	25.0 (9.9)	28.7 (11.3)	42.4 (16.7)
ANGLE FROM UPSTREAM, $\theta$ , DEG											
46.8	50.0	58.5	72.2	80	90.9	100	104	110	116.8	120	130.4

Figure E.2. Microphone locations - test cases 2, 3, 6 and 7 (from Ref. 46).

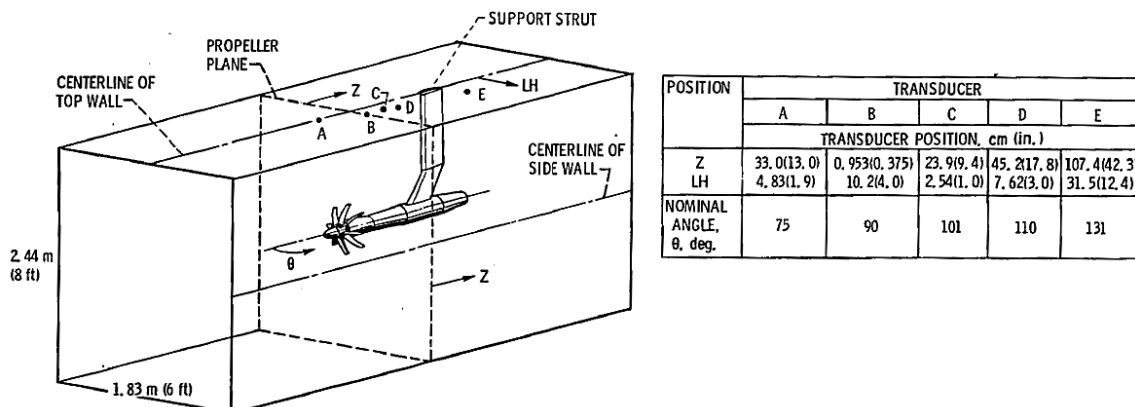


Figure E.3. Microphone locations - test cases 4 and 5 (from Ref. 6).

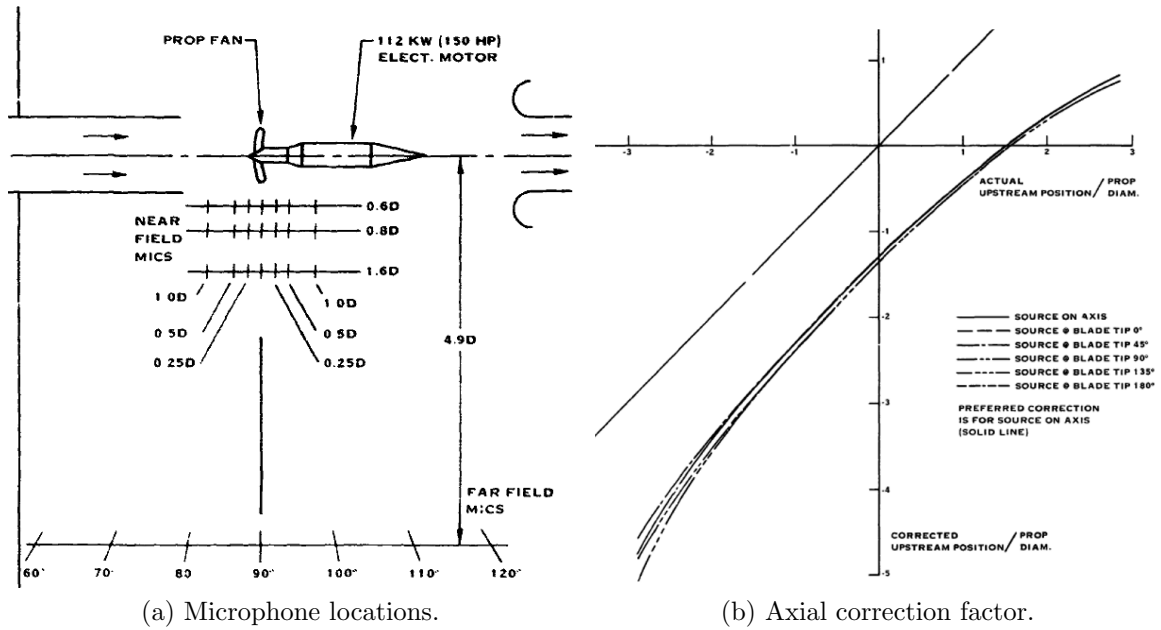


Figure E.4. Microphone locations and axial correction factor - test cases 8 and 9 (from Ref. 44).

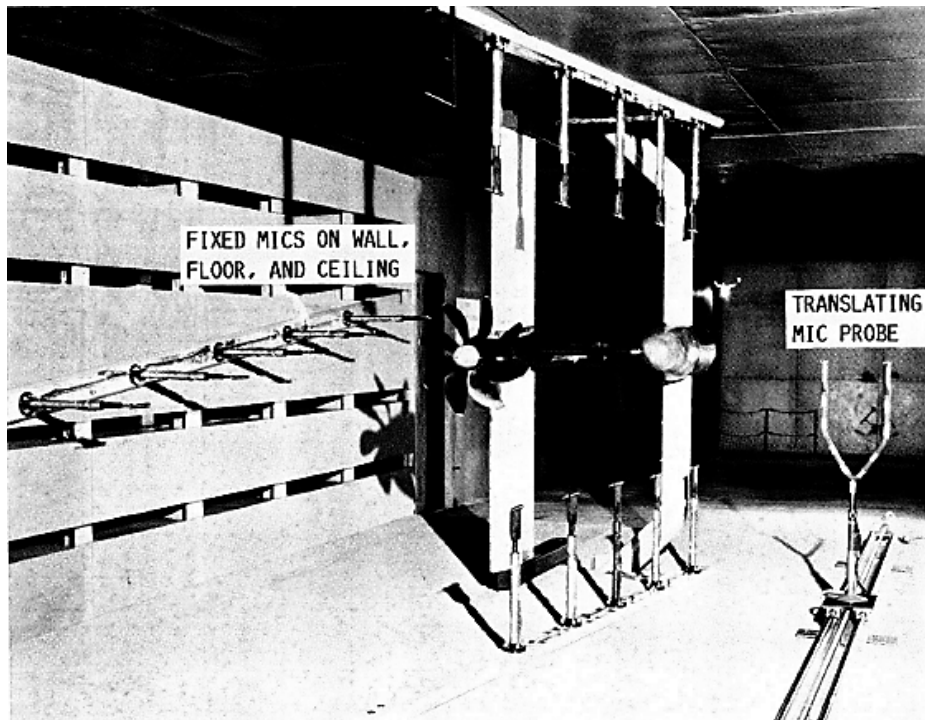


Figure E.5. Microphone locations - test case 10 (from Ref. 5).

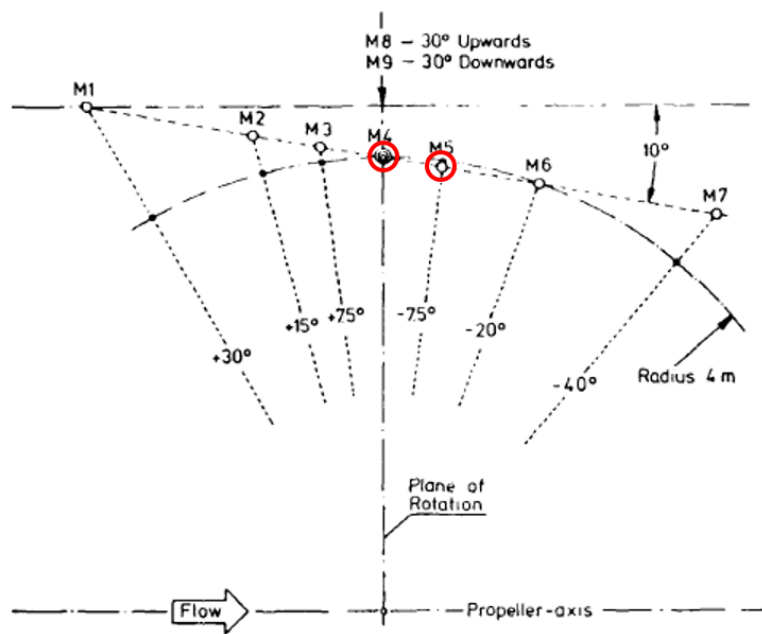


Figure E.6. Microphone locations - test case 14 (from Ref. 51).